DOI:10.14753/SE.2015.1798

Mapping the human brain with cortical electrical stimulation

PhD thesis

Dr. László Entz

Szentágothai János Neuroscience Doctoral School
Semmelweis University

Supervisors: Dr. István Ulbert, D.Sc.
Dr. Péter Halász, D.Sc.

Official reviewers:
Dr. Anita Kamondi, D.Sc.
Dr. Magdolna Szente, D.Sc.

Head of the Final Examination Committee:
Dr. István Nyáry, Ph.D.

Members of the Final Examination Committee:
Dr. László Détári, D.Sc.
Dr. Lajos Rudolf Kozák, Ph.D.

Budapest, 2015

DOI:10.14753/SE.2015.1798

Table of Contents:

DOI:10.14753/SE.2015.1798

DOI:10.14753/SE.2015.1798

DOI:10.14753/SE.2015.1798

DOI:10.14753/SE.2015.1798

DOI:10.14753/SE.2015.1798

Abbreviations

ANOVA:	analysis of variance
BA:	Brodmann's Area
BOLD:	Blood-Oxygen-Level Dependent contrast imaging
CES:	cortical electrical stimulation
CSD:	current source density
CT:	computer tomography
ECG:	electrocardiogram
ECoG:	electrocorticogram
EEG:	electroencephalogram
ESM:	electrical stimulation mapping
FFT:	fast Fourier transformation
FLAIR:	fluid attenuation inverse recovery sequence
fMRI:	functional magnetic resonance imaging
HS:	hippocampal sclerosis
LFP:	local field potential
LFPg:	local field potential gradient
ME:	multichannel microelectrode array
MRI:	magnetic resonance imaging
MUA:	multiple unit activity
NIN:	National Institute of Clinical Neuroscience
Non-REM:	non rapid eye movement
NSLIJ:	North Shore-LIJ Health System
REM:	rapid eye movement
RSFC:	resting - state functional connectivity
SD:	standard deviation
SE	standard error
SEM:	standard error of mean
SO:	slow oscillation
SPES:	single pulse electrical stimulation
SWA:	slow wave activity

DOI:10.14753/SE.2015.1798

SWS:	slow wave sleep
TBLA:	temporo-basal language area
tDCS:	transcranial direct cortical stimulation
TFR:	time – frequency analysis
TMS:	transcranial magnetic stimulation

DOI:10.14753/SE.2015.1798

1 Introduction (literature review)

1.1 Brief history of electrical stimulation of the neocortex

The first documented electrical stimulation of the living human brain occurred in 1874. A patient with a purulent ulcer of the scalp with skull osteomyelitis was admitted to Good Samaritan Hospital in Cincinnati by Dr Roberts Bartholow. The parietal area of the brain became exposed when debridement was done. Bartholow made a faradic stimulation device to stimulate the exposed brain, since there was no such device to be purchased. When mechanical stimulation was done, there was no response, but when electrical stimulation was applied, contralateral muscle spasm was seen, documenting that the cortex was responsive to electricity (Morgan, 1982). Ten years later, in 1884, the first intraoperative cortical electrical stimulation was performed by Sir Victor Horsley, the father of functional neurosurgery. He applied faradic electrical stimulation to the tissue within an occipital encephalocele, and he demonstrated conjugate eye movements that he concluded were due to stimulation of the corpora quadrigemina. Two years after that, in 1886, after a tumor resection, he identified the thumb area of the motor cortex that had been involved in localized seizures, and resected it, the first time intraoperative stimulation was used to guide a resection.

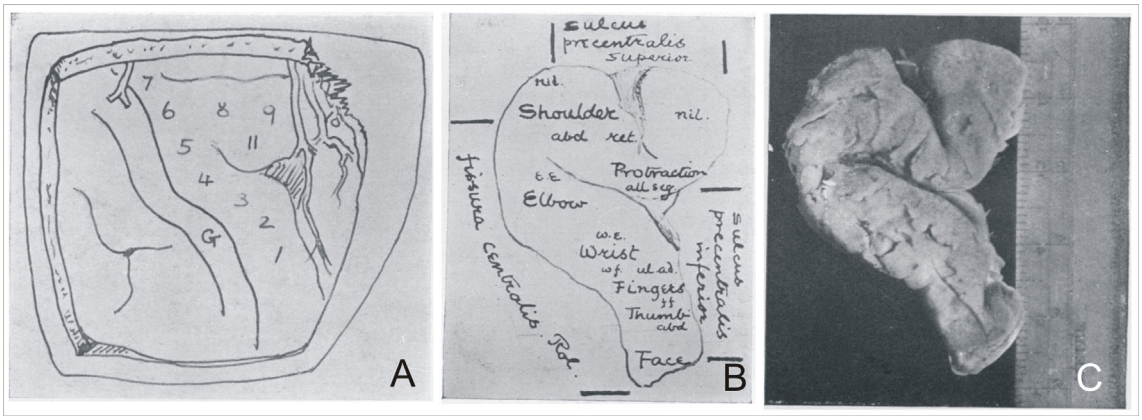

Fig. 1. A, 4.-Sketch of operation field in case of Hn. made immediately after operation. showing cut edge of bone. Fissure of Rolando or central fissure passes in front of G. The sulcus precentralis inferior is shaded. The numbers indicate the points stimulated. B, Outline of the gyrus pre-centralis removed. Abd., abduction; ret., retraction; e.e., elbow extend; w.e., wrist extend; w.f., wrist flexed; ul. ad.,

ulnar adduction; f.f., fingers flex. C, Photograph of the gyrus pre-centralis fixed in formol. The scale is that of centimetres and millimetres (Horsley, 1909).

Later in 1909 he reported in detail of a surgery performed in the precentral region to cure epileptic movement of the contralateral arm (Fig. 1.)(Horsley, 1909). Still in 1909, Harvey Cushing stimulated the postcentral gyrus in an awake patient and demonstrated contralateral motor movement (Peckham et al., 2009). In the mean time in Berlin Professor Fedor Krause reported on a 15-year-old girl he was operating on because of Jacksonian seizures and status since the age of 3. The girl had meningitis at the age of 2 and developed a postencephalic cyst, which was responsible for the seizures. Krause applied monopolar faradic stimulation to the brain (he believed it is less epileptogenic than galvanic stimulation, which was favored by Otfried Foerster), to reveal the function of the cortex he was about to resect. Although he published his experience in 1911, the surgery took place on November 16th in 1893. According to his report the patient was seizure free for 17 years and improved in her mental performance as well (Krause, 1911). Later Krause published a monograph on the topographical mapping of the motor cortex, according to his intraoperative findings with electrical stimulation. He based his functional map on the experience gained with 142 operations (Krause, 1931-1932). In the mean time Otfried Foerster performed similarly awake surgeries to be able to map functional areas of the brain prior to resection. His concept was more driven by epileptological considerations meaning that resecting more of the presumed epileptogenic cortex will more likely result in seizure freedom. He studied in great detail the semiology of the seizures and their localization value. Foerster and his student Penfield published a less detailed but much more extensive cortical map, which was based on the cytoarchitectonic map of O. Vogt (Foerster and Penfield, 1930).

The history of electrical stimulation of the cortex concurs with the beginning of modern epilepsy surgery. The need for better treatment of epilepsy in parallel with the advancement in neurosurgery led to the development of electrical stimulation methods to map essential brain functions prior to resections. The pioneers Horsley, Krause, Foerster and Penfield all realized the importance of not “just” curing epilepsy, which itself was a tremendous step forward, but in the meantime also to understand better the functional anatomy of the brain to be able to preserve essential functions. Penfield after spending 6 Months with Foerster observing his surgical technique, returned to North

DOI:10.14753/SE.2015.1798

America where he met Herbert Jasper who was one of the pioneers in using electrodes to record the electrical activity of the brain to localize epileptogenic areas. Jasper is one of the founders of electroencephalography which gained more and more importance in the localization of epileptogenic cortex prior to therapeutic resection. Penfield and Jasper at the Montreal Neurological Institute first performed an intraoperative electrophysiological recording of the brain on an awake patient in 1937 with subsequent cortical stimulation to map brain functions (Lüders, 1991) (Fig. 2.).

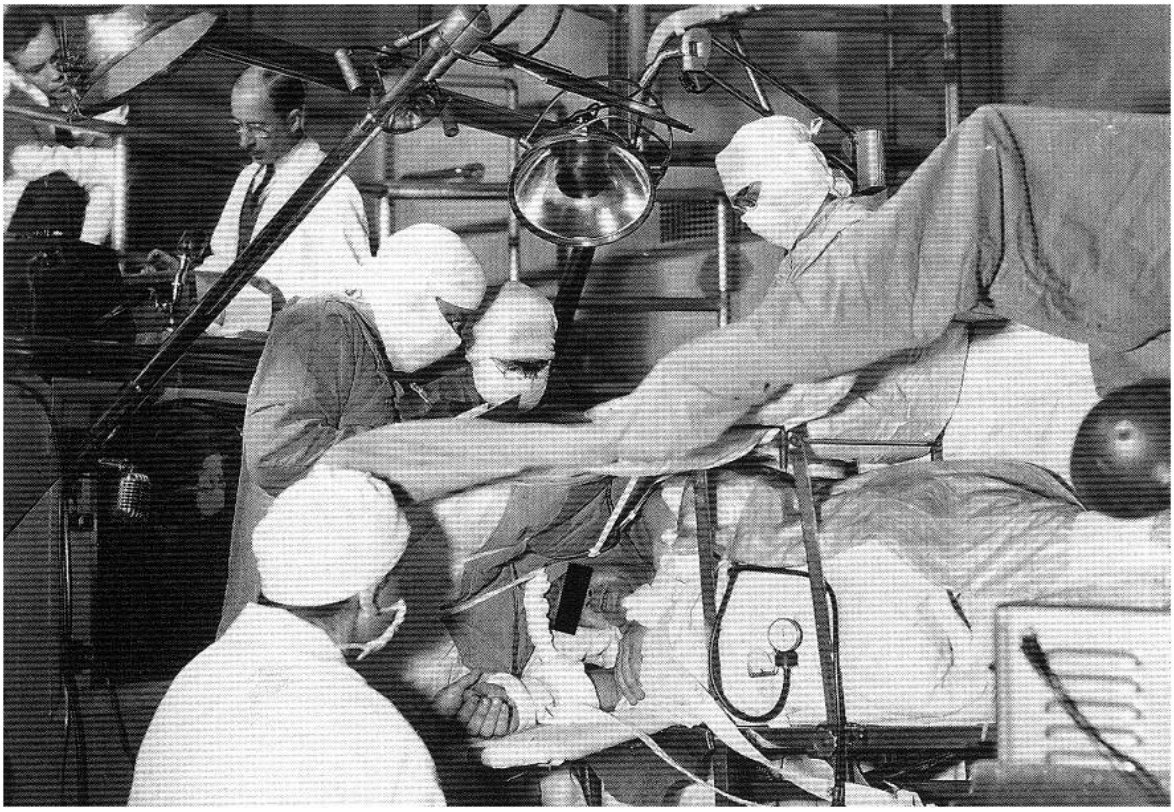

Fig. 2. W. Penfield and H. Jasper performing an awake craniotomy with electrocorticography at the Montreal Neurological Institute in the 1950's.

The routine use of intraoperative mapping led to the development of electrodes, which could be placed subdurally to reach cortical regions otherwise hidden. These electrodes could not only be used for recording brain activity but also for stimulating the underlying cortex. In the second half of the XXth century more and more centers started to develop their own method to stimulate the brain. Extensive discussions were started on the electrical parameters used for stimulating the cortex, some centers used the parameters from animal models, and some did develop their own protocol.

A major step was the recording of after discharges produced by the stimulation. After discharges are still not fully understood, it can be an incipient induced seizure evoked with the stimulation or reflecting areas with lower depolarization threshold. After discharges were registered and attention was paid to locations where it could be elicited with stimulation, when planning the surgical resection line. These technical and methodological findings and advancements led to the foundation of modern epilepsy surgery, which is based many ways on cortical electrical stimulation, which is still the gold standard of mapping brain function and pathology to some extent in the neurosurgical arena.

In the second half of the XXth century more and more neurosurgical centers around the world founded their own comprehensive epilepsy surgical program. The systematic work between epileptologists, psychiatrist, neuropsychologists and neurosurgeons led to the formation of strict protocols how patients with focal onset epilepsy resistant to medical treatment has to be evaluated before surgery.

In the last two decades with the technical innovations in the field of structural and functional neuroimaging the combined use of preoperative imaging with the information received from either intraoperative or extraoperative cortical mapping is the basis of defining eloquent areas of the brain. Precise localization of eloquent areas allows for safe planning of the cortical resection with the least (or none) postoperative neurological deficit for the patient.

The routine use of intracranial electrodes gave place to another form of electrical stimulation, which initially supported neuroscientific purposes, called single pulse electrical stimulation. The first report on single pulse electrical stimulation (SPES) evaluated the responses of the stimulation, which according to the report helps to identify epileptogenesis in human brain (Valentin et al., 2002). Evoked early and delayed responses were identified in the first second after stimulation, but only delayed cortical responses were associated with regions also participating in seizure genesis (Fig. 3.). The ‘early responses’ as defined by Valentin et al. is equivalent with the cortico-cortical evoked potentials defined by Matsumoto et al. in 2004 (Fig. **7.**). The parallel investigations of neuroscientists and clinicians led to the different interpretation of the stimulation evoked responses. While clinicians focused on the diagnostic and therapeutic effects (Valentin et al., 2002, Matsumoto et al., 2004, Kinoshita et al., 2005,

Valentin et al., 2005a, Valentin et al., 2005b, Matsumoto et al., 2007, Umeoka et al., 2009, Enatsu et al., 2011), scientists tried to investigate the electrophysiological changes induced by the stimulation (either cortical electrical or transcranial magnetic or trancranial electric stimulation) locally and globally both in animals and humans (Marshall et al., 2004, Marshall et al., 2006, Massimini et al., 2007, Vyazovskiy et al., 2009). The first report on SPES in humans in Hungary came from István Ulbert's laboratory performed by Loránd Erőss as the operating neurosurgeon reporting on intraoperative SPES through subdural electrodes over the temporal lobe and the evoked potentials were recorded both from the hippocampal formation with laminar microelectrodes and also from the neocortex with subdural electrodes (Fabo, 2008).

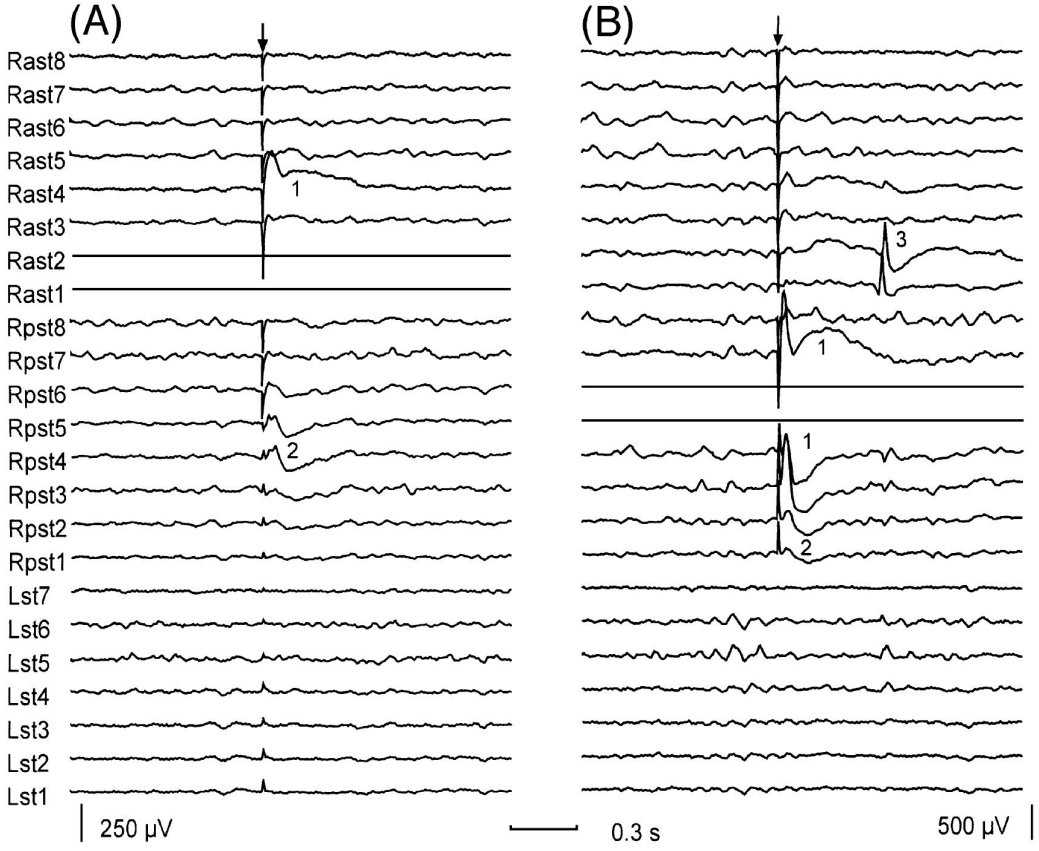

Fig. 3. Numbers inserted in the figure indicate different response types: (1) early responses seen at electrodes located close to the stimulating electrodes; (2) early responses seen at electrodes located >3 cm away from the stimulating electrodes; and (3) delayed responses seen with a latency of >100 ms. The arrows indicate the stimulation artifact. (Valentin et al., 2002)

1.2 Understanding human slow oscillation and its role in non-REM sleep

Brain rhythms, a prominent characteristic of EEG discovered in its initial recordings by Berger (Berger, 1929), are thought to organize cortical activity (Buzsaki and Draguhn, 2004). Especially prominent in sleep (Loomis et al., 1937), microphysiological studies of their neural basis have until now relied on animal models (Steriade, 2006). Presurgical diagnostic procedures in epilepsy may allow the experimenter to open an invasive window on the brain and record local field and action potentials to investigate the fine scale generators of electrical brain oscillations (Worrell et al., 2004, Jirsch et al., 2006, Clemens et al., 2007, Urrestarazu et al., 2007, Axmacher et al., 2008, Fabo et al., 2008, Worrell et al., 2008, Cash et al., 2009, Jacobs et al., 2009, Schevon et al., 2009, Crepon et al., 2010). Traditionally, cortical oscillations have been divided into distinct bands, with more or less distinct roles in, for example, vigilance states, various cognitive functions and pathology. Most importantly, the slow (delta) and especially the very fast rhythms (ripple and fast ripple) have been found with fine scale intracranial observations to effectively influence pathological excitability and may serve as a basic substrate underlying paroxysmal activity (Bragin et al., 2002, Worrell et al., 2004, Jirsch et al., 2006, Urrestarazu et al., 2007, Fabo et al., 2008, Worrell et al., 2008, Jacobs et al., 2009, Schevon et al., 2009, Crepon et al., 2010). More generally, during normal cortical function, oscillations are hierarchically organized and this oscillatory hierarchy can effectively control neuronal excitability and stimulus processing (Lakatos et al., 2005, Steriade, 2006). Low frequency oscillations seem to play an important role in cognitive functions even in the awake state (Lakatos et al., 2008, Schroeder and Lakatos, 2009), despite the fact that under other circumstances slow rhythms are usually good signatures of compromised cerebral functions (Ebersole and Pedley, 2003) and sleep (Achermann and Borbely, 1997).

The slow oscillation - as distinct oscillation from the delta band - was first described by Steriade in 1993 in cats (Steriade et al., 1993a, Fig. 4). A fundamental mode of cortical activity in mammals is the predominance of slow (<1Hz) oscillations (SO) during the deepest stage of non-rapid eye movement (NREM) sleep (Achermann and Borbely, 1997, Steriade et al., 2001, Timofeev et al., 2001, Luczak et al., 2007). In humans, this stage (the third and deepest stage of NREM sleep; N3, also called slow wave sleep; SWS) is reached when 20 % or more of an epoch consists of slow wave activity (SWA,

0.5-2 Hz) in the frontal EEG, having peak-to-peak amplitudes larger than 75 μV, and accompanied by the behavioral signs of sleep (Iber et al., 2007). Intracellular recordings in cats during natural SWS have revealed that SO are composed of rhythmically recurring phases of increased cellular and synaptic activity (up-states) followed by hyperpolarisation and cellular silence (down-states) (Steriade and Timofeev, 2003). In human SWS, the surface positive SWA half-wave (up-state) contains increased alpha and beta power compared to the surface negative SWA half-wave (down-state), suggesting that their basic neurophysiology may be similar to animal findings (Molle et al., 2002, Massimini et al., 2004). While the SO in animals is limited to below 1 Hz (Steriade et al., 1993c), the recent American Academy of Sleep Medicine (AASM) guidelines suggest the 0.5-2 Hz range for SWA in humans (Iber et al., 2007).

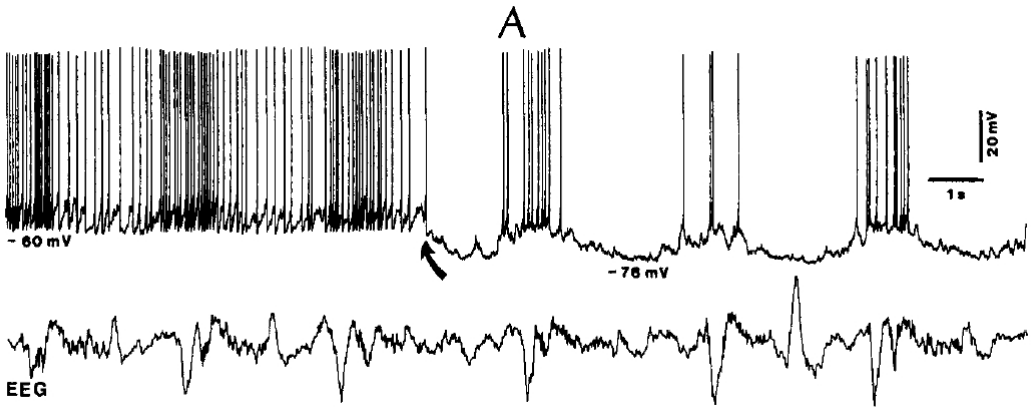

Fig. 4. Part of Figure 7. from the original publication of Steriade: The slow (~0.3Hz) oscillation of reticular thalamic cells and its relation with cortical EEG in cats. (Steriade et al., 1993a)

Studies into the neural mechanisms of slow waves have been motivated by reports that they underlie restorative sleep functions and serve memory consolidation (Huber et al., 2004, Marshall et al., 2006, Vyazovskiy et al., 2008) via ensemble reactivation (Born et al., 2006, Euston et al., 2007) and synaptic strength normalization (Vyazovskiy et al., 2008). SO can be induced artificially by various anesthetics in vivo (Steriade et al., 1993c, Volgushev et al., 2006, Luczak et al., 2007), and ionic environments in vitro (Sanchez-Vives and McCormick, 2000, Shu et al., 2003, Haider et al., 2006). SO are generated in cortico-cortical networks, since they survive thalamectomy (Steriade et al.,

1993b), but not the disruption of cortico-cortical connections (Amzica and Steriade, 1995). However, recent data suggest a complex thalamo-cortical interplay in SO generation (Crunelli and Hughes, 2010). Fine scale laminar analysis of neuronal firing activity revealed that artificial SO in slice preparations are the earliest and most prominent in the infragranular layers, where they are initiated, and spread towards the superficial layers with a long ~100ms inter-laminar delay (Sanchez-Vives and McCormick, 2000). Subthreshold membrane potential fluctuations giving rise to local field potentials (LFP), clearly precede neuronal firing at up-state onset, thus, firing may be the consequence rather than the cause of up-state initiation (Chauvette et al., 2010). Current source density (CSD) analysis of the low frequency (<1 Hz) components of the artificial, anesthesia induced SO (Steriade and Amzica, 1996), localized the most prominent up-state related sinks to the middle and deepest cortical layers (most probably layer III-VI). In contrast, the fast (30-40 Hz) components were more distributed, composed of "alternating microsinks and microsources" along the whole cortical depth (Steriade and Amzica, 1996). In another publication the same authors reported a massive up-state related sink in layers II-III besides weaker ones in the deeper layers during spontaneous and evoked K-complexes (Amzica and Steriade, 1998). The laminar distribution of the major up-state related sink in the rat primary auditory cortex was variable (Sakata and Harris, 2009). On average across animals, the maximal up-state related sink was located in middle and deep layers (most probably layer III-V) in natural sleep, whereas it was located in superficial layers (most probably layer II-III) under urethane anesthesia (Sakata and Harris, 2009). In intact animals the up-state onset related initial firing, intracellular membrane potential and LFP changes could be detected in any layer in a probabilistic manner, with a short inter-laminar delay (~10ms), however, on average, the earliest activity was found in the infragranular layers (Sakata and Harris, 2009, Chauvette et al., 2010). Although the cellular and synaptic/trans-membrane mechanisms of slow waves during natural sleep are thus under intense investigation in animals, these mechanisms have not previously been studied in humans.

DOI:10.14753/SE.2015.1798

1.3 Complex propagation patterns characterize human cortical activity during slow-wave sleep

Cortical slow-wave activity (SWA; in the ~0.5–2 Hz frequency range) is the EEG correlate of synchronized active (up) and silent (down) states of large populations of neocortical neurons during deep non-rapid eye movement (non-REM) sleep or slow-wave sleep (SWS) (Steriade et al., 1993c, Cash et al., 2009, Csercsa et al., 2010). Although synchronous up and down states were observed in isolated neocortex *in vitro* (Cossart et al., 2003), several studies showed that the thalamus might also play an active role in shaping cortical SWA (Sirota and Buzsaki, 2005, Volgushev et al., 2006, Crunelli and Hughes, 2010, Magnin et al., 2010). Large-scale thalamocortical networks were shown to engage in synchronous low-frequency oscillations (Sirota and Buzsaki, 2005, Volgushev et al., 2006). Furthermore, the hippocampus as well as subcortical centers could also participate in this process (Isomura et al., 2006, Wolansky et al., 2006, Mena-Segovia et al., 2008), indicating that slow oscillations could provide a general clockwork for a large variety of neural operations (Sirota and Buzsaki, 2005, Buzsaki, 2006). This view is further strengthened by a series of observations indicating that SWA is indispensable for precisely coordinating hippocampal and thalamocortical oscillations. Population activity patterns like hippocampal ripples and synchronously appearing cortical spindles are orchestrated by the cortical SWA, being entrained to the first half of the surface positive, active phase or up state of slow-wave cycles (Siapas and Wilson, 1998, Molle et al., 2006, Clemens et al., 2007, Csercsa et al., 2010). Also, cortical SWA was shown to propagate over large distances as traveling waves (Massimini et al., 2004, Murphy et al., 2009). From another point of view, memory consolidation processes are often reflected in local changes of cortical SWA (Huber et al., 2004, Massimini et al., 2009) and asynchronies in thalamocortical slow rhythms at different recording sites, were reported in some studies (Sirota and Buzsaki, 2005). Recent reports of regional and temporal heterogenicity of cortical slow waves (Mohajerani et al., 2010), as well as alternative propagation patterns such as spiral waves (Huang et al., 2010), raise the possibility that, in addition to the large-scale orderly traveling of slow waves, complex propagation patterns emerge in a temporally parallel manner at a finer spatial scale. Signals from subdural electrodes provide

substantially better spatial localization compared with scalp recordings as a result of the absence of distorting, integrating, and attenuating effects of interleaved tissues (Buzsaki, 2006, Bangera et al., 2010). These advantages allowed us to investigate the fine-scale (~1 cm) propagation patterns of sleep slow waves such as convergence, divergence, reciprocal, and circular propagation.

1.4 Electrical stimulation triggered slow oscillation and its effects on physiological and pathological brain functions

Animal and human studies show that SO can also be triggered with different types of cortical stimulation. One of the first human studies that focused on the effects of low frequency transcranial electrical stimulation of the brain was written by Marshall and her group in 2004 and then in more detail in 2006 (Marshall et al., 2004, Marshall et al., 2006). They focused on the effects on declarative memory and found that the recall of a paired-associate learning task in the morning in the stimulation group was significantly higher compared to sham stimulation group. Transcranial electrical stimulation was applied during the early stages of non-REM sleep and then the applicants were tested next morning. They also found that the analyzed EEG segments in the stimulation free intervals and after stimulation had an increased slow wave activity compared to sham stimulation. Interestingly, slow oscillation stimulation simultaneously enhanced EEG power within the slow spindle frequency range (8–12 Hz, peaking at: 10.5 Hz) as well as spindle counts (Fig. 5.).

DOI:10.14753/SE.2015.1798

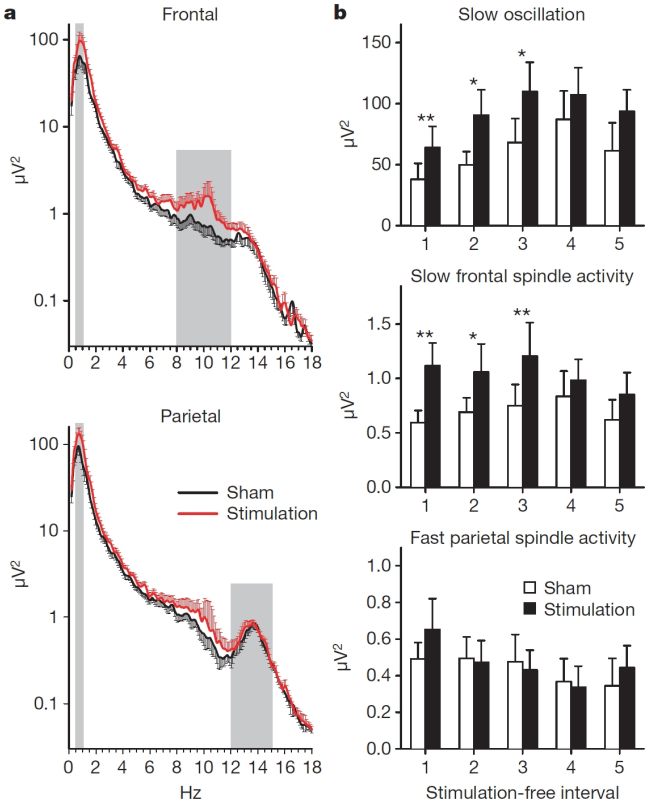

Fig. 5. EEG activity during the 1-min intervals between periods of slow oscillation stimulation and between corresponding periods of sham stimulation. a, Average power spectrum (across first three stimulation-free intervals) at the midline frontal and parietal sites. Shaded areas indicate frequency bands for slow oscillations (0.5–1 Hz), slow frontal spindle activity (upper panel, 8–12 Hz), and fast parietal spindle activity (lower panel, 12–15 Hz). b, Time course of power in the five stimulation-free intervals for slow oscillations, slow frontal spindle activity and fast parietal spindle activity (Marshall et al., 2006).

Massimini and his group applied transcranial magnetic stimulation (TMS) to the brain of healthy volunteers to analyze the effects of TMS on sleep and slow oscillations. They found that on a site, state and dose dependent manner every appropriate stimulation could evoke a slow wave similar to the spontaneous ones and also to K-complexes (Massimini et al., 2007). Although stimulation could evoke a slow wave in non-REM sleep, this was not possible during wakefulness. Beside the effects of the acute stimulation, similarly to transcranial electric stimulation, TMS also resulted in deepening of sleep and increase in slow wave activity.

DOI:10.14753/SE.2015.1798

The first study that compared the effects of intracortical stimulation with the spontaneous slow waves was done by Vyazovsky et al. They used intracortical electrodes to stimulate and also to record ECoG signals in rats. They found that stimulation of the cortex reliably induces slow waves which were very similar to the spontaneous ones and also behaved as travelling waves over cortical areas (Vyazovskiy et al., 2009) (Fig. 6.). These studies all share the fact that using these methods SO was only evoked during non-REM sleep and stimulation in the awake phase did not produce any SO (Massimini et al., 2009).

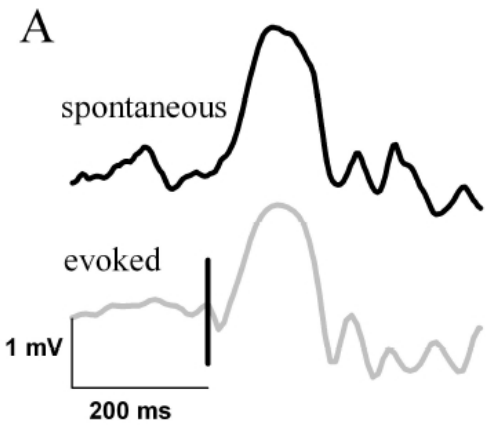

Fig. 6. Comparison between evoked and spontaneous sleep slow waves in rats. A. Individual traces depicting typical spontaneous (black) and evoked (grey) slow waves from one representative rat. Positivity – upward. Vertical bar denotes the timing of the trigger ((Vyazovskiy et al., 2009) modified Fig. 2.).

Single pulse electrical stimulation may also be useful in localizing an epileptic focus and in assessing antiepileptic effects. Valentin et al. found with SPES that late responses can be evoked from the presumed epileptogenic regions of the brain. According to their results, the total resection of the sites which produced late responses was associated with better seizure outcome (Valentin et al., 2005b). Kinoshita et al. have shown that both low (0,9Hz) and high frequency (50Hz) cortical electrical stimulation (CES) can suppress interictal epileptic activity. In the same study they also analyzed the effects of the stimulation on the logarithmic power changes of the ECoG activity in the 0-50Hz band. They found that after high frequency stimulation the stimulated and the neighboring electrodes show significant power decrease from 10-35Hz, which last about

15 minutes after stimulation (depending on the band). They also looked at low frequency stimulation, but here they found only very brief and small changes in power (Kinoshita et al., 2005). Fregni et al. found significantly decreased epileptiform activity after cathodal DC stimulation (Fregni et al., 2006). The link between the animal models and the clinical observations made by the above cited groups is still missing, to understand the effects of single pulse electrical stimulation on the cortex. The hypothesized anti epileptic affect of the stimulation and the ability to reveal epileptogenic areas (networks) is not fully understood. The explanation to these phenomena might be found in the detailed analyzes of the stimulation evoked electrical changes in the cortex both locally and generally on the global networks of the brain.

1.5 Intracranial electrode reconstruction on individual brain surface

Since the introduction of intracranial EEG by Penfield and Jasper there is need for a method, to localize and visualize the electrodes in the skull at their actual location. Up until recently it was very difficult to localize the electrodes, even with high resolution CT and MRI images. The major issue is the implantation procedure itself, due to the deformity of the skull, caused by the craniotomy, the coregistration of the preimplantation images to the postimplantation images is difficult. Another common problem is the artifact or its absence (MRI) of the implanted electrodes, which makes it difficult to exactly locate the center of the electrodes. Several solutions to this problem have been proposed, utilizing photography (Wellmer et al., 2002, Mahvash et al., 2007, Dalal et al., 2008), 2D radiography (Miller et al., 2007), postoperative MRI (Kovalev et al., 2005), or postoperative CT (Grzeszczuk et al., 1992, Winkler et al., 2000, Noordmans et al., 2001, Nelles et al., 2004, Hunter et al., 2005, Tao et al., 2009, Hermes et al., 2010), each with inherent limitations. There is still no standard method to use for electrode reconstruction on the surface of the preimplantation brain. One of the most advanced and probably best suited method is the one proposed by Dykstra et al, from Boston. In their method they combine the imaging possibilities of a freely available software package Freesurfer (Dale et al., 1999) for brain surface reconstruction with the mathematical possibilities of MATLAB (MathWorks, Natick, MA). This method allows of creating high resolution 3D brain reconstructions from preoperative MRI, and co-registering the postimplantation CT to that space. By doing

so one of the difficulty is the consequences of the craniotomy, which always deforms the outer contour of the brain at the site of the surgery. To bypass this problem a special Matlab script was created which locates the center of the electrode (according to previous manual selection) and snaps it to the pial surface of the brain. Our international research group in cooperation with Dykstra and his colleagues adopted the published method and modified it to the needs of the following research.

1.6 Mapping brain networks with SPES evoked cortico-cortical potentials

To be able to study the anatomico-functional organization of the brain, we have to combine methods which can provide very precise anatomical locations, but in the mean time also bears information of the functional role of that specific brain region.

One of the most used method to anatomically specify different brain regions is Brodmann's cytoarchitectonic subdivision (Brodmann, 1909). The combination of Brodmann's brain map with today's sophisticated imaging methods allows to precisely localize individual cortical regions to a standard which can be a basis of comparing anatomical regions across individuals.

A large body of clinical and scientific evidence supports a functional organization of brain areas into processing modules that are distributed over noncontiguous brain regions (Felleman and Van Essen, 1991). It is widely accepted that cortical regions interact over varying distances to form local and long-range networks that cooperate and form the basis of both normal brain function as well as pathological processes such as seizure spread. CCEP mapping using SPES in patients undergoing seizure monitoring with invasive intracranial electrode arrays is one means to delineate these networks and at the same time localize them to distinct brain regions.

The term 'cortico-cortical evoked potentials' was introduced by Matsumoto et al. from Hans O. Lüders's group at The Cleveland Clinic Foundation (Cleveland, Ohio, USA). In their initial paper they studied the connections between the well known perisylvian and extrasylvian language areas, and their idea was to develop a technique which may reveal the otherwise hidden functional connections between eloquent (e.g. language, motor) areas (Matsumoto et al., 2004)(Fig. **7.**).

Such mapping has been used to define functional networks related to language (Matsumoto et al., 2004) (Fig. **7.**) and motor function (Matsumoto et al., 2007) and pathological networks that support ictal onset (Valentin et al., 2002, Enatsu et al., 2011). Umeoka et al. found neural connection between the two temporo-basal regions, indicating the existence of a direct connection between these areas which also represent the temporo-basal language areas, investigated with bitemporal subdural electrodes (Umeoka et al., 2009).

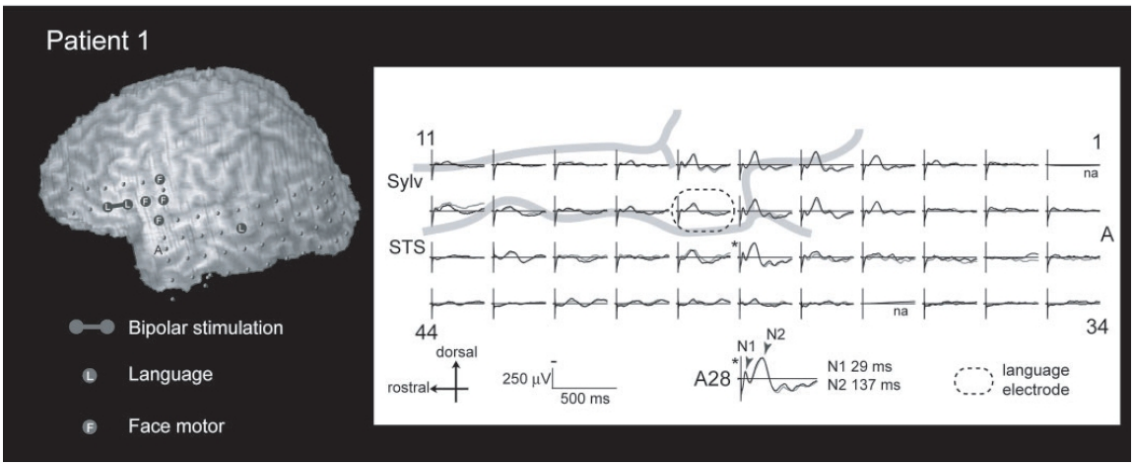

Fig. 7. CCEPs AL→PL in patient 1 recorded from the posterior language area (plate A), time-locked to single pulse electrical stimulation delivered at the anterior language area. Two trials are plotted in superimposition for each electrode. The vertical bar corresponds to the time of stimulation. The anterior language, posterior language and face motor areas were identified by standard cortical stimulation. Evoked responses were recorded mainly from the posterior part of the superior temporal gyrus and the adjacent portion of the middle temporal gyrus in and surrounding the language electrode defined by standard cortical stimulation (A18: highlighted with a dotted circle). Maximal activity was seen at electrode A28 with a clear early N1 and a late N2 potential, peaking at 29 and 137 ms, respectively. STS = superior temporal sulcus; Sylv = sylvian fissure; AL = anterior language area; PL = posterior language area; na = CCEP not available due to high impedance in the recording electrode (Matsumoto et al., 2004).

The implanted subdural electrodes in patients with epilepsy provide high spatiotemporal resolution that can permit the identification of the ictal onset and propagation. However,

it is difficult to characterize excitability and connectivity of cortical regions with this approach. In the past decade, an interventional approach has been adopted within a few groups (Valentin et al., 2002, Matsumoto et al., 2004, Valentin et al., 2005b, Matsumoto et al., 2007) which involve single pulse stimulation at one cortical region and recording the response at other regions. These protocols are to be distinguished from the typical invasive electrical stimulation mapping (ESM) protocols that involve high frequency (20-50Hz) electrical stimulation to elicit behavioral changes and attribute them to the function sub served by the brain areas underlying the stimulated electrode. While this identifies 'eloquent' functional areas of the neocortex, high frequency ESM disrupts the function of the underlying brain and carries the risk of producing seizures. Furthermore, it is difficult to ascertain whether the elicited behavior is originating from the region underlying or regions strongly connected to the stimulated electrode. SPES typically does not elicit any obvious behavioral effect, but the ability to deliver multiple pulses allows computation of a CCEP profile over the array of implanted electrodes. These responses consist of an initial early biphasic activation (10-30ms) and a delayed (50-300ms) slow wave. The early response, which has been referred to as the N1 response is thought to be the result of direct activation of the local cortex (Purpura et al., 1957, Goldring et al., 1994), while the later N2 slow wave seems to represent a widespread induced cortical downstate. Recently, the N1 and N2 time period of the CCEP has been shown to correlate with connectivity measures defined by resting state fMRI (Keller et al., 2011), while the latency and amplitude of the N1 correlates with diffusion tensor imaging (Conner et al., 2011).

1.7 Resting state functional magnetic resonance imaging as a tool to reveal intrinsic architecture of the brain

There is mounting evidence that the temporally correlated low-frequency fluctuations that engender the brain's intrinsic functional architecture are relevant to brain function. One of the first scientists who looked at these very low frequency fluctuations in the brain was Bharat Biswal. He reported on the first fMRI recorded in resting state of 11 healthy volunteers. According to his findings brain areas involved in motor function have a high degree of temporal correlation even in resting state, when choosing a

reference in the middle of the motor cortex (Biswal et al., 1995). His findings with resting state fMRI were very similar to the results obtained with task based fMRI (Fig. 8.).

Studies relating variation within this intrinsic architecture to behavior, cognition, psychopathology, and neurological disease have captured the attention of the neuroscientific, psychological, and clinical communities alike (Hampson et al., 2006, Fox et al., 2007, He et al., 2007a, Greicius, 2008). Despite early controversies regarding the origins of the BOLD signal fluctuations commonly used to map the intrinsic architecture, recent work demonstrating their electrophysiological correlates suggests a neural origin (He et al., 2008, Shmuel and Leopold, 2008, Sadaghiani et al., 2010, Scholvinck et al., 2010).

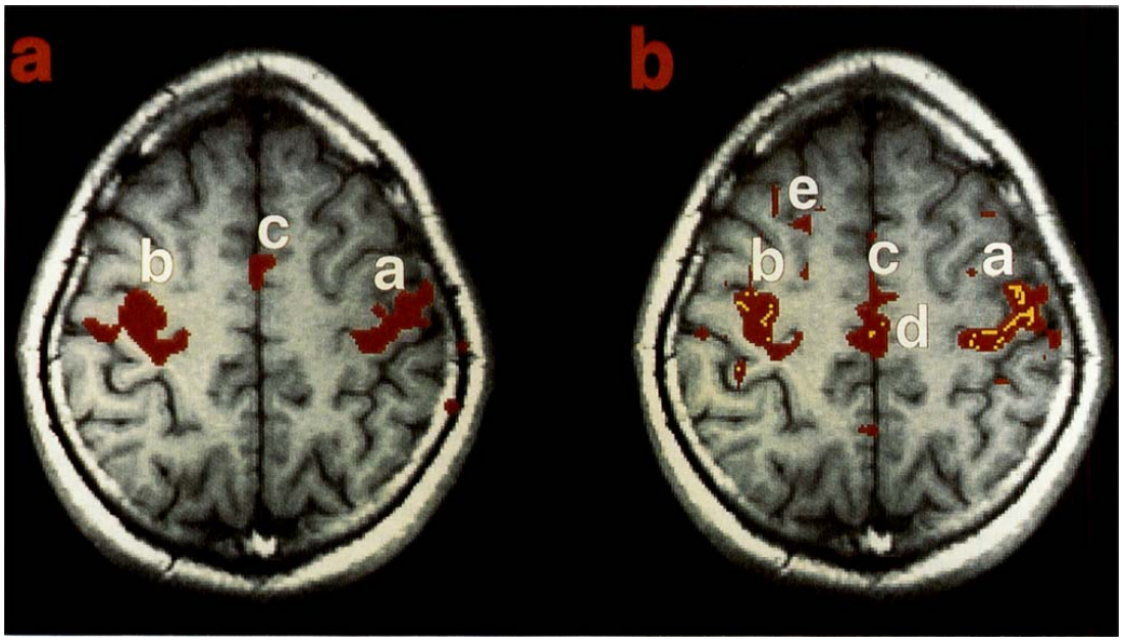

Fig. 8. (Left) FMRI task-activation response to bilateral left and right finger movement, superimposed on a GRASS anatomic image. (Right) Fluctuation response using the methods of this paper. Red is positive correlation, and yellow is negative. Fig. 3. from: (Biswal et al., 1995); a-b:motor cortex; c: SMA; d: paracentral lobule; e: premotor area.

Yet, the neurophysiological significance of correlated brain activity occurring on such slow time scales remains elusive. Emerging hypotheses suggest a role for this slow

activity in the maintenance and reinforcement of the synaptic connections that support cognition and action (Pinsk and Kastner, 2007, Nir et al., 2008). Central to this suggestion is the assumption that cortico-cortical dynamics that take place over faster time scales are embedded in its intrinsic functional architecture; however, to date no direct evidence of this exists.

1.8 Graph theoretical approaches to analyze brain networks

Graph theoretical measures may be adopted to CCEP defined local and long range connections to help to describe the connectivity of different brain regions and networks. The human brain is a large-scale complex network, simultaneously segregated and integrated via specific connectivity patterns (Tononi et al., 1994, Bullmore and Sporns, 2009, He and Evans, 2010). Bullmore and colleagues summarized the graph theoretical approaches and definitions in their 2009 paper, which we followed in our analysis, see figure below (Fig. **9.**). A quantitative analysis of complex brain networks, largely based on graph theory (Bullmore and Bassett, 2011) is typically conducted through either the structural or functional domain (Damoiseaux and Greicius, 2009, Guye et al., 2010). Structural connectivity networks can be based on white matter tracts quantified by diffusion tractography (Hagmann et al., 2008, Iturria-Medina et al., 2008) or correlations of morphological measures (He et al., 2007b, Bernhardt et al., 2009) they give insight into structural architectural features. Functional connectivity networks, on the other hand, can be calculated via temporal correlations or coherences between blood oxygen level-dependent functional MRI signals from distinct brain regions (Salvador et al., 2005, Achard and Bullmore, 2007) or similarly by measuring correlations between electrocorticographic recordings from different cortical regions using scalp or intracranial electrodes (Kramer et al., 2011, Stam and van Straaten, 2012). It has been suggested that the human network is organized to optimize efficiency, due to a small-world topology allowing simultaneous global and local parallel information processing (Kaiser and Hilgetag, 2006, Bassett et al., 2008, Bullmore and Sporns, 2009).

DOI:10.14753/SE.2015.1798

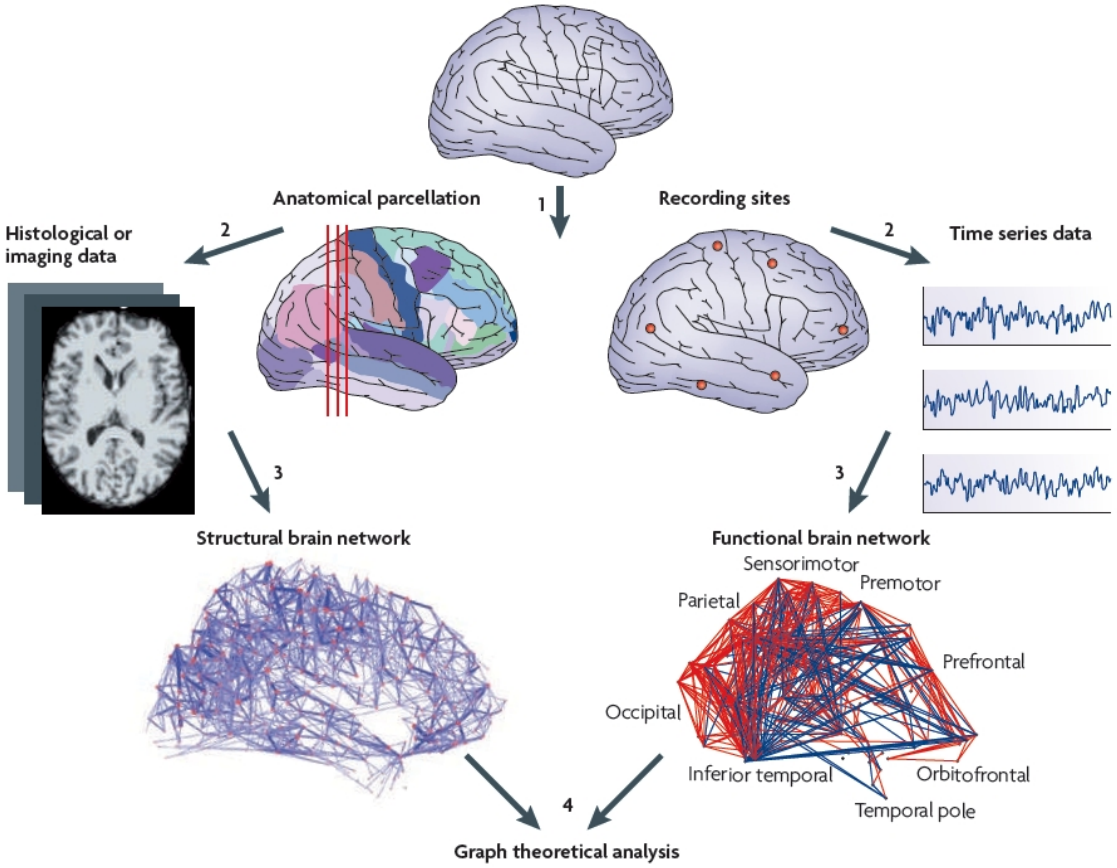

Fig. 9. Structural and functional brain networks can be explored using graph theory through the following four steps (see the figure):

• Define the network nodes. These could be defined as electroencephalography or multielectrode-array electrodes, or as anatomically defined regions of histological, MRI or diffusion tensor imaging data.

• Estimate a continuous measure of association between nodes. This could be the spectral coherence or Granger causality measures between two magneto encephalography sensors, or the connection probability between two regions of an individual diffusion tensor imaging data set, or the inter-regional correlations in cortical thickness or volume MRI measurements estimated in groups of subjects.

• Generate an association matrix by compiling all pair wise associations between nodes and (usually) apply a threshold to each element of this matrix to produce a binary adjacency matrix or undirected graph.

• Calculate the network parameters of interest in this graphical model of a brain network and compare them to the equivalent parameters of a population of random networks. (Bullmore and Sporns, 2009).

Indeed, a small-world architecture has been shown for functional connectivity networks (Salvador et al., 2005, Achard et al., 2006) and structural connectivity networks (Hagmann et al., 2008, Iturria-Medina et al., 2008). The analysis of functional and structural connectivity networks using electrophysiological and imaging data provides new avenues for assessing complex network properties of the healthy and diseased brain (Zhang et al., 2011). However, these measures do not assess relationships of causal influence that one brain area may have over another. Quantifications of this influential relationship, termed *effective connectivity,* are more difficult to study. Prior attempts have relied upon Granger causality (Brovelli et al., 2004) and dynamic causal modeling (McIntosh and Gonzalez-Lima, 1994, Friston et al., 2003). However, these observational methods rely upon statistical covariance (Smith et al., 2011) as opposed to interventional empiric testing. Combining transcranial magnetic stimulation (TMS) with electroencephalography (EEG), magnetoencephalography (MEG) or functional MRI (fMRI) provides a more empiric effective connectivity assessment (Massimini et al., 2005), but this method also has limitations related to the difficulty of inferring intracranial neural measurements from extracranial stimulation by utilizing assumptions of EEG/MEG source modeling or indirect measures of neural activity with fMRI. Epilepsy patients undergoing surgical evaluation provide an opportunity to directly record human brain electrophysiology with high spatiotemporal resolution. In these subjects, effective connectivity may be assessed empirically by applying single pulses of electrical current at one cortical region and recording the cortico-cortical evoked potential (CCEP) at other remote locations (Valentin et al., 2002, Matsumoto et al., 2004, Catenoix et al., 2005, Valentin et al., 2005b, Lacruz et al., 2007, Matsumoto et al., 2007, Catenoix et al., 2011, Matsumoto et al., 2012, David et al., 2013, Enatsu et al., 2013, Keller et al., 2013, Entz et al., 2014). CCEP mapping typically does not elicit the behavioral effects that are observed with clinical electrical stimulation mapping (ESM; 20-50Hz stimulation, 1-15ma amplitude, .2-.5ms pulse width, 1-3s duration) protocols in order to map eloquent cortical areas (Gordon et al., 1990, Hamberger, 2007). Instead, field potentials evoked by SPES can be averaged to compute a CCEP profile over the remainder of implanted electrodes. CCEPs consist of an initial early (10-50ms) biphasic N1, and a delayed (50-500ms), slow N2 wave (Creutzfeldt et al., 1966, Lacruz

et al., 2007). The N1 is thought to reflect direct activation of the local cortex (Purpura et al., 1957, Goldring et al., 1994, Matsumoto et al., 2004), while the N2 may represent a later inhibition (Creutzfeldt et al., 1966, Entz et al., 2009), similar to spontaneously recorded and induced human slow oscillations generated by cortical and subcortical (thalamic) interactions (Steriade, 2003, Matsumoto et al., 2004, Cash et al., 2009, Rosenberg et al., 2009, Csercsa et al., 2010, Logothetis et al., 2010, Catenoix et al., 2011, Hangya et al., 2011)

DOI:10.14753/SE.2015.1798

2 Aims

2.1 Evaluate the appropriate settings for single pulse electrical stimulation (SPES)

One of our principal aim is to define the appropriate stimulation paradigms for single pulse electrical stimulation. We plan to systematically analyze the effects of various stimulation parameters, such as amplitude, cortical location, vigilance states and the duration of the implantation on the evoked potentials. After defining the optimal parameters, these are planned to be used in all further stimulation sessions.

2.2 Description of the effects of SPES on the neocortex recorded with electrocorticography and with a laminar multielectrode recording system in the deeper layers

We would like to use standard electrophysiological analyzes methods to describe the spatio-temporal properties of the evoked potentials beside looking only at the cortical surface recordings, our special aim is to define the contribution of each lamina to the evoked potential results seen on the ECoG. For the laminar analysis we plan to use a custom built microelectrode system, which penetrates the cortex and enables to record the local field potential gradient across all six layers.

2.3 Comparison between spontaneous and cortical stimulation evoked slow oscillation

We have previously shown the laminar profile of the human spontaneous slow oscillation (Csercsa et al., 2010), but our special aim is to compare the spontaneous slow oscillation with the evoked SO using the same multielectrode system which was used earlier. Single pulse electrical stimulation evoked neuronal silence followed by neuronal hyperactivity in the cortex recorded as a cortical surface negative wave followed by a positive peak may be generated by the same cortical mechanisms as the spontaneous SO.

2.4 Description of propagation patterns of human slow wave sleep using a non-linear mutual information based correlation technique

Recent reports of regional and temporal heterogenicity of cortical slow waves (Mohajerani et al., 2010), as well as alternative propagation patterns such as spiral waves (Huang et al., 2010), raise the possibility that, in addition to the large-scale orderly traveling of slow waves, complex propagation patterns emerge in a temporally parallel manner at a finer spatial scale. We aim to describe these complex propagation patterns by applying information based correlation techniques on human SWA recordings.

2.5 Standardization of electrode reconstruction and visualization for patients with intracranial electrodes

The major advancements in the field of neuroimaging allows now to standardize the protocol for visualizing electrodes implanted in the skull and also to localize them to the underlying cortical surface for sophisticated imaging and electrophysiological data analysis. Our goal was to create such a protocol for every epilepsy surgical candidate implanted at NSLIJ and NIN, which strictly defines the imaging modalities and timing both for structural and functional imaging data. After image acquisition we plan to standardize the procedures to create brain surface reconstructions and also to develop our own electrode localization method.

2.6 Resting state fMRI predicts the spatial distribution of CCEPs

Electrical stimulation of the cerebral cortex with intracranial electrodes of patients with intractable seizures provides us means for directly relating electrical activity that occurs over faster time scales throughout the brain to the intrinsic functional architecture previously mapped in the same individual using resting state - fMRI data.

Here, we use this approach to test the hypothesis that the spatial distribution and magnitude of evoked neuronal activity is predicted by the pattern and strength of temporal correlations among the spontaneous BOLD fluctuations exhibited by spatially distinct regions, commonly referred to as resting state functional connectivity (RSFC). Specifically, we predicted that: 1) the spatial distribution of the electrical response to direct stimulation (i.e., CCEP) would follow that of the intrinsic functional architecture (i.e., RSFC) associated with the stimulated site, and 2) regions within the architecture

exhibiting the strongest connectivity with the stimulated site would show the highest magnitude electrically evoked responses.

2.7 Mapping of functional areas using CCEP

In order to account for inter-subject variability in electrode placement, in this report we map intracranial electrodes to a modified parcellation scheme based upon Brodmann areas (BAs) defined by Montreal Neurological Institute (MNI) space. This permitted us to combine results across 25 subjects at two different institutions to present a more comprehensive CCEP-based effective connectivity map of the human neocortex. Our results demonstrate both a consistency of certain connections as well as the fact that many connections are directed.

DOI:10.14753/SE.2015.1798

3 Materials and Methods

3.1 General methodologies and materials

3.1.1 Patient selection

Patients participating in these studies have medically intractable seizures and were referred for epilepsy surgical evaluation. The studies were performed in two different major epilepsy surgical centers either at the Department of Functional Neurosurgery of the National Institute of Clinical Neuroscience (NIN, Budapest, Hungary) or at the Comprehensive Epilepsy Center at North Shore - LIJ Health System (NSLIJ, Manhasset, NY, USA). All patients had pharmaco-resistant epilepsy and prior to surgical intervention were presented at the local epilepsy surgical conference for multidisciplinary discussion of the planned therapy. The multidisciplinary team consists of epileptologists, neurosurgeons, neuropsychologists, psychiatrist and neuroradiologists. Only those patients were included who was offered an invasive presurgical evaluation for better localization of epileptogenic areas solely based on clinical decision. Fully informed consent was obtained from each subject under the auspices of the Hungarian Medical Scientific Council and local ethical committee; National Institute of Clinical Neuroscience, or along institutional review board guidelines (protocol #07-125) of North Shore- LIJ Health System, according to the World Medical Association Declaration of Helsinki. The patients were informed that participation in this study would not alter their clinical treatment in any way, and that they could withdraw at any time without jeopardizing their clinical care.

	Hospital	**Gender**	**MRI abnormality**	**Age at surgery**	**Implanted side**
Pt1	**NIN**	1	normal	33	acute
Pt2	**NIN**	1	R central flair abnormality	34	acute
Pt3	**NIN**	1	L temporo-polar microgyria	26	L
Pt4	**NIN**	1	R superior frontal gyrus flair abnormality	16	R
Pt5	**NIN**	2	normal	34	R
Pt6	**NIN**	1	L sclerosis tuberosa	42	L

Pt7	**NIN**	1	normal	31	R
Pt8	**NIN**	1	normal	40	L
Pt9	**NIN**	1	L parietal and insular flair abnormality	29	L
Pt10	**NSLIJ**	2	L occipitotemporal dysplasia	22	L
Pt11	**NSLIJ**	1	R hemiatrophy	21	R
Pt12	**NSLIJ**	2	normal	36	Bilateral
Pt13	**NSLIJ**	2	normal	48	R
Pt14	**NSLIJ**	2	R Cortical Dysplasia	17	R
Pt15	**NSLIJ**	1	hypothalamic hamartoma,	21	R
Pt16	**NSLIJ**	1	normal	22	R
Pt17	**NSLIJ**	1	R Temporal lobe encephalomalacia	47	R
Pt18	**NIN**	2	R temporo-polar dysgenesis	35	L
Pt19	**NSLIJ**	2	L temporal encephalomalacia	55	Bilateral
Pt20	**NSLIJ**	2	L frontal tumor	39	L
Pt21	**NIN**	2	R cingular and frontal CD	20	R
Pt22	**NSLIJ**	1	L frontal encephalomalacia	18	Bilateral
Pt23	**NSLIJ**	1	L temporal arachnoid cyst	60	L
Pt24	**NSLIJ**	2	R Multiple gangliogliomas	25	R
Pt25	**NSLIJ**	1	normal	15	Bilateral
Pt26	**NSLIJ**	1	R occipitotemporal encephalomalacia	30	R
Pt27	**NSLIJ**	2	normal	30	R
Pt28	**NSLIJ**	2	normal	26	Bilateral
Pt29	**NSLIJ**	1	R occipitotemporal encephalomalacia	32	R
Pt30	**NSLIJ**	2	normal	23	L
Pt31	**NIN**	1	L occipito-temporal dysgenesis	17	L
Pt32	**NSLIJ**	2	L mesial temporal sclerosis	40	L
Pt33	**NSLIJ**	2	L mesial temporal sclerosis	36	L
Pt34	**NSLIJ**	1	R hemiatrophy	22	R

Table 1.: Summary of all patients included in the different studies. R=right, L=left. NSLIJ: North Shore – LIJ Health System, NIN: National Institute of Clinical Neuroscience.

Patient enrollment started in 2006 and went on till 2012 at NIN and from 2009-2012 at NSLIJ. We analyzed the data of 34 patients coming from both centers (12 patients from NIN and 22 patients from NSLIJ, Male: 19, Female: 15, Average age at surgery: 30,9±11,4 years). 11 patient's preoperative MRI was considered normal, without any known pathology.

3.1.2 Electrode implantation, ECoG recording and imaging

Following non-invasive evaluation patients underwent subdural strip, grid and depth electrode implantation (NSLIJ: Integra Lifesciences Corp., Plainsboro, New Jersey, USA, NIN: AD TECH Medical Instrument Corp., Racine, WI, USA). Subdural electrodes were implanted with the aid of neuronavigation and fluoroscopy to maximize accuracy (Eross et al., 2009). Grids were implanted through standard craniotomy over the target area defined by the Epilepsy Surgical Team (EST) prior to surgery using non-invasive data. If the EST decided to use only strip electrodes a burr whole technique was used.

Video-EEG - monitoring was carried out using Xltek EMU 128 LTM System (San Carlos, CA, USA) at NSLIJ and a Brain Quick System 98 (Micromed, Mogliano Veneto, Italy) at NIN. All signals were recorded to a skull electrode at NSLIJ Acquisition rate: 2 kHz, no filtering) and to a mastoid reference at NIN (Acquisition rate: 1 kHz, no filtering). Most of the times the intracranial electrodes were supplemented with scalp electrodes in the frontal region, ECG and zygomatic electrodes for recording electrooculograms. ECoG recordings were made over the course of clinical monitoring for spontaneous seizures. The decision to implant the electrode targets, and the duration of implantation was made entirely on clinical grounds without reference to this investigation. The long-term video-EEG monitoring of the patients took place at a highly specialized unit, with 24 hour service of EEG assistants and nursing care.

As a routine between 2006 and 2009 every patient at NIN had a preoperative 1,5Tesla, T1 weighted MRI with 1mm 3D axial slices for reconstruction of the brain surface

beside or within the clinical epilepsy protocol. After 2009 every patient at both centers had a preimplantation 3Tesla, T1w. MRI with 1mm 3D axial slices. After 2010 every patient had a postimplantation 1mm slice 3D axial CT scan and a postimplantation 3D 1mm T1w axial 1.5T MRI with the electrodes in the skull to aid electrode reconstruction and localization. Every patient after the resection between 3 to 6 Months had a postresection 3T MRI scan with 1mm 3D T1w axial slices. Beside these scans most of the patients had extensive functional MRI done as required for localization of eloquent areas including a 5 minute resting state fMRI scan and also at least once diffusion tensor imaging.

3.1.3 Brain surface reconstruction and electrode localization

In order to map evoked responses to anatomical locations on the cortex, subdural electrodes were identified on the pre-operative MRI by first registering the locations of the electrodes on the post-implantation CT to the equivalent location in the post-implantation structural MRI. Pre- and post-implantation MRIs were both skull-stripped using the BET algorithm from the FSL software library (www.fmrib.ox.ac.uk/fsl/) followed by coregistration to account for possible brain shift caused by electrode implantation and surgery (Mehta and Klein, 2010). Electrodes were identified in the postimplantation CT using BioImageSuite (Duncan et al., 2004) and subsequently snapped to the closest point on the reconstructed pial surface of the pre-implantation MRI in MATLAB using custom scripts (Dykstra et al., 2010). The reconstructed pial surface was computed using Freesurfer (Dale et al., 1999). Intraoperative photographs were used to corroborate this registration method based on the identification of major anatomical features. See in detail in the results section.

3.1.4 Functional electrical stimulation mapping of the neocortex

For localization of functional cortical areas electrical stimulation mapping (ESM) was carried out according to standard clinical protocol (bipolar stimulation, train lengths: 2-5sec, Amplitude: 3-15mA, Frequency: 20-50Hz, Pulse width: 0,5msec). ESM was always performed in the presence of an epileptologist and neuropsychologist.

Areas were defined as expressive language sites when stimulation resulted in speech arrest. When stimulation resulted in a naming deficit based on auditory or visual cues or an interruption in reading or comprehension an area was deemed as a non-expressive

DOI:10.14753/SE.2015.1798

language site. Sensory and motor areas were identified when stimulation caused movement or changes in sensation. ESM was conducted on all implanted electrodes and functional areas were mapped with the lowest current to find the most specific function under the stimulated contact pairs. A typical result of an ESM is seen in Fig.10.

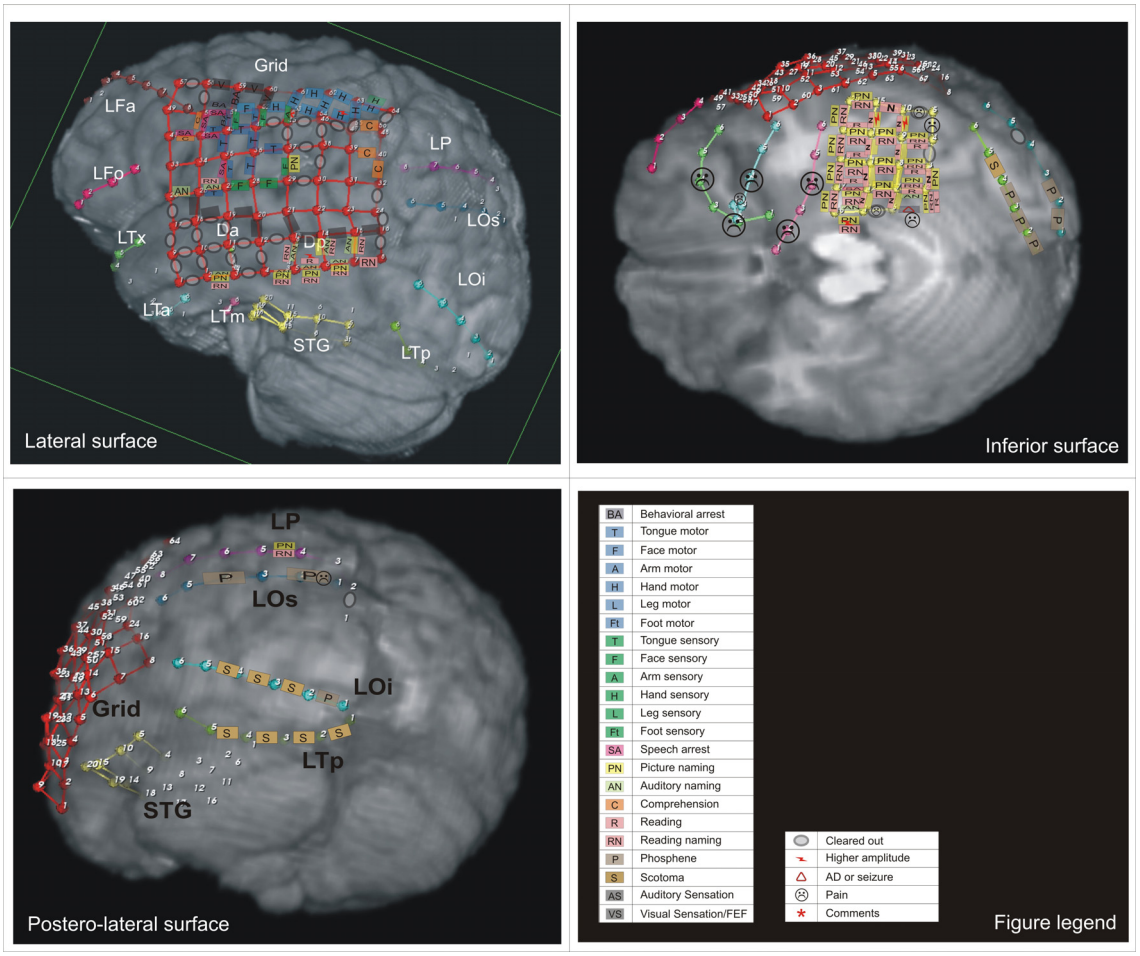

Fig. 10. Functional electrical stimulation map of a patient with left sided seizure onset as defined with non-invasive investigations. Note the extremely dense language network in the temporo-basal area.

3.1.5 Single pulse electrical stimulation of the neocortex

Following implantation of intracranial electrodes, patients were monitored for epileptic activity. During this time, CCEP mapping was performed using single pulse stimulation. Systematic bipolar stimulation of each pair of adjacent electrodes was administered with single pulses of electrical current (Amplitude: 10mA, Frequency: 0.5Hz, pulse width: 0.2 msec, 20-100 trials per electrode pair) using a Grass S12 cortical stimulator at NSLIJ (Grass Technologies Inc., West Warwick, RI, USA) and an

IRES Surgical 600 cortical stimulator at NIN (Micromed S.p.A. Via Giotto, 2-31021, Mogliano Veneto - Italy). The associated evoked responses (CCEPs) were measured at all other electrode sites. The current amplitude of 10mA activated the maximal number of neuronal elements without inducing epileptic after discharges or other behavioral changes. An inter-stimulation interval of 2s was utilized to minimize the effect of overlapping evoked responses and to leave enough restitution time for the cortex. The stimulation was performed extra-operatively on average 5 days after electrode implantation surgery after seizures had been recorded and anti-epileptic medications had been resumed. Stimulation was performed at the bedside while the patient was either in a restfully awake state or in the deep stages of non-REM sleep in the early hours of sleep. In 3 cases we performed SPES intraoperatively when the patient was under general anesthesia (i.v. Propofol with Fentanyl).

3.1.6 Analysis of CCEP

Electrophysiological data analyses were performed using Neuroscan Edit 4.3 software (Compumedics, El Paso, TX) and custom MATLAB scripts (MathWorks, Natick, MA). Evoked responses to stimulation were divided into 2s epochs (500ms pre-stimulation to 1500ms post-stimulation) time-locked to stimulation pulse delivery. The early CCEP consists of two major deflections (usually negative in polarity) termed N1 and N2, peaking at approximately 20-30ms and 150-500ms respectively. To quantify the magnitude of the CCEPs in the time window of the N2, we measured the peak voltage of the absolute value of the response between 50-500ms and computed a z-score using the standard deviation of the baseline. Prior to averaging low pass filtering (30 Hz) and baseline correction (-500 to -50 ms) was performed. The standard deviation was computed for each electrode separately using all time points in the baseline window of the averaged signal. CCEPs were considered significant if the N2 peak of the evoked potential exceeded the baseline amplitude by a threshold of ±6SD as determined from the ROC curves (see below). Evoked responses exceeding ± 500uV were excluded as these most likely indicate electrical artifacts. Responses were color-coded according to significance and plotted on the co-registered cortical pial surface (Fig. 11.).

DOI:10.14753/SE.2015.1798

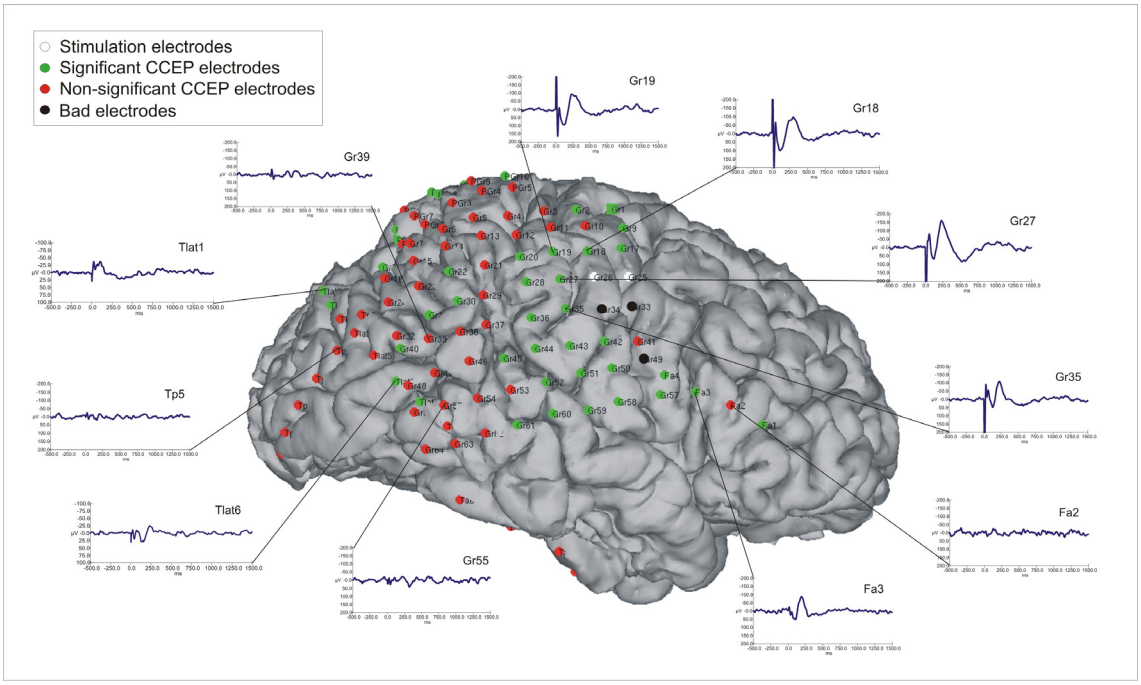

Fig. 11. 3D surface reconstructed (freesurfer) preimplantation MRI with electrodes overlaid and snapped to the surface. Electrodes are shown with different colors according to the legend. Little inlays show the averaged CCEPs according to its position on the cortex. Significance was defined according to the protocol. Most of the significant responses are in the close vicinity of the stimulation electrodes, but some are also more distant (e.g.: Tlat1, Tlat6, Fa3). Also note the disappearance of the N1 peak on the electrodes further away from the stimulation site (e.g.: Tlat1, Tlat6, Fa3). Negative potentials are shown upward.

3.1.7 Determination of amplitude threshold of CCEP.

Direct stimulation on the cortex evokes large responses; therefore, it is not ideal to employ conventional statistical thresholds to quantify significance. We relied on a well-established intracortical pathway to calculate a receiver operating characteristic (ROC) curve to determine the optimal threshold for significance of the evoked response. It is well known that neuro-anatomical (Damasio and Damasio, 1980, Petrides and Pandya, 2009) and functional connections (Kelly et al., 2010, Koyama et al., 2010) exist between Broca's and Wernicke's area, and stimulation of Broca's area evokes CCEPs in Wernicke's region (Matsumoto et al., 2004). To both validate our technique and calculate the threshold response, we stimulated Broca's area and examined the evoked

responses in Wernicke's region in the subjects with electrode coverage in language areas. Sensitivity and specificity were calculated based on the evoked response with reference to clinical findings from electrical stimulation mapping. True positives were those electrodes with CCEPs above the threshold and eliciting a response on functional mapping (e.g. speech arrest). False positives were those where CCEPs were above threshold and ECM had no effect. An optimal threshold, showing the best trade-off between sensitivity and specificity was found at six standard deviations (SD) from baseline and was chosen for significance and was used for the duration of the study (Fig. 12.) The correlation analysis was repeated with other thresholds which did not alter results significantly.

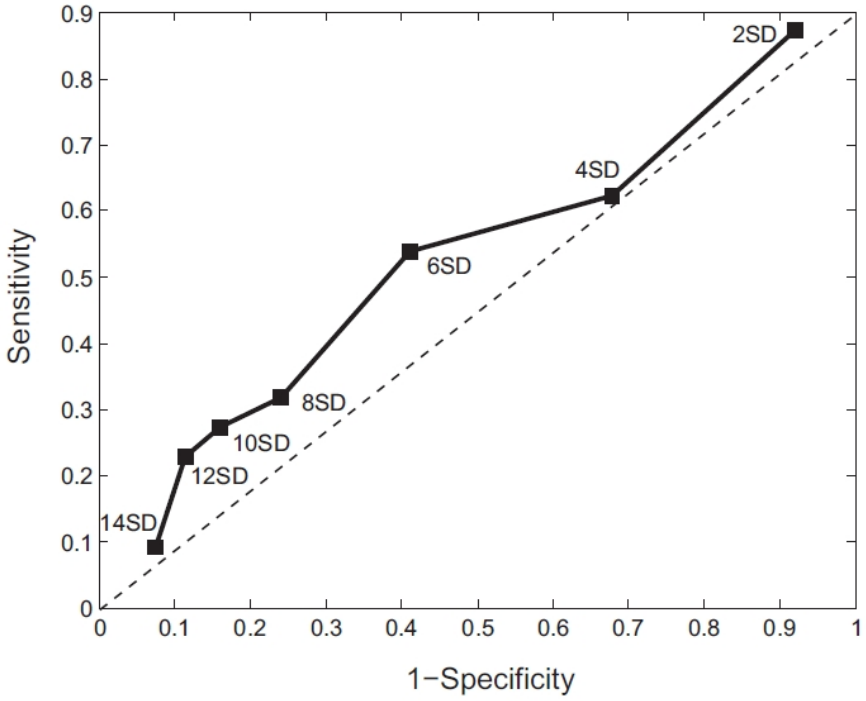

Fig. 12. Determining the CCEP threshold. Receiving operating curves were produced from responses in Wernicke's area after stimulation of Broca's area in two subjects who had electrode coverage over these language regions. The greatest discriminability is towards the top-left hand corner of the graph. Thus, the point furthest away from the dotted line (R = 1) represents the largest discriminability (d' in signal detection theory). The best tradeoff between sensitivity and specificity was found at 6 SDs from baseline, so this threshold was used to determine significant CCEPs.

DOI:10.14753/SE.2015.1798

Special methodologies according to individual studies

3.2 Analysis of spontaneous and evoked slow oscillation

3.2.1 Patients and electrodes

Five patients (Pt. 1-5.) were included in the first part of the study (stage 1) dealing with the analysis of spontaneous slow oscillations of the brain, which has been published earlier (Csercsa et al., 2010) and five patients (Pt. 4-7. and pt. 35.) were included in the second part of the study (stage 2) describing the effects of SPES evoked potentials with laminar multielectrode.

In addition to the surface electrodes, a 350 μm diameter, 24 contact experimental laminar multichannel microelectrode array (ME) was implanted perpendicular to the cortical surface, underneath the clinical grids (Fig. 13.) (Ulbert et al., 2001a, Ulbert et al., 2001b, Ulbert et al., 2004a, Cash et al., 2009, Keller et al., 2009). The 40 μm diameter Pt/Ir contacts were spaced evenly at 150 μm providing LFP recordings from a vertical, 3.5mm long cortical track, spanning from layer I to layer VI. A silicone sheet attached to the top of the ME shank prevented the first contact from sliding more than 100 μm below the pial surface (Ulbert et al., 2001a). In each case, the explanted ME was visually inspected under a microscope for structural damage, and we did not find any alteration, indicating intact structure throughout the recordings. The location and duration of the clinical electrode implantation were determined entirely by clinical considerations, the ME was placed in cortex that was likely to be removed at the definitive surgery.

DOI:10.14753/SE.2015.1798

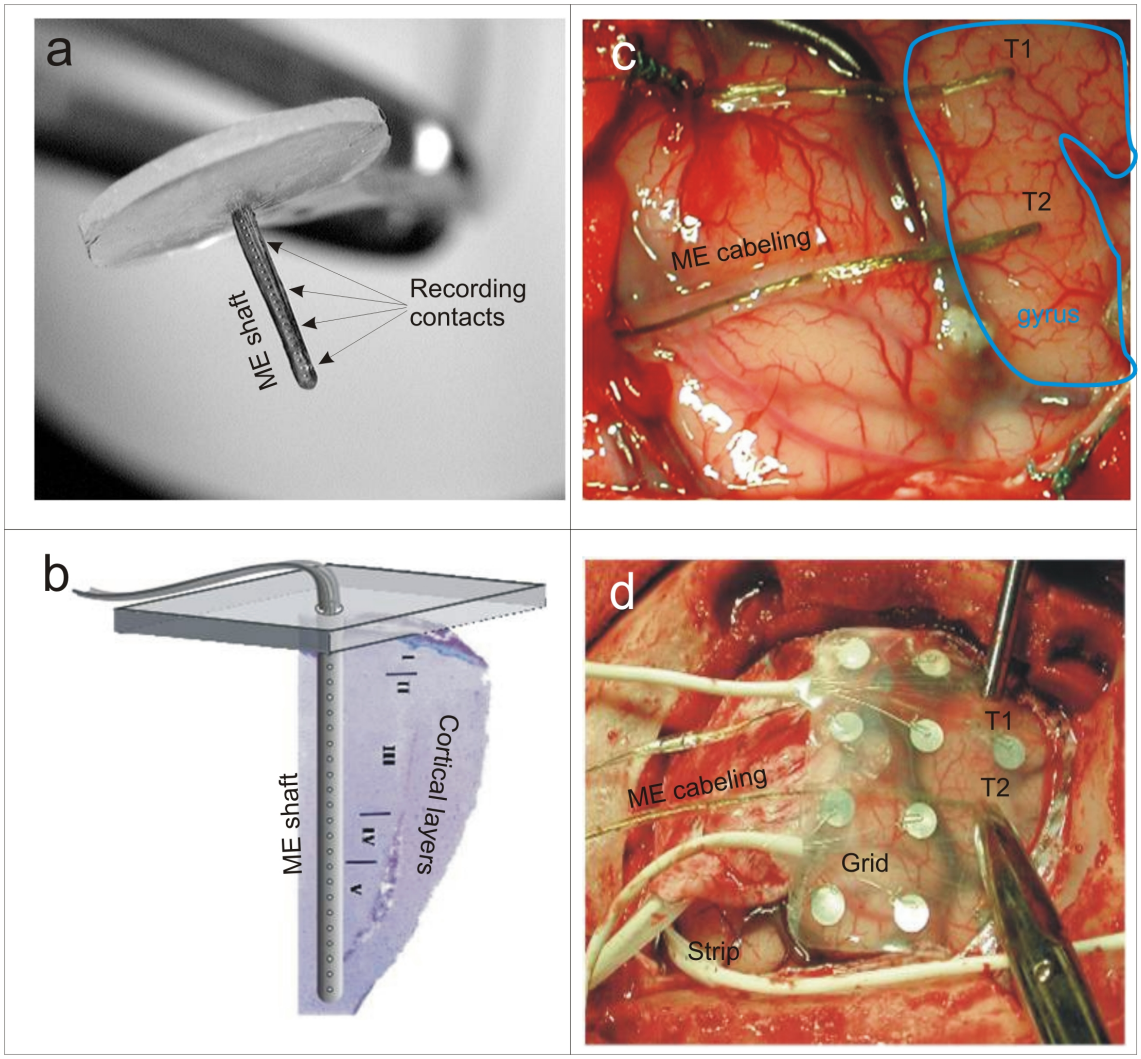

Fig. 13. Intracortical "thumbtack" multielectrode for LFP recordings of all 6 layers of the cortex; a) microphotograph of the electrode shaft and silicone top for stabilization in the cortex; b) schematic figure showing the histological reconstruction of the electrode penetration track and the position of each microelectrode contact to the individual cortical layers; c) Intraoperative photograph of two thumbtack electrodes in the cortex of an epileptic patient, note the perpendicular implantation in the middle of a gyrus; d) Intraoperative photograph of the same patient as 'c', final position of the thumbtack electrodes covered with a subdural grid for clinical purposes.

DOI:10.14753/SE.2015.1798

3.2.2 Histology

The positions of the electrodes were confirmed by intraoperative navigation, co-localization of intraoperative photographs, pre- and postoperative MR scans and 3D MR reconstructions of the 7 patients included in the study (Fig. 14.).

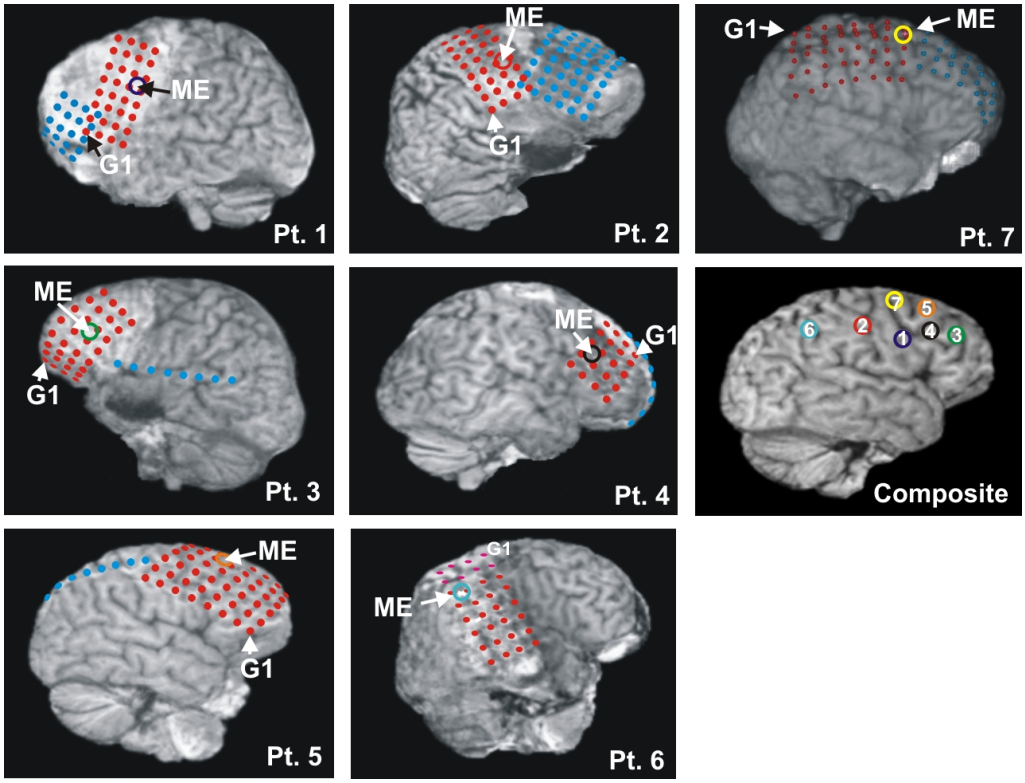

Fig. 14. Grid, strip and multielectrode array (ME) locations in the seven patients included in the study. Locations are superimposed on 3D reconstructions of MRIs taken with the electrodes in place, aided by intraoperative navigation and photographs. Grid and strip electrode contacts are depicted in red and blue colors; the first grid contact is marked with G1. ME locations of the patients are marked with circles. Patient 1 (blue): left Brodmann's area (BA) 9, Patient 2 (red): right BA 2, Patient 3 (green): left BA 46, Patient 4 (black): right BA 9, Patient 5 (orange): right BA 8, Patient 6 (turquoise): right BA 7, Patient 7 (yellow): BA 8

Photographs were also taken during the resective surgery to confirm that the surface electrodes did not shift during monitoring. The brain tissue containing the electrode track in Patients 4 and 5 was removed en-bloc for further anatomical analysis (Ulbert et al., 2004b, Fabo et al., 2008, Csercsa et al., 2010). See details in References.

3.2.3 Recordings

After electrode placement, the patients were transferred to the intensive monitoring unit for 5-7 days, where continuous 24 hour video-EEG observation took place in order to localize the seizure focus. ECoG from clinical strip and grid electrodes (32-92 channels, mastoid reference) was recorded concurrently with patient video using the standard hospital system (band-pass: 0.1-200 Hz, acquisition rate: 400-5000 Hz / 16 bit). Video-EEG data for the duration of monitoring were stored on hard disks for later analysis. Spatial LFP gradient (LFPg), the voltage difference between consecutive laminar electrode contacts was provided by a special preamplifier placed inside the head bandage of the patient (Ulbert et al., 2001a). For simplicity, throughout the text the spatial potential gradient is expressed in μV unit rather than the formally correct μV per inter-contact distance (150 μm). This reference independent measurement method was proven to be effective in minimizing the motion related and electro-magnetic artifacts (Ulbert et al., 2001a). The LFPg was split to EEG range (0.1-300 Hz) and single (SUA), multiple unit activity (MUA) frequency range (300-5000 Hz) by analogue band-pass filtering at the level of a custom made main amplifier (Ulbert et al., 2001a). EEG range signal was sampled at 2 kHz / 16 bit; MUA range was sampled at 20 kHz / 12 bit and stored on a hard drive.

3.2.4 Slow wave activity detection (stage 1.)

Patients 1-5. (Table) were included in this stage of the study.

We have analyzed the LFPg, MUA and ECoG data acquired from each patient during one to three nocturnal recording sessions. Since the sleep of the patients was fragmented due to medical care, distress from the hospitalization and head wound, we cannot provide standard hypnograms that are usually obtained from healthy subjects without a recent craniotomy. Craniotomies may also distort the scalp distribution of the EEG due to lack of bone and excessive fluid accumulation below the scalp, furthermore scalp electrodes if placed close to the frontal craniotomy wounds may induce infection, this why we avoided placing more than two frontal scalp EEG electrodes. Partial sleep staging was performed based on readings of the available scalp EEG and ECoG electrodes by expert neurologists. In this study, we have analyzed electrophysiological data obtained only from the deepest stage of NREM sleep (N3, or SWS) (Iber et al.,

2007). Behavioral sleep was confirmed by the video recording, while SWS was electrographically identified in accordance with the recent AASM guidelines (Iber et al., 2007). SWS periods were identified when 20% or more of an epoch consisted of SWA (waves in the 0.5–2 Hz frequency range with peak-to-peak amplitude larger than 75 μV, measured over the frontal regions) (Iber et al., 2007). Data containing interictal spikes (within 1 min) and seizures (within 60 min) were excluded from the study to avoid epileptic contamination.

In addition to spectral, and autocorrelation analyses, SWA cycle detection was based on phase and amplitude information, extracted from the narrow-band filtered (0.3-3 Hz, 24 dB/octave, zero phase shift) layer II LFPg and ECoG data. Instantaneous phase of the filtered signal was calculated by the Hilbert transformation. In our implementation, a single SWA cycle was defined between -180 ° and +180 ° phase. The -180 ° phase value corresponded to the trough of the negative half-wave (down-state) preceding the 0 ° phase, which corresponded to the peak of the positive half-wave (up-state) and finally the +180 ° phase corresponded to the following negative half-wave trough (down-state). At each +180 ° crossing the phase was wrapped -360 ° for better visualization. To avoid the detection of higher frequency (e.g.: theta) oscillations, waves with shorter than 500 ms cycle lengths (corresponding to higher than 2 Hz frequency) were excluded from the analysis. Waves with non-monotonic phase runs were also excluded, since phase inversions may also indicate higher frequency contamination. In addition to phase constraints, valid SWA cycles had to fulfill the following amplitude criteria: the up-state peak amplitude had to be more positive than +50 μV and the preceding or following down-state trough amplitude had to be more negative than -50 μV. The SWA detection algorithm parameters were tuned and carefully validated by expert electroencephalographers. Similar algorithmic parameters were used for all of the patients. To facilitate comparison of our results with previous animal studies, the threshold level was set to +50 μV on the filtered (0.3-3 Hz, 24 dB/octave, zero phase shift) upper layer III LFPg, and the wave triggered (up-state locked) averages were calculated on the un-filtered LFPg and MUA. For further details see reference (Csercsa et al., 2010).

3.2.5 Current source density analysis

CSD analysis identifies synaptic/trans-membrane generators of LFP in laminated neural structures (Freeman and Nicholson, 1975, Nicholson and Freeman, 1975). The negative of the second spatial derivative of the LFP closely approximates the macroscopic current density over unity cell membrane area. Since LFPg is the first spatial derivative of LFP, one additional spatial derivation yielded the CSD for the EEG range (0.1-300 Hz) data. Inhomogeneous conductivity and electrode spacing were not taken into account (both were substituted by the dimensionless number 1 in the calculations); high spatial frequency noise and boundary effects were reduced by Hamming-window smoothing and interpolation (Ulbert et al., 2001a) thus CSD was expressed in μV units. It was shown previously (Ulbert et al., 2001a, Ulbert et al., 2001b, Ulbert et al., 2004a, Ulbert et al., 2004b, Wang et al., 2005, Halgren et al., 2006, Knake et al., 2007, Fabo et al., 2008, Cash et al., 2009, Steinvorth et al., 2009, Wittner et al., 2009), that our recording and analysis techniques can reliably detect CSD activity in each layer of the human cortex and hippocampus.

3.2.6 Multiple unit activity analysis

A continuous estimate of population neuronal firing rate was calculated from the MUA range (300-5000 Hz) data. The signal was further filtered (500-5000 Hz, zero phase shift, 48 dB/octave), rectified and decimated at 2 kHz, applying a 0.5 ms sliding average rectangular window, followed by a final, smoothing low-pass filter (20 Hz, 12 dB/octave).

We have shown previously (Ulbert et al., 2001a, Ulbert et al., 2001b, Ulbert et al., 2004a, Ulbert et al., 2004b, Wang et al., 2005, Halgren et al., 2006, Fabo et al., 2008, Cash et al., 2009, Wittner et al., 2009) that our SUA, MUA recording and analysis techniques can reliably detect task or epilepsy related modulation of neuronal firing from each layer of the human cortex and hippocampus.

3.2.7 Evoked slow oscillation analysis (stage 2.)

Patients 4-7. (Table) were included in this stage of the study.

Brief single current pulses were injected into adjacent grid contacts (10mA, 0.2ms, 0.5Hz) using a Micromed IRES Surgical 600 cortical stimulator. The bipolar stimulations were repeated 20-150 times between the same contacts. All responses were

averaged both from the clinical and the laminar electrodes. Since the stimulation artifact was apparent both on the surface recordings and on the ME recordings, we used the artifact as the link between the two recordings. For more details on single pulse electrical stimulation see general methods section.

Spectral, Current Source Density and Multi Unit analysis

The same set up and analysis methods were used as described in detail in the spontaneous SO section, here we give a brief overview and highlight the minor differences.

To measure the oscillatory power changes after stimulation we used wavelet based joint time-frequency domain analysis (TFR). First all bad channels and the stimulation channels were removed from the recording. After generating single sweeps from the raw data, time locked to the stimulus artifact, baseline correction and re-referencing was done to the mean average reference an all sweeps. The analysis was performed in the 1-200Hz band, time locked to the stimulus presentation, baseline period: -500ms to -50ms, test period: 0ms to 1500ms post stimulation. Averages were made both from the ME and the surface electrodes.

CSD was our technique for localizing synaptic activity, see details above. Simultaneous multi unit activity (MUA) lends convergent information to the definition of these processes and provides insight into local cellular responses to the field potential being analyzed. One-dimensional CSD data are presented on depth-versus-time maps, with color – coded sink (red) and source (blue) amplitudes. The second spatial derivative of the field potentials approximates the depth distribution of the current sources in laminated structures, such as the neocortex. Inhomogeneous conductivity was not taken into account. Hamming-window spatial smoothing and additional 0.1Hz to 100 Hz bandpass filtering (zero phase shift, 12dB/oct) was applied on the continuous CSD data derived from the low-frequency band recordings.

3.3 Methods of non-linear mutual information based correlation technique

3.3.1 Patient selection

Patients (Pts.) participating in this study [n= 6, five men (Pt. 3, 4, 6, 8, 9) and one woman (Pt. 5)] had medically intractable complex partial seizures and were referred to

our epilepsy surgical center (NIN) for presurgical evaluation (Table). All patients underwent intracranial electrode implantation as required for localization of epileptogenic tissue before therapeutic resection. For electrode implantation and recording see details in the general methods section. For slow wave sleep detection see details in 3.2.4.

3.3.2 Data analysis

Data preprocessing.

Subgrids of 4x4 (Pts. 3, 5, and 8) or 4x5 (Pts. 4, 6, and 9) electrodes were selected for analysis (Fig. 15.A). The reduction of the number of grid electrodes was necessary to analyze similar number of channels for comparability reasons and to reduce computational time. Selection of subgrids was based on grid location [an attempt was made to include frontal electrodes where SWA is typically more pronounced (Kurth et al., 2010)] and recording quality (channels not functioning were excluded). For each patient, three to five 1-min-long segments (26 segments in total) of normal SWS were selected. Principles of segment selection were to avoid epileptic contamination (see below) and to include deep-sleep epochs with prominent SWA. In Pt. 9, all segments were recorded in a single night, whereas in the other patients, segments from different nights were also included. Selected segments were preceded and followed by 30 min of seizure-free activity (except Pt. 6, where it was preceded by 30 min and followed by 10 min) and were free from interictal spikes. ECoG traces were resampled at 1000 Hz and bandpass filtered (0.1–40 Hz) with a finite impulse response filter using zero phase shift filtering (fir1.m and filtfilt.m built-in Matlab functions) to remove high frequency ECoG components and electrical noise.

Calculation of propagation maps.

We assessed associations between ECoG traces from different channels using mutual information (MI). MI provides the amount of information shared by two variables and is considered a nonlinear measure of covariation (Na et al., 2002, Kajikawa and Hackett, 2005, Hangya et al., 2009). The choice of MI instead of linear correlations was motivated by its ability to detect any kind of dependency without assumptions about the structure of correlations or the underlying distributions (Na et al., 2002, Kajikawa and Hackett, 2005, Paz et al., 2010), which is important because nonlinear correlations are

generally common among neural signals (Freiwald et al., 1999, Hangya et al., 2009). We further justified this choice by comparing MI with linear cross-correlation analysis (see Results, below). For each 1000 ms segment, ECoG values were binned into fixed bins between the overall minimal and maximal value. MI was calculated between different ECoG channels using the classic formulation in combination with Panzeri–Treves bias correction (Shannon, 1948, Panzeri et al., 2007), as described previously (Hangya et al., 2009). The basic idea of timeshifted correlations or cross-correlations was applied (Ostojic et al., 2009), using MI instead of linear correlation, as follows. On each channel, 1-s-long ECoG segments (X_t to X_{t+1000}) were correlated to later segments from all other electrodes separately ($Y_{t+\tau}$ to $Y_{t+\tau+1000}$, $0 < \tau < 1000$ ms) by calculating MI (temporal resolution, 1 ms) (Fig. 15.B). Maximal MI in the function of the time lags (τ) was calculated for all time points (t) and channel pairs. The choice of 1-s-long time windows was motivated by the observation that SWA frequency is around or below 1 Hz (Crunelli and Hughes, 2010, Csercsa et al., 2010, Diekelmann and Born, 2010), thus these time windows were able to approximately include a slow-wave cycle. However, it has been shown that MI calculations are robust in the selection of the time windows (Paz et al., 2010). The above calculations were repeated for overlapping 1-s-long ECoG segments (900 ms overlap). Next, correlations were destructed by cutting the ECoG data to 1–1.2-s-long segments, which were then shuffled using the randperm.m built-in Matlab function, which randomly permutes integers based on a uniform distribution. Permutation was repeated if a data segment remained in its original position. Significance of maximal MI was tested by comparing it to a distribution of MI values calculated from such shuffled versions of the original data (number of shuffles ranged from 151,296 to 236,400). A significance level of $p = 0.0001$ was used to reduce the number of false-positive detections according to high numbers of statistical tests (this choice corresponds to approximately one false detection in 2.5 s). In case a significant maximal MI was found, waveform correlation was established between the two channels at time point *t*. It should be noted that according to the binning between the minimal and maximal data values, MI reflected predictability between slow-wave cycles rather than higher frequency (lower amplitude) oscillations such as spindles (see Results, below). Thus, significant maximal MI showed the propagation of SWA between two cortical areas, the temporal maximum location provided propagation time,

and the maximal MI value indicated correlation strength. Propagation speed was calculated by dividing electrode distances by propagation time values. Time-resolved propagation maps were created using the above parameters, visualized as movies and further analyzed (see below). Unitary propagation events (Fig. 15. C, bottom left, arrows) were assessed by significant propagation between two ECoG channels. Start and end points of such events were defined by the zero (t) and maximal location ($t + \tau$) points in the time lag–MI plot (Fig. 15. B, right). According to the overlapping windows (see above), the time resolution of propagation map frames was 100 ms, whereas the temporal resolution of time delays was 1 ms (see above). Consistency of time delays for direct and indirect associations as checked to test the robustness of the method.

DOI:10.14753/SE.2015.1798

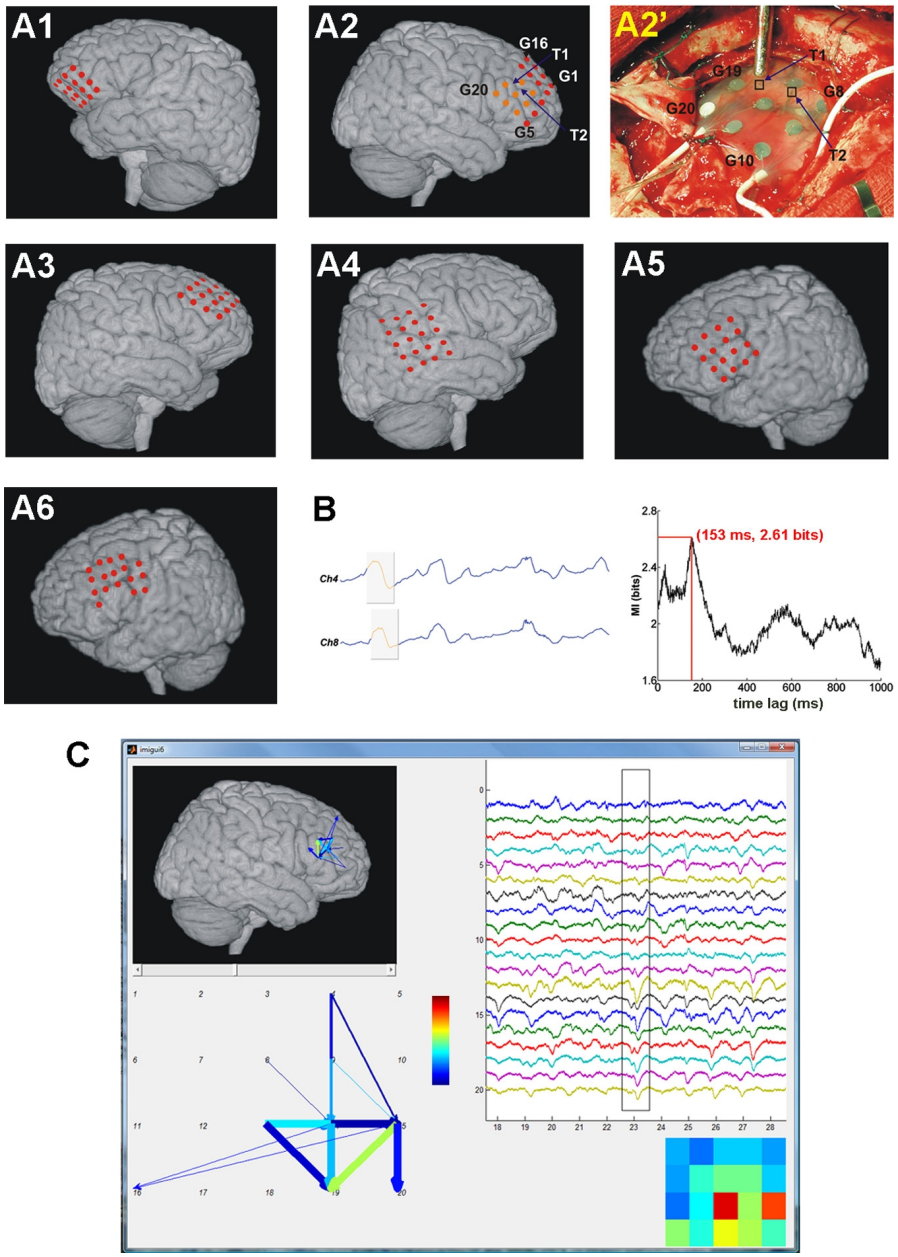

Fig. 15. Recording and analysis of SWA propagation. *A*, Estimations of the positions of recording sites on standard human brain images based on intraoperative photographs and postoperative structural MR images (*A1–A6* correspond to Pts. 3-6, 8, 9 respectively). *A2*', Photograph taken during the operation. Marked points and electrodes are also exhibited in the corresponding reconstruction image (*A2*). Recording sites visible in *A2*' are displayed in orange in *A2*. Channel 18 in Pt. 4 as well as channels 5, 17, and 18 in Pt. 9 were dysfunctional (i.e., either no data were recorded by the electrode, or a disproportionate amount of non-biological noise showed the malfunction of the contact site) and thus left out

from the analysis. *B*, Filtered (0.1– 40 Hz) ECoG data were subjected to MI analysis for all pairs of recording channels (see Materials and Methods). One-second-long data segments were compared with time-lagged data from the other channel and the extent of nonlinear correlation (predictability) was measured by MI. Left, Short data segments from two ECoG channels (Ch). Gray shading designates examples of 1-s-long temporal windows for MI calculations. Right, MI was displayed as the function of time lags (1 ms resolution). A significant maximal MI (in this case, 2.61 bits at 153 ms temporal delay) was considered to be a sign of significant correlation between the two channels, which corresponded to propagating sleep slow waves (see Materials and Methods and Results). Left, Time lag between the data windows (gray) was set to the optimal delay (153 ms) at the given time point. Note the similarity of slow-wave cycles (orange) in the windows. This analysis was repeated for all fixed time instances and for all pairs of recording channels. *C*, Based on the MI analysis, SWA propagation time, distance, and association strength could be assessed for all significant unitary propagation events, from which a time-resolved propagation map was drawn and visualized in a custom-built graphical user interface. A screenshot from this interface is shown with all ECoG channels (top right), amplitude map [bottom right; coldest/warmest color correspond to smallest/largest ECoG amplitude (color bar); 5x4 squares correspond to the 5x4 grid electrodes; amplitude was calculated as the difference of maximal and minimal ECoG value in the data window], propagation map displayed in a schematic form (bottom left) and also projected to the brain surface (top left). For every time point, arrows on the propagation map designate unitary propagation events between two recording sites (marked by numbers on the schematic view). The color of each arrow shows association strength (warmer colors are stronger) and the width corresponds to propagation time (thicker lines show shorter time).

Correlation triggered average.

To visualize ECoG patterns giving rise to significant correlations, we calculated ECoG averages triggered by significant MI values. That is, if a significant MI was detected at a certain time, a 1-s-long ECoG segment centered to that time point was stored. At the

end, these segments were averaged for each recording channel. The average signal reflected typical ECoG patterns underlying significant correlations.

Linear cross-correlations.

Linear cross-correlation analysis was conducted by replacing time-shifted mutual information values with linear cross-correlations. To facilitate the comparison of the results of linear and nonlinear analyses, all other parameters of the calculations were left unchanged (including significance testing using shuffled data; see above). Thus, a directional correlation was established when a significant cross-correlation with a positive time lag was observed (positive and negative correlation were not differentiated to allow the comparison with the MI measure). We also calculated the input– output functions related to significant linear (cross-correlation) and nonlinear (MI) correlations. For each pair of recording channels, we collected pairs of ECoG segments where a significant association was found, and plotted average ECoG amplitude values of a recording channel as a function of binned ECoG values of the other channel. All data analysis procedures were implemented in Matlab development environment (MathWorks) using custom-built and built-in functions. For further methodologies see reference (Hangya et al., 2011).

3.4 Resting state connectivity analysis and CCEP

3.4.1 Patient Selection

Six patients (4 female, aged 35.8 ± 13.4 years; range 17-47) with pharmaco-resistant epilepsy at North Shore - LIJ Health System participated. Those with overtly abnormal brains including extensive cortical dysplasia, tumors with vasogenic edema, and strokes were excluded from this study.

3.4.2 Imaging

Patients were scanned on a General Electric Signa HDx 3T scanner. Resting state fMRI data were acquired using a EPI gradient echo sequence (FOV = 220mm, voxel size 4x3.5x3.5, matrix 64x64, flip angle = 70, TR = 2000ms, TE =30, acquisition plane = axial, 150 contiguous volumes). Participants were instructed to rest with their eyes closed. An anatomical T1-weighted image was acquired using SPGR sequence (FOV =

256mm, voxel size 1x1x1, matrix 256x256, flip angle = 8, TR = 2500ms, TE = 30, TI = 650ms, acquisition plane = axial, 180 slices).

3.4.3 Resting State Functional Connectivity

Resting state data preprocessing was performed using AFNI (Cox, 1996) and FSL (Smith et al., 2004), and included slice timing correction for interleaved slice acquisition, motion correction, de-spiking, spatial smoothing (6mm full-width at half-maximum Gaussian blur), band-pass filtering (0.009-0.1Hz), and linear and quadratic de-trending. To remove variance associated with processes such as breathing, cardiac activity and motion, we regressed each patient's preprocessed time series on 9 nuisance covariates (6 head motion parameters, signals derived from the ventricles, white matter, and the global signal). The resultant 4-D residuals volume was registered to the patient's anatomical image using a linear transformation with 6 degrees of freedom.

For each patient, and each stimulation site, spherical seed regions of interest (ROI; 6mm radius) were constructed centered at each electrode. The mean time course for the seed was computed by averaging across all voxels within the seed. A whole-brain map of RSFC was created by computing the correlation between the seed time course and that of every other voxel in the brain, and applying Fisher's r-to-z transformation to the resultant correlation coefficients. For visualization purposes, the resultant RSFC map was projected from a three-dimensional volume to the individual's pial surface and plotted using MATLAB. In these graphs Z-values ≥ 0.3 were considered statistically significant (corresponding to a Bonferroni-corrected threshold of $P < 0.05$ considering all correlations computed).

3.4.4 Correspondence between CCEPs and RSFC.

To quantify the correspondence between CCEP and RSFC, for each stimulation site, we computed the correlation between CCEP z-scores at each electrode site and Fisher z-transformed correlation (RSFC) values at each corresponding electrode site. The resultant correlations were transformed to z-values using Fisher's r-to-z transformation, and averaged across all stimulation sites for a given individual. The mean z-value was reverse-transformed to an r-value and the statistical significance of the r-value was assessed based on the degrees of freedom (number of trend lines – 1) for each subject individually. No thresholding was applied for this analysis.

In a second statistical analysis, we compared the mean RSFC across the electrodes sites that exhibited a significant CCEP response (±6SD from baseline) to those exhibiting a non-significant CCEP response using a two-tailed *t*-test. To rule out the possibility that the differences between RSFC at significant and non-significant electrodes were driven primarily by electrodes proximal to the stimulation site, this analysis was repeated excluding those electrodes located within 25mm of the stimulation site).

3.5 Mapping of functional areas using CCEP

25 patients (11 Male, 14 Female) with medically refractory epilepsy were enrolled at the Comprehensive Epilepsy Center at North Shore LIJ Health System (LIJ, New Hyde Park, NY USA) and the National Institute of Clinical Neuroscience (NIN, Budapest, Hungary).

Patients participating in this study had medically intractable seizures and were referred for epilepsy surgical evaluation. All patients underwent intracranial electrode implantation for localization of epileptogenic tissue prior to therapeutic resection. Patients included in the study are: 7,9,10, 12-33 as seen in Table 1.

3.5.1 Defining electrodes not involved in seizure genesis.

To be able to differentiate between electrodes strongly connected to epileptic activity and those which do not show epileptic activity in the early phase of a seizure we defined some criterion. Every electrode was categorized into two groups according to the epileptologists description of the seizures. If there was any sign of high frequency pathological activation (>30Hz) within the first 10 seconds of a clinical seizure as defined by the epileptologist, that electrode was labeled as ictal if no such activation was detected, the electrode was labeled as non-ictal and it was included in the analysis.

DOI:10.14753/SE.2015.1798

3.5.2 3D Electrode reconstruction and Brodmann's area co-localization as the standard system to compare results from patients.

In order to map evoked responses to anatomical locations on the cortex we first applied the same cortical surface reconstruction and electrode localization techniques as described in the general methods section.

Co-registering the preoperative MRI to standard MNI space allowed the identification of the nearest BA to each electrode using AFNI (http://afni.nimh.nih.gov/). This automated process was corroborated with manual inspection of two independent researchers and set against the results of ESM to avoid any mislabeling. Only those bipolar stimulations were used where both electrodes covered the same BAs and only those BAs were included where none of the electrodes showed ictal onset. Using this method most of the BAs were covered in the patient population examined in this study except for the following (Table 2). BAs not covered with electrodes: 12, 23, 25, 26, 30, 33, 48, 49, 52.

We computed connectivity among functional regions of the cortex by grouping BAs of similar function. This way we are able to create maps of individual functions rather than strict BAs. The groups created are as follows: BA1-3: somato-sensory (SS); BA 44,45: Broca's area (BR); BA 11,12,25,47: prefrontal cortex (PFC); BA 23,26,29,30,31: posterior cingulate cortex (PCC); BA 24,32,33: Anterior cingulate cortex (ACC); BA 34,35,36: parahippocampal gyrus (PHG); BA 41,42: auditory cortex (AU). These categories were combined across hemispheres.

Pt.	Brodmann's Areas																													
16	1	2	3	4	6	8	9	10	11	20	21	22	24	31	34	35	36	37	38	39	40	42	44	45	46	47				
17	2	3	4	5	6	7	9	10	11	19	20	21	22	28	36	37	38	39	40	42	43	44	45	46	47					
13	1	2	3	4	6	8	9	10	11	19	20	21	22	34	36	37	38	40	41	42	43	44	45	46	47					
18	1	4	5	6	8	9	10	11	20	21	22	24	31	36	38	44	45	46	47											
10	1	2	3	4	6	7	8	9	10	11	17	18	19	20	21	22	28	34	36	37	38	39	40	42	43	44	45	46	47	
12	3	4	6	8	9	10	11	18	19	20	21	22	37	38	39	40	43	44	45	46	47									
19	1	2	4	6	8	9	10	11	19	20	21	22	37	38	40	41	42	44	45	46	47									
20	2	3	4	5	6	7	9	10	20	21	22	40	42	43	44	46														
21	6	8	9	10	11	25	32	44	45	46																				
22	3	4	6	7	8	9	10	21	22	40	44	46																		
23	1	2	3	4	5	6	7	9	10	11	19	20	21	22	28	36	37	38	39	40	42	43	44	45	46	47				
24	2	3	4	5	6	7	9	17	18	19	20	21	22	23	29	31	37	39	40	42										
25	1	2	3	4	6	8	9	10	11	19	20	21	22	28	36	37	38	39	40	42	43	44	45	46	47					
26	1	2	3	4	6	7	9	10	11	20	21	22	36	37	38	40	42	44	45	46	47									
27	1	2	3	4	5	6	7	8	9	10	11	18	19	20	21	22	37	38	39	40	42	44	45	46						
28	1	2	3	4	5	6	7	8	9	10	11	18	19	20	21	22	24	28	35	36	37	38	39	40	42	43	44	45	46	47
29	2	3	4	5	6	7	20	21	22	37	39	40																		
15	2	3	4	5	6	7	18	19	20	21	22	30	37	38	39	40	41	42	43	44	45									
30	2	3	4	6	8	9	10	18	19	20	21	22	24	25	32	35	36	37	38	39	40	42	44	45	46	47				
14	2	4	5	6	7	10	11	19	20	21	22	28	36	37	38	39	40	41	42	43	46	47								
7	2	3	4	5	6	7	8	9	10	31	39	40	46																	
31	7	18	19	20	21	22	28	29	30	31	35	37	39	40	42															
32	1	2	3	4	6	7	8	9	10	11	18	19	20	21	22	28	32	36	37	38	40	42	43	44	45	46	47			
33	2	3	4	6	9	10	11	19	20	21	22	25	30	35	36	37	38	40	42	44	45	46	47							
34	2	3	4	6	7	8	9	10	11	18	19	20	21	22	24	28	32	36	36	37	38	39	40	42	43	44	45	46	47	
9	2	4	6	8	9	20	21	22	27	38	40	41	44	45	46	47														

Table 2.: Brodmann's areas covered with electrodes in each patient.

3.5.3 Correlation between amplitude and distance from stimulation electrode

Z score calculation of the CCEP amplitude.

We calculated the statistical Z-score of every significant evoked potential by taking the baseline from: -500ms to -50ms before the stimulus as the reference period and the peak of the N1 or N2 wave. The standard deviation was calculated from the baseline period. Z is the number of standard deviations between the value and the mean.

Defining the distance between electrodes.

To measure the distance between two implanted electrodes we used the coordinates derived from the electrode localization procedure. We simply calculated the Euclidean distance of the two center points of the electrodes and used it as a measure of distance.

According to this the distance was always the shortest possible route between the two nodes irrespective of the convolutions of the brain. When calculating the distance between an electrode pair (stimulation electrodes) and a single electrode (recording electrode), we calculated the midpoint of the shortest line between the two stimulation contacts.

3.5.4 Calculation of the connectivity between BAs and Graph analysis to visualize connections.

In order to examine the network topology of the connections between brain regions, graph theoretical measures were applied to the CCEP matrices (Bullmore and Sporns, 2009, Wang et al., 2011, Bassett et al., 2012). Specifically, indegree (the number of significant connections recorded on a BA from every other stimulating BA), outdegree (the number of significant connections measured on all BAs after stimulating a BA), and degree (the sum of indegree and outdegree) were computed using the Brain Connectivity Toolbox (Rubinov and Sporns, 2010).

Indegree and outdegree were calculated two ways. First, we looked at the single electrode level and second at the Brodmann's area or group level. On single electrode level for indegree we calculated every connection to a node (single electrode) from all other electrodes which were stimulated, and then divided the number with the stimulations actually performed (possible maximum number of connections) in order to reduce variability due to different electrode configurations and stimulation trials. For outdegree on the single electrode level, we calculated the number of outgoing connections from every node, which was also normalized with the possible maximum number of connections (e.g the total number of recording electrodes minus the two stimulated electrodes).

To examine in- and out-degree at the BA level, we first averaged together all the connections from the electrodes which were placed within the same Brodmann's area on a single patient level and took every connection where the z-score exceeded a threshold of 3SD. Then we grouped all the BA's of all the patients together to see the grand mean average of connections, excluding all connections which were only present in 10% of the patients, to exclude inconsistent under represented connections. Graph theory

DOI:10.14753/SE.2015.1798

measures were normalized such that the sum of the indegree, degree, and outdegree of all stimulation sites for each patient was divided with the possible stimulations for indegree and the possible recording BAs for outdegree to reduce inter-individual variability. Plots of the graph theoretical measures were created using custom scripts (MATLAB, Natick, MA).

DOI:10.14753/SE.2015.1798

4 Results

4.1 Evaluation of the appropriate settings for single pulse electrical stimulation (SPES)

4.1.1 Surface ECoG recordings

We were able to record cortically evoked potentials in every patient in our study. Evokability varied across patients and sites. Typically the evoked potentials consisted of brief biphasic activation between 10-30ms (also called N1-P1 peak) after stimulus, which was followed by a negative trough and peak, lasting from 50-500ms (also called N2-P2) (Fig. 16.). Depending on the location, the polarity might invert due to the known effect of bipolarity, resulting in passive current flow. Using our criteria for selecting the significant evoked potentials compared to baseline, detailed above, we found that most of the evoked potentials occurred adjacent to the stimulation electrodes, but in most of the cases we also found significant CCEPs on electrodes 3 to 15cm distant from the stimulation sites, sometimes on different lobes and hemispheres of the brain (Fig. 11.).

To test the consistency of the latency of the N2 wave, we calculated the delay from the stimulus artifact until the peak of the N2 wave in every patient. We found that the majority of the N2 waves fall between 100 and 250ms (Fig. 17. A).

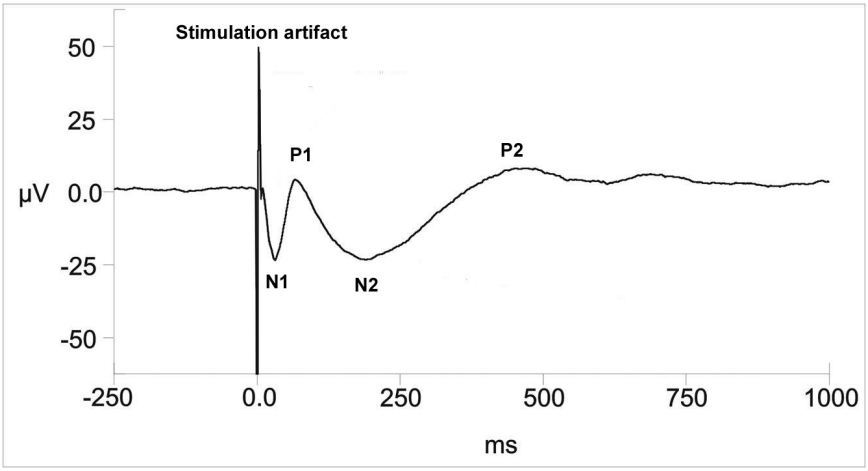

Fig. 16. Typical CCEP from a subdural electrode next to the stimulation contacts. After the stimulation artifact, which is on average below 10ms, a brief (10-40ms)

DOI:10.14753/SE.2015.1798

trough (N1) and peak (P1) is followed by a longer (50-1000ms) trough (N2) and a peak (P2).

To see the relationship between the amplitude of the N2 wave and the latency from the stimulus artifact, we created a scatter plot with the Z-score of the amplitude on the y-axis and the latency on the x-axis (ms). No significant correlation was found in this analysis though an inverse relationship was observed (Fig. 17. B).

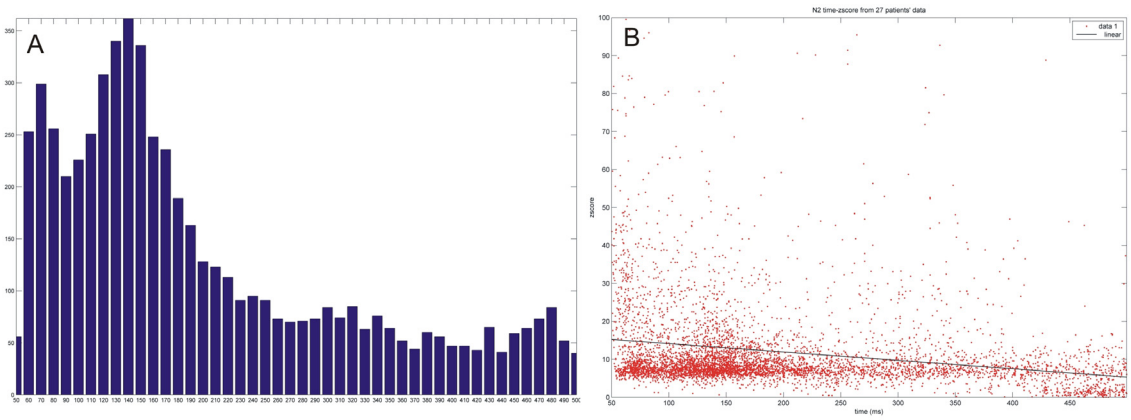

Fig. 17. A, Bin count shows the number of N2 peaks in every bin from 50-500ms (10ms bin) from all of the patients averaged. The majority of the N2 peaks fall between 110-200ms. B, Scatter plot of the delay from the stimulation artifact of the N2 wave (X-axis) and the Z-score of the amplitude of the peak of the N2 (Y-axis).

To describe the timing of the N2 wave we correlated the delay of the N2 peak from the stimulation artifact with the distance from the stimulation electrode pair. The scatter plot shows this correlation which does not show any significant correlation, but a non significant tendency of the more distant electrodes being further away in time from the stimulation artifact (Fig. 18.).

DOI:10.14753/SE.2015.1798

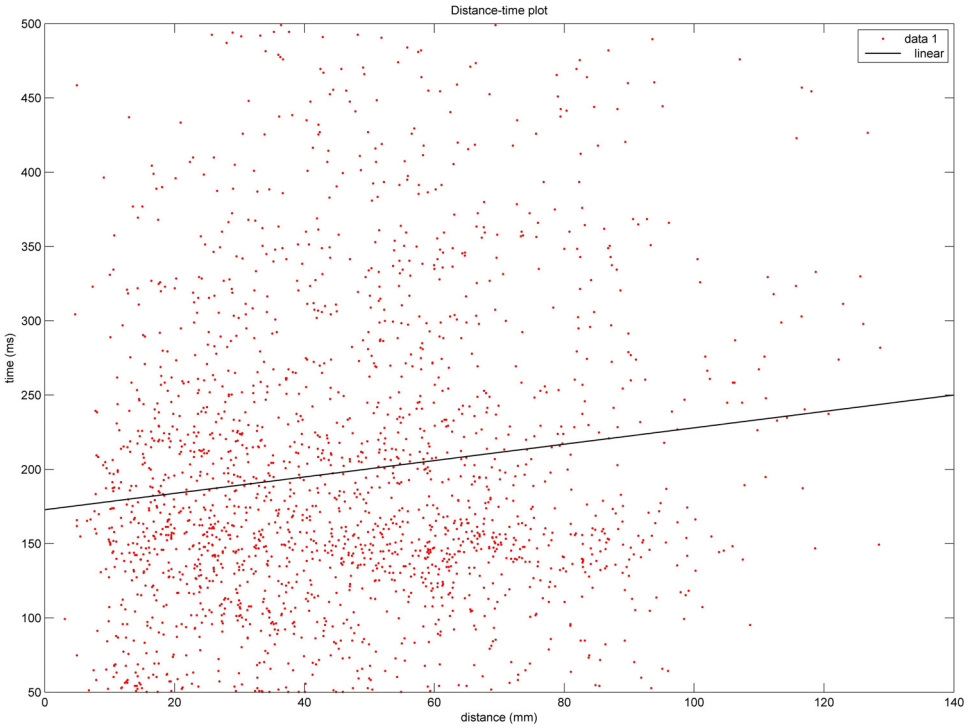

Fig. 18. Scatter plot shows the delay of the N2 peak from the stimulation artifact (Y-axis) compared to the distance of the stimulation electrodes to the recording electrodes, which registered a significant CCEP. We did not find any significant correlation between the two datasets, but a mild tendency if the electrode are further away the stimulation latency appears to be higher.

To test the effects of the stimulation current on the CCEP, we applied increasing amplitudes of electrical current between the same electrode pairs. The recorded CCEP increased gradually starting with 3ma till 9ma. 3ma was on many electrodes not sufficient to evoke a significant evoked potential, but 6ma was typically enough. By increasing the stimulation amplitude until 9ma-s the evoked potential increased as well. Above 9ma we could not register significant increase in the amplitude of the N2 wave, up to 15ma, which is considered the upper limit of safe stimulation. We repeated the same protocol on the same electrodes also at night, when the patient was in the early deep stages of non-REM sleep. The results are the same also in sleep, meaning that the vigilance state of the patient has no effect on the evoked potential characteristics (Fig. 19.). This pilot study was the basis of the stimulation protocol we applied to all of our patient. The use of 10ma as a standard stimulation parameter yielded the maximum amplitude of the N2 wave, but in the mean time still safe enough not to cause any

behavioral change or epileptic activity. Since the actual current flow between the two stimulation electrodes lasts for such a short time period (200μs) the activation of the neuronal elements is only possible within a very small circumscribed area below the electrodes, compared to the mass effect of the high frequency stimulation mapping performed for clinical reasons. During the entire period of the study we did not record any stimulation induced seizures. We observed 4 clinical seizures of over 60 stimulation sessions, but all of them showed the typical complex partial semiology, which was judged as the habitual seizure of the patient, meaning that it was independent from the stimulation, rather a habitual seizure, coincide with the time of the stimulation.

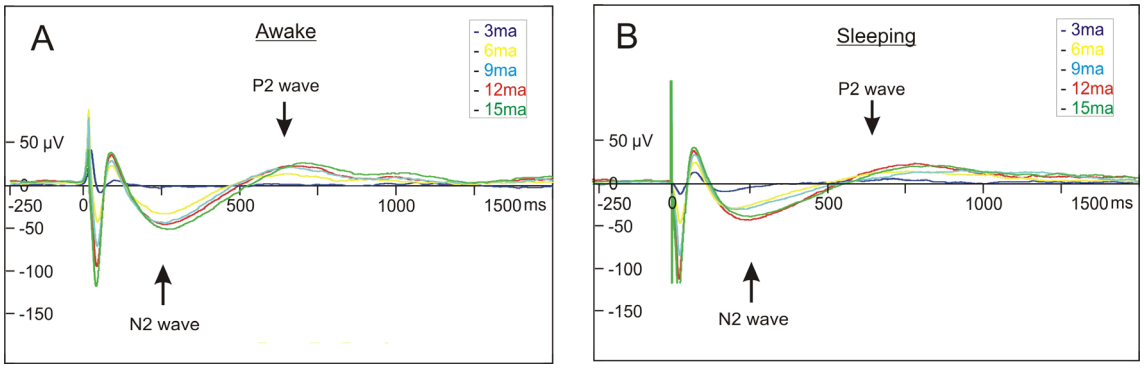

Fig. 19. The effect of different stimulation amplitude (3-15ma) on the CCEP. A) shows the bipolar stimulation during awake state, B) shows the stimulation of the same electrode pair during the early deep stages of sleep.

We tested the effect of the duration of the video-EEG monitoring on the CCEP pattern and amplitudes. In one of our patient (Pt. 14.) we could perform SPES at postimplant day 4, 7 and 13 (Fig. 20.). Due to clinical reasons the patient needed longer monitoring so we were able to record multiple sessions. The amplitude of the N2 wave show minimal variations, without any significant differences in the shape and timing of the evoked potential peaks.

DOI:10.14753/SE.2015.1798

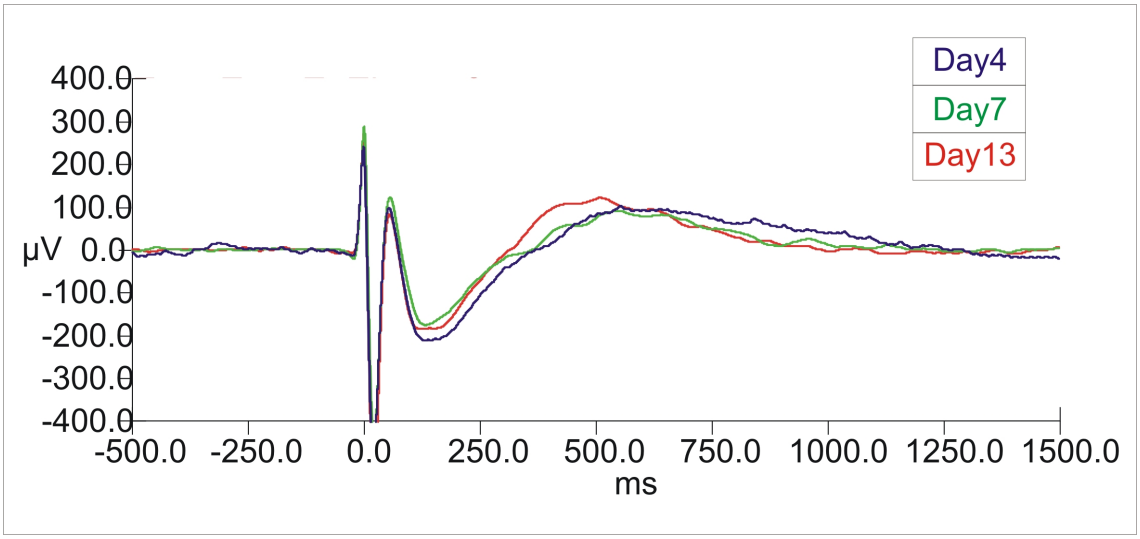

Fig. 20. Averaged and filtered (Low pass: 30Hz, 24db, zero phase shift) CCEPs of the same patient and stimulated close to the recording site on postop day: 4, 7, 13. We applied the same filtering to all 3 curves to clearly see the waveform without any high frequency noise.

4.2 Description of the effects of SPES on the neocortex recorded with ECoG and with a laminar ME recording system

4.2.1 Comparison between anesthetized, awake and sleep stages

Cortical stimulation has been performed in different vigilance states. First under general anesthesia in the operating room as part of the intraoperative mapping procedure, second at the bedside during long – term video-EEG monitoring with implanted electrodes in awake and third in deep non-REM sleep. The cortical evoked potentials in awake and naturally sleeping patients did not show any significant difference. The natural vigilance states compared to the artificial sleeping state of anesthesia did show some differences, but mostly in the latencies. Cortical stimulation under general anesthesia prolonged the evoked potentials, but did not change its shape (Fig. 21.).

DOI:10.14753/SE.2015.1798

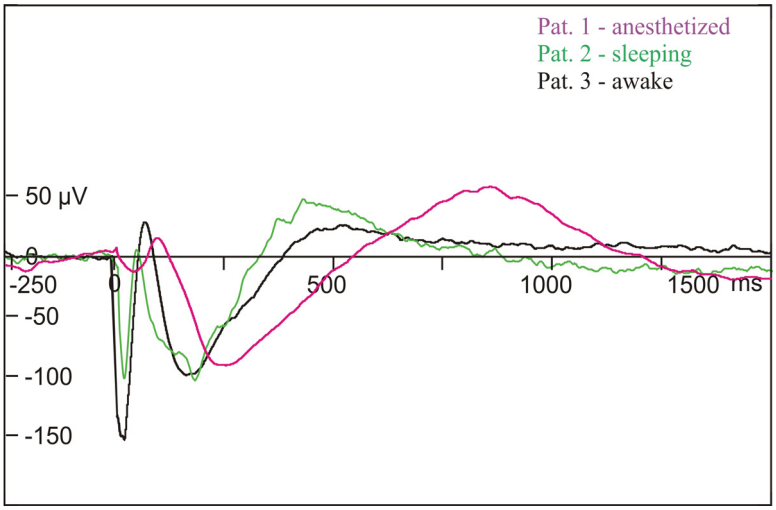

Fig. 21. Averaged electrocorticograms of three different patients in three different vigilance states before and after cortical electrical stimulation, the stimulation artifact was removed for better visualization and a short segment was interpolated instead. Patient 38 (O27, purple) was anesthetized (intraoperative registration), patient 5 (O39, green) was sleeping and Patient 6 (O40, black) was awake (chronic implants) during the stimulation.

4.2.2 Potential map and time-frequency (TFR) analysis of the CCEPs on the surface recordings

We created surface potential maps of a grid electrode (Pt.5.) to describe the spatial effects of the cortical stimulation. According to our hypothesis the potential map of the N1 peak show a well circumscribed localized surface negativity in the surrounding electrodes to the stimulation. According to the maximum amplitude of the N2 wave almost the entire grid showed a surface negative potential, even in distant areas from the stimulation site. The P2 wave showed a moderate, but larger positive area than the P1. We calculated the time frequency spectrum (TFR) on all channels to see the oscillatory power changes in the 0-200Hz range. We found that under the electrical stimulation induced surface negative potentials there is a wide band (0-100Hz) spectral power decrease on the grid electrodes compared to the baseline. This power decrease lasts under the first part of the negative slope of the surface negative potential (N2) (Fig. 22).

DOI:10.14753/SE.2015.1798

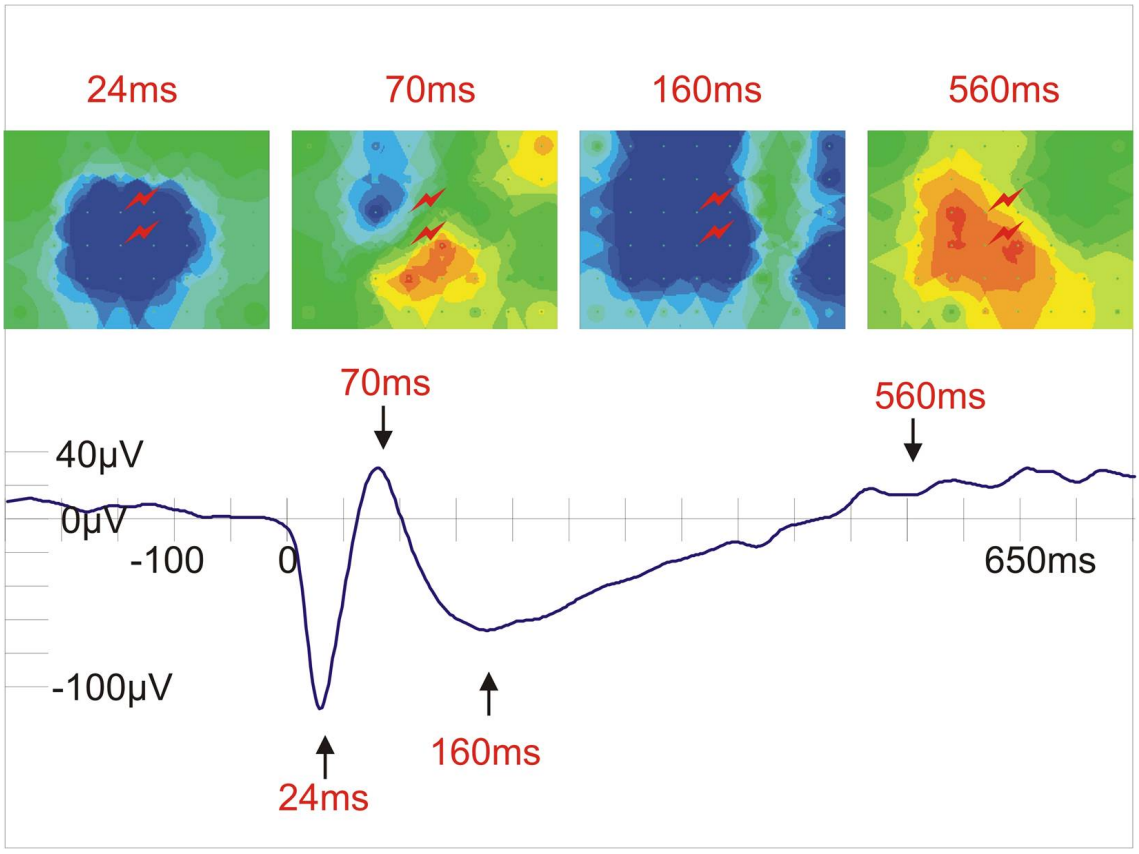

Fig. 22. Potential map of the grid (Pt. 5.) after single pulse electrical stimulation. Maps in the upper part show the potential map of the grid at the appropriate time after stimulation. The stimulation artifact was removed for better visualization and the missing segment was interpolated. N1=24ms, N2=160ms.

During the rebound positivity (P2) we found significant spectral power increase, which was most pronounced during the first part of the positive slope. Looking at the distribution of the power changes, we found that the areas close to the stimulation electrodes were involved most of the times, but there were distant regions as well which showed significant /power alterations. Due to the high frequency noise caused by the stimulation, the appropriate TFR analysis of the N1 peak was not possible (Fig. 23).

DOI:10.14753/SE.2015.1798

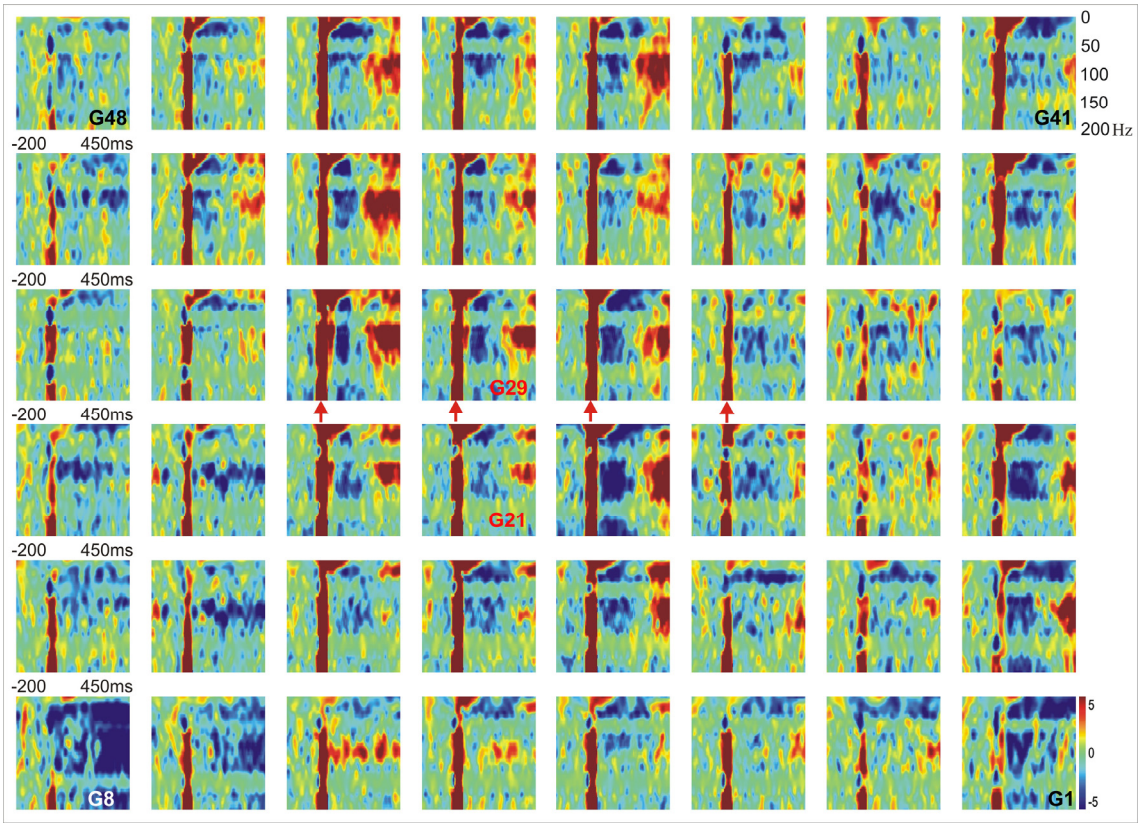

Fig. 23. Wavelet based time-frequency analysis of a 48chanel grid (Pt. 5). Each little inlay represents one channel's peristimulus interval (-50- 450ms). The Y axis represents the frequency between 0-200Hz. Colors show the spectral power changes over time (blue: spectral power decrease compared to baseline, red: spectral power increase compared to baseline) Stimulation artifact is marked with red arrows. Gr21-Gr29 were stimulated, the responses are interpolated from the neighboring channels for better visualization.

4.2.3 Laminar properties of the evoked potential

After histological reconstruction of the penetration tracks we were able to co-localize the 24 electrode contacts of the shaft to the different laminas of the neocortex. According to this the thumbtack electrode penetrated successfully through all the 6 layers of the cortex, enabling us to record from all of them.

Looking at the local field potentials recorded with the microelectrode we were able to see the vertical bipolarity of the cortex, since during the N2 phase we found negative potentials in the upper layers and positive potentials in the deeper layers, during P2 the opposite.

We also calculated the time-frequency power spectrum of the evoked potentials in the same time frame as on the surface (-200ms - 450ms).

Interestingly during the descending part of the surface potential N2 wide band (30-200Hz) power decrease was observed across all layers, whereas during the ascending phase of N2 (early phase of P2) we found less pronounced but still significant power increase. These spectral changes were consistent across patients and sites.

Calculating the second derivative of the local field potential shows us the local current source density (CSD) along the shaft. In parallel with the TFR results during N2 a current source was measured and during P2 a significant current sink. These changes spanned between layer II-IV in most of the cases, involving mostly the middle-upper layers.

Multi unit activity (MUA) revealed decreased cellular spiking activity during N2 and increased activity under the P2 phase of the surface CCEP. (Fig24.)

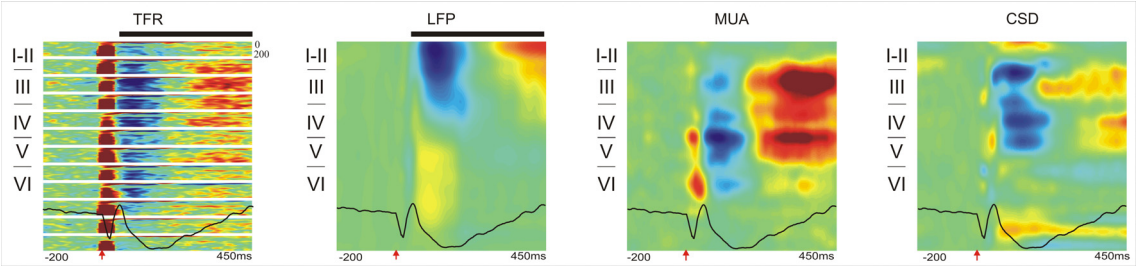

Fig. 24. TFR: Laminar spectral power changes (0 - 200Hz) over time recorded with the intracortical multielectrode after cortical electrical stimulation. Blue = power decrease, red = power increase. LFP: Laminar local field potential changes over time recorded with the intracortical multielectrode after cortical electrical stimulation. Blue = negativity, Red = positivity. MUA: Laminar multi unit activity changes over time recorded with the intracortical multielectrode after cortical electrical stimulation. Blue = decrease in activity, Red = increase in activity. CSD: Laminar current source density changes over time recorded with the intracortical multielectrode after cortical electrical stimulation. Blue = source, Red = sink.

4.2.4 General features of human SWA

Clinical subdural strip and grid electrodes and MEs were implanted into the frontal and parietal cortices of patients with intractable epilepsy in order to identify the seizure focus and eloquent cortex prior to surgical therapy. The focus was eventually localized

DOI:10.14753/SE.2015.1798

to the frontal lobe in four patients, and to the temporal lobe in one. Histology of the ME penetration track was recovered in two patients; it showed intact laminarization (Fig.25), well preserved pyramidal cells and glia (Fig.25, B-C), indicating no discernible epilepsy or implantation related damage of the examined cortex. None of the patients had pre-operative pathological MRI findings in the 1-2 cm vicinity of the ME implantation site.

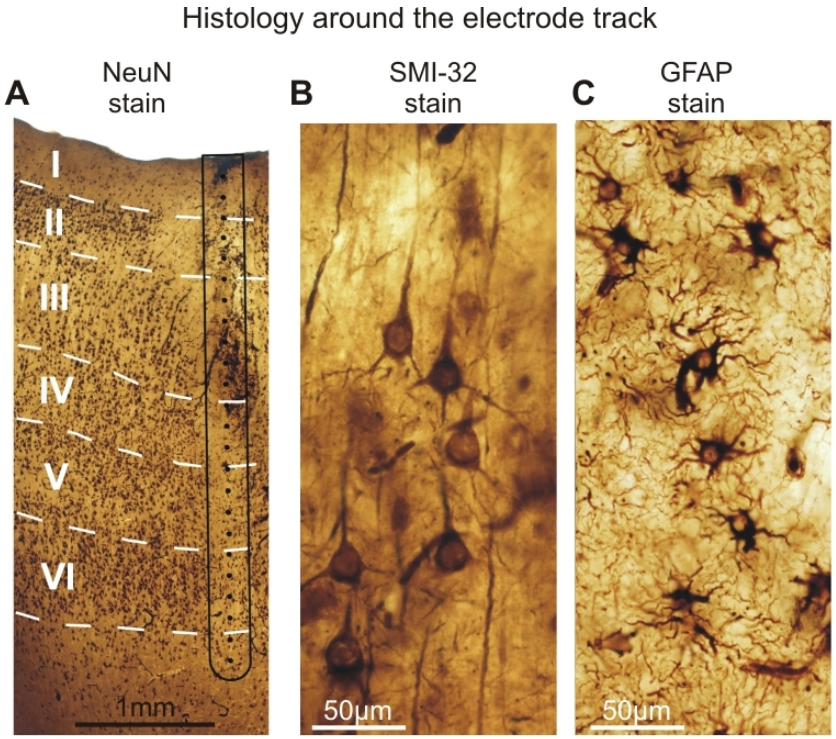

Fig. 25. Electrode track histology, representative examples from Patient 4. (A) The MEelectrode track (black contour line) and inferred contact locations (black dots) are shown relative to cortical layers (Roman numbers) revealed by the NeuN stain. Laminarization appears to be intact. (B) Well preserved pyramidal (SMI-32 stain) and (D) glial cells (GFAP stain) next to the electrode track.

Automatic SWA cycle detection was based on amplitude and phase information using LFPg (Fig.26, A) and ECoG (Fig.26, B) recorded during SWS. On average, 20 SWA cycles (*mean*=20 1/min, *range*=12-26 1/min, *SD*=7 1/min) were detected per minute. Cycle length peaked on average at 0.8 sec (*mean*=0.8 sec, *range*=0.6-1.4 sec, *SD*=0.3 sec). Interdetection interval peaked on average at 1.1 sec (*mean*=1.1 sec, *range*=0.8-1.2 sec, *SD*=0.4 sec), all comparable to healthy subjects (Massimini et al., 2004). LFPg and ECoG FFT power spectrum and autocorrelation also corresponded well to previous

human (Achermann and Borbely, 1997) and animal (Isomura et al., 2006) findings, indicating correct SWA cycle identification and relatively normal SWA production.

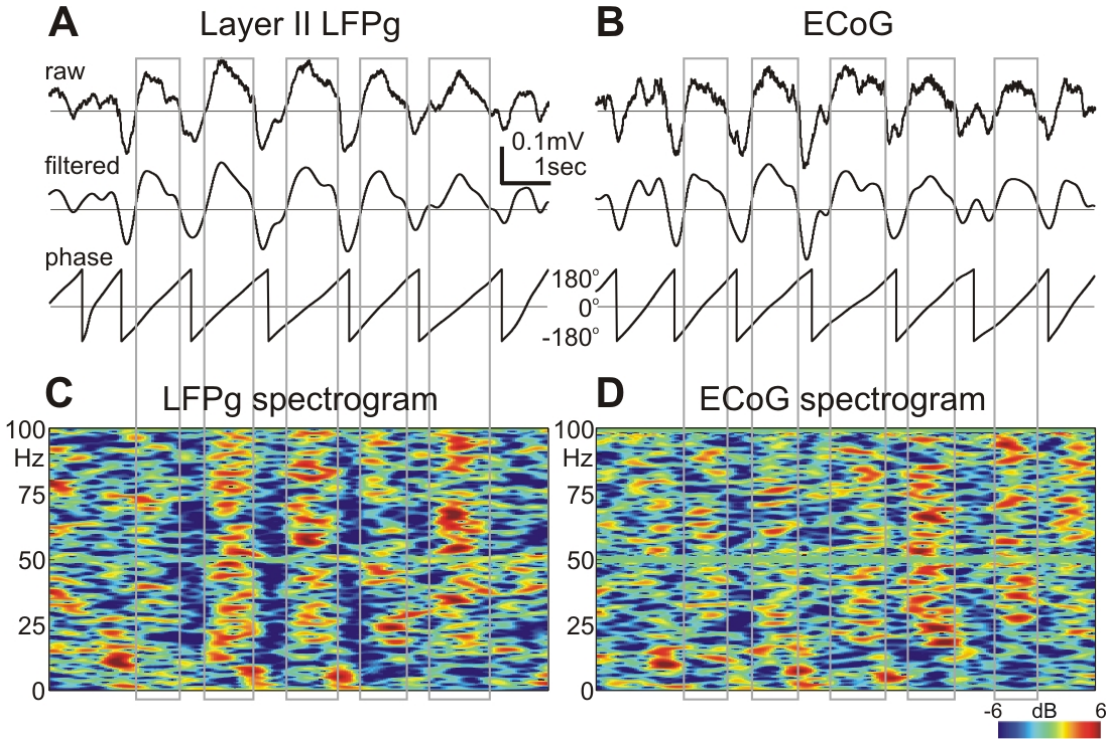

Fig. 26. Similarity between LFP gradient recorded with a microelectrode array within the cortex and ECoG recorded from macro contacts subdurally. (A) Upper: 'raw' traces of single sweeps containing slow wave activity; broadband (0.1–300 Hz) LFP gradient from layer II. Middle: 'filtered' traces after band-pass (0.3–3 Hz) filtering. Lower: 'phase' traces showing the instantaneous phase of the 'filtered' trace above derived by the Hilbert transform. Grey rectangles indicate automatically detected up-states (surface positive half-waves). Patient 4. (B) Same as (A), but recorded from neighboring ECoG contacts. (C) Color map of LFP gradient and (D) ECoG spectral power during the slow wave activity shown in (A) and (B). x-axis: time, y-axis: frequency, z-axis: color coded relative spectral power in dB, compared with the mean of the entire interval in each frequency band (relative spectrogram).

LFPg recorded in layer II (Fig.26, A) closely resembled to the locally recorded ECoG (Fig.26, B), with Pearson $r>0.9$ ($p<0.01$) in all patients. Time-locked averages to the peak of the surface positive half-wave (up-state) showed similar LFPg and ECoG

waveforms regardless if time locking was based on the LFPg or ECoG. Both LFPg and ECoG (Fig.26, C-D) showed broadband (10-200 Hz) spectral increases during up-states and decreases during down-states.

4.2.5 Laminar distribution of SWA

To estimate the laminar contribution of various activities, ME channels were assigned into six putative layers (I-VI) based on the histological findings (Fig.25, A) when available, and cortical depth when not. This analysis revealed substantial concentration of the 0.3-3 Hz band LFPg FFT power within layers I-III in each patient, indicating strong supragranular synaptic/trans-membrane activity. The SWA shape similarities between electrode contacts were significantly greater in supragranular versus infragranular layers in each patient, (0.634 versus 0.423, grand average pair wise coherence, Kruskal-Wallis ANOVA, $p<0.01$), while autocorrelation profiles revealed a more precisely paced rhythm supragranularly in each patient.

Several measurements, both in individual patients (Fig.27, A-D) and in grand averages, reflecting different aspects of population synaptic/trans-membrane and firing activity, were maximal in supragranular layers at the up-state peak.

Laminar analysis of spontaneous slow wave activity

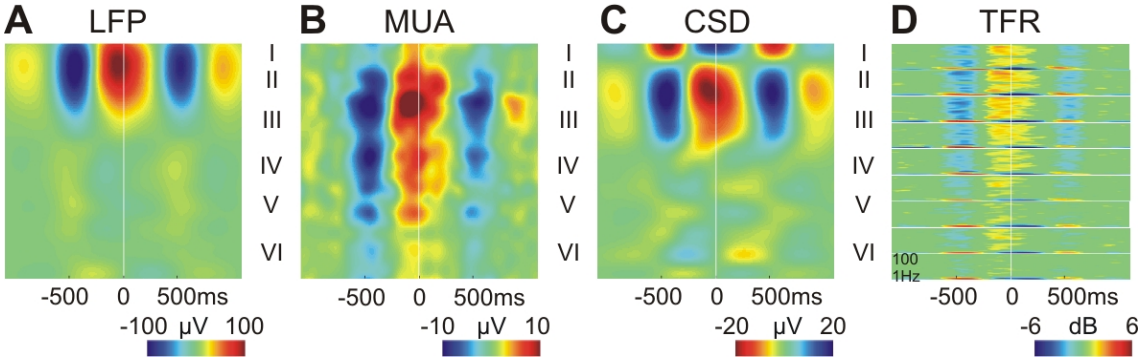

Fig. 27. Role of supragranular layers in slow wave activity generation. Representative depth profile map examples from Patient 4 (A–D). (A) LFP gradient (LFPg), (B) multiple-unit activity and (C) CSD depth profile maps. x-axis: time, y-axis: cortical depth, with corresponding laminarization, z-axis: color-coded amplitude of LFP gradient, multiple-unit activity and CSD units. Positive values are red, negative are blue, except for CSD, where sink is depicted in red and source in blue. (D) LFP gradient spectrograms (SPC) from nine representative channels in layers I–VI.

Normalized, grand average depth profiles of LFPg were marked by maximally positive deflections in layers I-III, inverting in layers V-VI into a small negativity. MUA was also maximal in layer III. The CSD depth profile at the peak of the SWA up-state showed a maximal source (outward current) in layer I and maximal sink (inward current) in layers II-III, only very small CSD deflections were observed infragranularly. In contrast, the CSD depth profile of a population of interictal spikes detected manually and locked to the surface positive LFPg (similarly as in the case of the up-state), were markedly different, exhibiting a large sink-source pair in the infragranular layers. Significant increases (bootstrap analysis (Delorme and Makeig, 2004), $p<0.01$) in LFPg spectral power were detected in all layers at 10-100 Hz frequencies during up-states (Fig.27, D). Gamma power of LFPg and CSD was maximal in layer III.

4.2.6 Comparison of the evoked SO with the spontaneous SWA

According to our previous findings the cortical generators of the spontaneous SO if time locked to the up-state were localized to the supragranular layers (I-III). Similarly to the spontaneous SO the major changes in the CSD profile was localized also to the middle-upper layers representing the supragranular portion of the cortex after cortical stimulation (SPES) evoked SO. Comparing the changes in the TFR domain did not reveal any difference, both analysis show wide band (0-200) spectral decrease across the whole cortex during down-state and wide band increase during the early up-state phase. We also looked at the local field potential gradient changes where we found negative potentials in the upper layers during the down-state and positive potentials during the up-state in both situations. The MUA pattern did also prove our hypothesis in trying to corroborate the findings of the evoked SO with the spontaneous ones (Fig.28). The TFR, CSD and MUA changes during the evoked down state fulfill the criteria set for the K-complexes or spontaneous SO (Cash et al., 2009, Csercsa et al., 2010), and the rebound surface positivity shares most of the laminar features with the spontaneous SO.

DOI:10.14753/SE.2015.1798

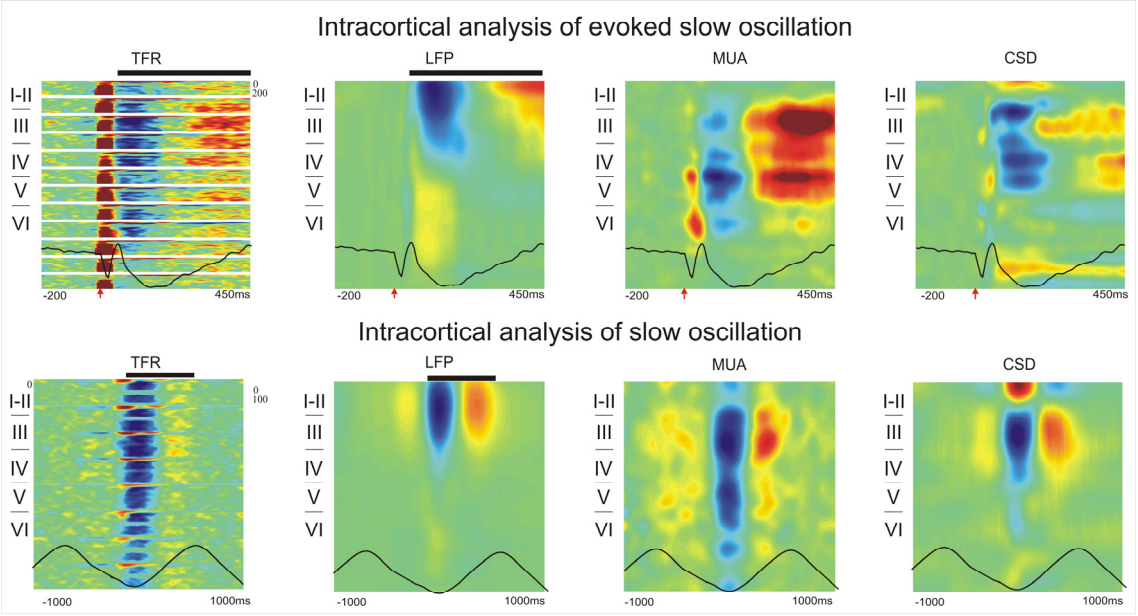

Fig. 28. Comparison of the evoked and spontaneous slow oscillation in the depth of the cortex. Upper part of the figure represents the laminar profile of the SPES evoked SO time locked to the stimulation artifact. Lower part of the figure shows the laminar profile of the spontaneous slow oscillation from the same patient (Pt. 5.) time locked to the down state. Note the time scale differences between the two analysis (-200-450ms for the evoked SO and -1000-1000ms for the spontaneous SO).

4.3 Non-linear mutual information based correlation show complex SWA propagation patterns

Nonlinear associations during human SWS

The nonlinear nature of neural communication was shown in several systems (Freiwald et al., 1999, Darvas et al., 2009, Chen et al., 2010); however, it is unclear whether such nonlinearities also appear in the course of slow oscillation propagation. We investigated 1-min-long segments of SWS in six epileptic patients. ECoGs from 16–20 subdural recording sites were analyzed in each patient. We first searched for associations between ECoG waveforms recorded from different brain areas and compared the results of a linear (cross-correlation) and a nonlinear (MI) correlation analysis (see Materials and Methods, above). Both linear and nonlinear types of dependencies were present in

ECoG channels in all analyzed sleep segments. Significant linear correlation and MI values were summed over time for each pair of recording channels for each recording segment, resulting in linear and nonlinear correlation profiles. Although some similarities between the two types of profiles were discoverable (Fig.29), significant nonlinear correlations were more abundant [5687 of 7266 channel pairs in all recordings (78.3%) compared with 1292 of 7266 (17.8%)], showing additional associations compared with the linear analysis. It should be noted however, that linear correlations were detected in a very few cases where nonlinear correlations were not (36 of 7266 channel pair comparisons, 0.5%), showing that in cases of pure linear associations, cross-correlation analysis can be more sensitive than MI. To visualize the associations between channel pairs, we calculated the input–output functions related to significant linear and nonlinear correlations. If all such input/output curves are line-shaped even for the MI calculations, then nonlinear analysis is unnecessary and the cross-correlation technique is sufficient to detect all associations. As expected, cross-correlations mainly captured linear relationships (Fig.29, A). However, we found that input–output curves were highly complex and often nonlinear in a number of cases for MI analysis (Fig.29, B). Thus, as nonlinear associations were present during human SWS, the MI analysis was more appropriate in characterizing slow oscillation propagation.

DOI:10.14753/SE.2015.1798

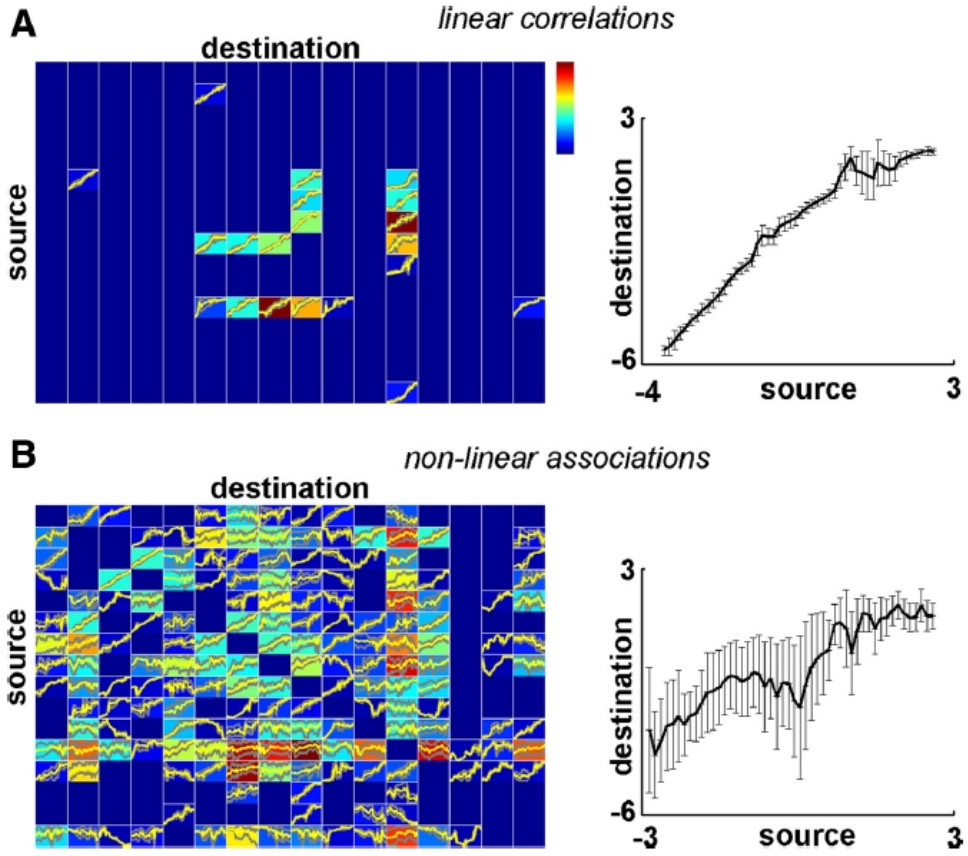

Fig. 29. Nonlinear associations during SWA propagation. A, Left, Correlation profile and input– output curves of linear cross-correlation analysis from a representative subject. Each colored field corresponds to a pair of recording channels (y-axis, source channel; x-axis, destination channel). Colors indicate the total strength of (significant) directional correlation between the source and destination channels (i.e., significant cross-correlation with a positive time lag when calculated with reference to the source channel; warm colors are high correlation values). A significant cross-correlation between two channels at τ milliseconds means that the ECoG segment of the source channel is correlated with that of the destination channel shifted by τ milliseconds. We collected these correlated pairs of data segments for each pair of channels and plotted the ECoG values of the destination channel against corresponding values of the source channel (binned and averaged). These input– output functions are plotted in the colored fields for all channel pairs (yellow, mean; gray, SD). Right, A typical input– output function (source, channel 8; destination, channel 9) is enlarged. Error bars indicate SD. ECoG segments were standardized (i.e., transformed to

zero mean and unitary SD); thus, tick labels on both axes show standardized voltage values. Note the line-like shape of these input– output curves. B, Left, Nonlinear correlation profiles and input– output curves for the same sleep segment calculated by the MI method. Arrangement follows that of A. Right, An example input– output function (source, channel 2; destination, channel 11) is enlarged. Note the higher abundance of significant nonlinear associations, the moderate similarities of linear and nonlinear correlation profiles (e.g., low rate/absence of correlations for channels14 and 15, strong correlation between channels 8 and 12), and the more complex and variable shape of nonlinear input– output curves. Higher SD values and noisier appearance of the nonlinear input– output functions show that the nonlinear correlation functions between pairs of channels exhibit temporal changes.

Characteristics of SWA propagation

The significant correlation of time-shifted waveforms recorded from pairs of electrodes was established by the MI technique. The resulting associations at each time point (Fig. 15., B,C) served as unitary events for the subsequent calculations. First, we investigated what characteristic patterns in the ECoG traces gave rise to significant waveform correlations. Raw ECoG segments showing significant nonlinear correlation with data segments recorded from other electrodes were averaged for each recording site (see Correlation triggered average, above). Significant waveform correlations usually corresponded to the rising phase of cortical SWA (Fig.30, A), which further supports the view that waveform correlations detected by the MI method reflect slow-wave propagation between different cortical areas. Moreover, it implies that the most conservative segment of the slow-wave cycle is its ascending phase, showing more pronounced correlation across areas compared with other phases of the oscillation. Next, we calculated general characteristics of SWA propagation. The distribution of propagation distance (Fig. 15., C, length distribution of the arrows) showed that SWA correlations were most common among neighboring cortical areas, although associations between distant sites were also observed (Fig.30, B). These unexpected

spatial noncontinuities, or jumps, of SWA do not fit the general idea of traveling waves, i.e., propagation of slow waves as single lines over large cortical areas (Massimini et al., 2004). Propagation speed of cortical slow waves (calculated by dividing electrode distances with propagation time values) showed large variability with an overall mean ± SEM of 3.33 ± 0.96 m/s, which is approximately in agreement with previous studies (Massimini et al., 2004, Murphy et al., 2009). The distribution shape of correlation strength (MI) showed marked similarity across recording segments and subjects (Fig 30., C). these propagation statistics were not statistically independent. Specifically, weak but significant negative correlations were found between correlation strength and propagation time [significant correlation ($p < 0.01$) in 24 of 26 sleep segments with a mean ± SEM correlation coefficient of -0.17 ± 0.01] as well as propagation distance [significant correlation ($p < 0.01$) in 22 of 26 sleep segments with a mean correlation coefficient of -0.16± 0.01], whereas it was positively correlated with propagation speed [significant correlation ($p<0.01$) in 19 of 26 sleep segments with a mean correlation coefficient of 0.10 ± 0.01]. Thus, fast propagation to short distances was accompanied by higher correlation strength. Expectedly, propagation time was usually positively correlated with propagation distance [positive correlation ($p < 0.01$) in 23 of 26 sleep segments with a mean correlation coefficient of 0.28 ± 0.02; negative correlation in one and no significant correlation in two cases].

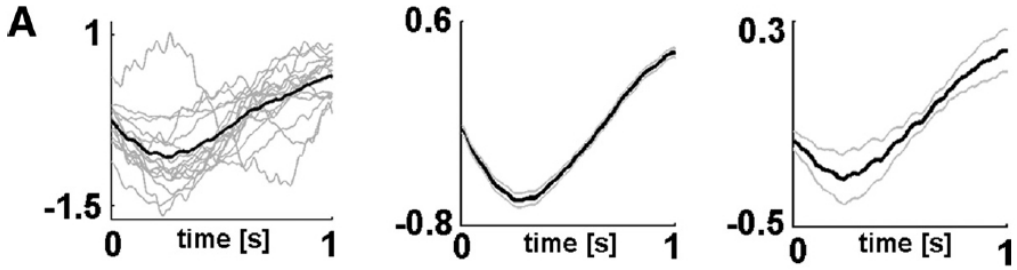

Fig. 30. SWA propagation characteristics. *A*, Average waveforms of data segments with significant nonlinear correlations across ECoG channels. Left, Mean waveform from all ECoG channels separately (gray) and averaged (black) from a representative sleep segment of a single subject. Only data segments that showed significant correlations with other recording channels were included in these calculations. Middle, Mean waveform of significantly correlated data segments from the same subject including all analyzed sleep segments (black). Gray lines

show SEM. Right, Grand average from all patients (black, mean; gray, SEM across patients). It should be noted that ECoG segments were standardized before the calculation of waveform averages; thus, tick labels of the *y*-axis show standardized voltage values. Average waveforms of data segments with significant waveform correlations across channels showed characteristic down-to-up state transitions, including the rising phase of SWA

4.4 Brain surface reconstruction and co-registration to standard space

In order to avoid the artifacts and distortions caused by the electrode implantation procedure on the postimplantation images with the electrodes, we needed to create a protocol for using preoperative images to display the electrodes and localize them to distinct anatomical regions. As described in the methods section we used a freely available software package (Freesurfer) which allows us to create segmented brain volumes and surfaces, which we can use for any type of imaging as a basis (Fig. 31.). To have the possibility to reconstruct the pial surface of the preoperative MRI is essential for being able to snap the electrodes to the preoperative brain surface since at the site of implantation the outer contour of the brain is always shifted on the postimplantation images toward the midline. To be able to create high resolution images we successfully developed a standard imaging protocol at both Centers. The protocol used at NSLIJ is as follows: General Electric Signa HDx 3T scanner. An anatomical T1-weighted image using SPGR sequence (FOV = 256mm, voxel size 1x1x1mm, matrix 256x256, flip angle = 8, TR = 2500ms, TE = 30, TI = 650ms, acquisition plane = axial). The patients for NIN are scanned at the MR Research Center of Semmelweis University with the following parameters: 3T Philips Achieva Scanner 3D T1-TFE sequence (voxel size 1x1x1mm, TR: 9.816ms, TE: 4.6ms, matrix: 512x512, acquisition plane = axial).

DOI:10.14753/SE.2015.1798

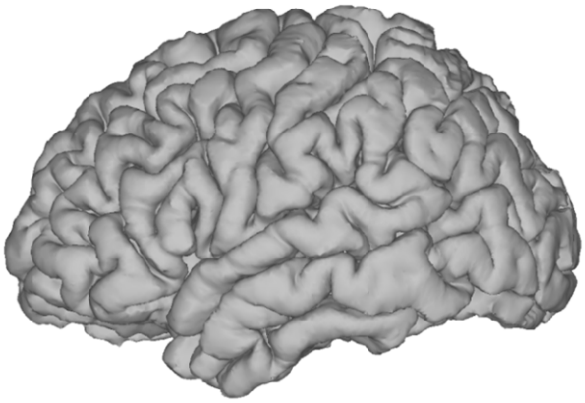

Fig. 31: 3D reconstructed cortical surface of Pt. 10. using Freesurfer.

4.4.1 Electrode localization using postimplantation CT

At our co-operational research program between NSLIJ and NIN we developed our own method to visualize the electrodes on the basis of Dykstra et al's publication (Dykstra et al., 2011). Instead of using Freesurfer and localize the electrodes there manually, we proposed the use BioImageSuite (BIS) (Duncan et al., 2004), which has an electrode localization interface (Electrode Editor) and makes the estimation of the center of the electrodes more robust. Beside the electrode localization, BIS enables to add every electrode to its database and plot them onto the surface of any image type (CT, MRI, fMRI), which is co-registered to the same 3 dimensional space. We first calculate the pial surface of each individual in Freesurfer (see above), which is the basis of any future imaging, because the brainmask created with freesurfer is co-registered automatically to standard MNI space, which makes the transition between different modalities (e.g. CT, MRI, fMRI) possible. After postimplant day 2-3 we perform a thin slice spiral CT (1mm) and T1 weighted 3D MR (1mm) without contrast. The acquired DICOM formatted images are then converted to the compressed single file format called NIFTI. The images are then co-registered to the preimplantation images as follows. To avoid the effects of the surgery we first co-register the postimplantation CT to the postimplantation MR. This intermodal linear (FSL software library, FLIRT: 12 degrees of freedom (affine)) co-registration is done very precisely due to the same anatomical

DOI:10.14753/SE.2015.1798

distortions recorded both after surgery. To perform the co-registration between the preoperative MR and the postoperative MR we found the best solution using the BET 2 algorithm from FSL to remove the bony structure from the brain. Having the two skull stripped MR-s the distortions are less pronounced and the linear transformation can be precisely performed. To transform the postimplantation CT to the same 3D space with the preoperative MR we concatenate the two transformation matrices described above, and in one step transform the CT in the same space where the MR is (Fig. 32). This protocol has been tested in over 30 patients with regular testing using intraoperative photographs. Once the CT has been transformed to the space where the surface reconstructed preoperative MR is, we can use the electrode editor function of BIS to localize the center of every electrode by clicking on the electrode artifact as seen in the figure (Fig. 32).

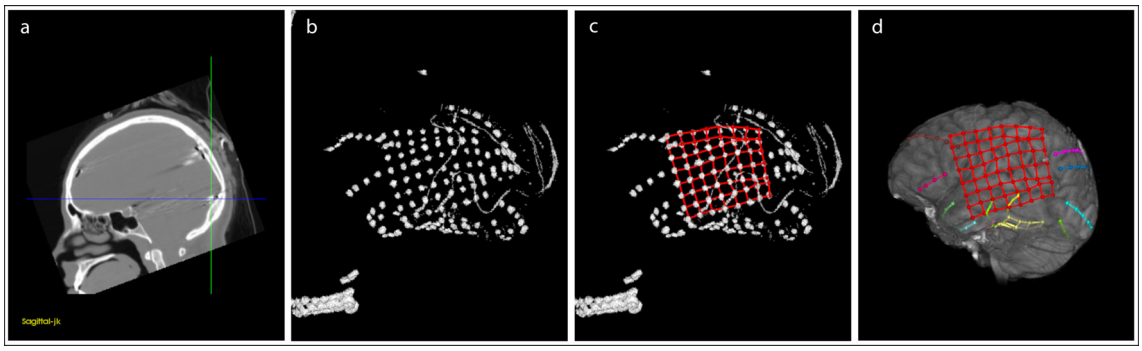

Fig.32. a) Saggital slice of a thin slice CT scan of a patient with implanted intracranial electrodes. b) 3D reconstruction of the same patient's CT scan, thresholded at the maximum intensity of the artifact caused by the metal of the electrode contacts. c) Using the interface of Bioimagesuite we manually associate every contact with a virtual electrode, which will bear the same coordinates as the real one. d) Electrodes can be overlaid on any 3D imaging of the patient which is co-registered to the same MNI standard space. Different grid and strip electrodes are individually color coded to aid visualization. The electrode localization interface of Bioimagesuite allows to rotate and cut the actual 3D volume in any direction.

The virtual color coded electrodes are defined in the same standard space, which allows to plot them onto any surface. To bypass the misalignments caused by the surgery we apply the same protocol (custom Matlab scripts to snap the electrodes to the

reconstructed surface) as described by (Dykstra et al., 2011) on the electrode coordinates in our pipeline. The electrodes can be visualized on the freesurfer brainmask for future analysis (e.g. resting state fMRI, fMRI, DTI, etc.) (Fig.33).

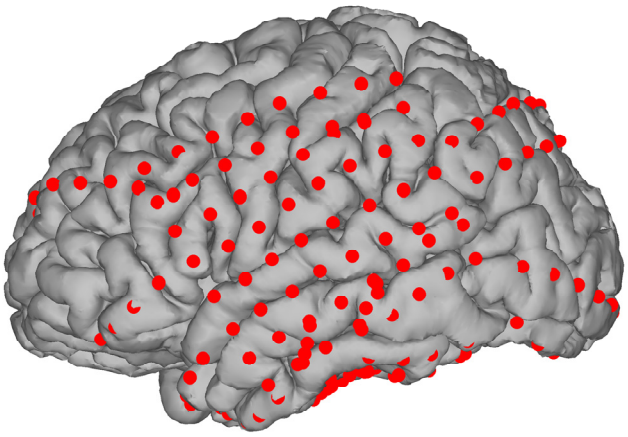

Fig. 33. 3D reconstructed brain surface of Pt. 10. with the subdural electrodes overlaid (red circles).

4.5 Resting state fMRI correlates with CCEP

For each of 6 patients (Pt. 10-15. = S1-S6) with intractable epilepsy, we investigated the relationship between RSFC and CCEPs. CCEPs are elicited in response to single pulse electrical stimulation of the cortex with subdural electrodes implanted for the purpose of seizure localization. CCEPs permit us to "electrically track" cortico-cortical neuronal connections *in vivo* by stimulating one cortical region and recording the evoked potentials at another location, since responses at the recorded site are the direct result of neuronal projections from the stimulation site (Matsumoto et al., 2004, Lacruz et al., 2007, Matsumoto et al., 2007). To obtain CCEPs, we administered repeated brief single-pulse electrical currents between adjacent electrodes and recorded the evoked electrophysiological responses at all other implanted electrode sites as described earlier. This procedure was repeated for all possible adjacent stimulation sites. To derive RSFC maps, we first localized the implanted electrodes via co-registration with the patient's anatomical MRI and CT scan (see Methods). The obtained coordinates formed the

centers of spherical regions-of-interest (‘seeds’), and the temporal correlation (RSFC) between each seed’s mean time series and the BOLD signal at every other voxel in the brain was then calculated (Fig.34, b). The fMRI scan was acquired prior to electrode implantation.

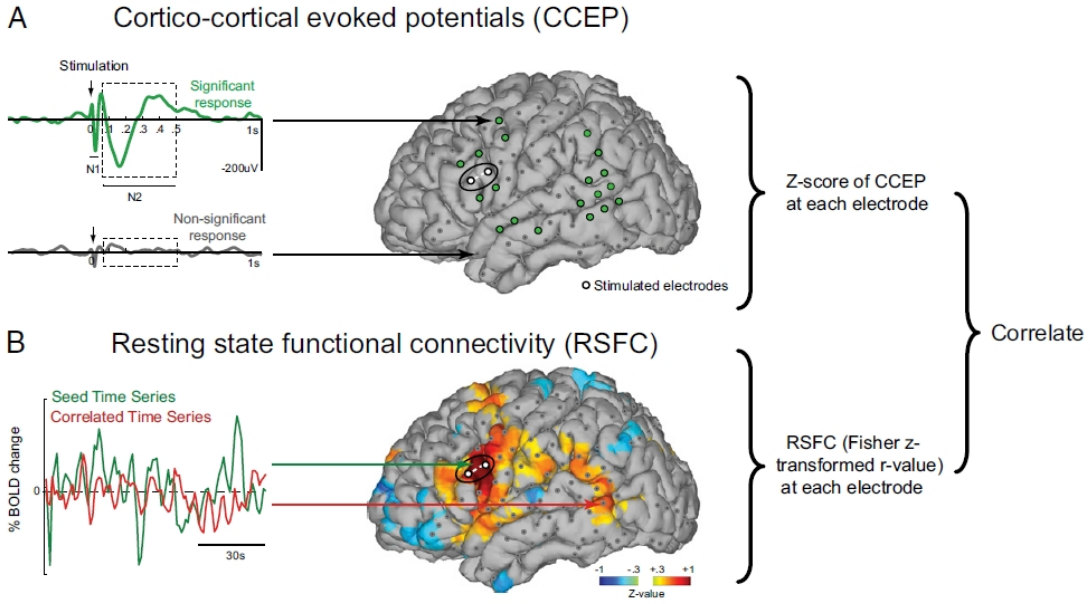

Fig. 34. Analysis schematic. (A) CCEPs in response to single-pulse electrical stimulation of each electrode pair were recorded at all implanted electrodes. For visualization purposes, the locations of significant responses were overlaid onto the individual’s reconstructed pial surface. The magnitude of CCEPs at each electrode was computed as a z score relative to baseline of each stimulation site. (B) RSFC maps associated with spherical ROIs underlying the stimulated electrodes were computed for each stimulation site. For visualization, the RSFC maps were displayed on the reconstructed pial surface. To examine the correlation between RSFC and CCEP values, Fisher’s z-transformed correlation coefficients were extracted from the voxels underlying each electrode and correlated with the CCEPs recorded from the same electrodes. The schematic shows data from Subject 1 (Pt. 10) as an illustration.

For each stimulation site, we first computed the correlation between CCEP amplitudes and RSFC values at each electrode without applying any thresholding (Fig.35, c). The average correlation across all stimulation sites was significant in all subjects, [S1: t(44)

= 37.9, P < 0.001; S2: t(15) = 36.7, P < 0.001; S3: t(39) = 26.5, P < 0.001; S4: t(35) = 23.9, P < 0.001; S5: t(20) = 41.9, P < 0.001; S6: t(25) = 53.4, P < 0.001] as well as across all six subjects [t(5) = 21.4; P < 0.001] indicating that correlations between RSFC correlation values and CCEP amplitudes are present independent of the stimulated brain area. Next, we computed a binary response matrix for each stimulation site by identifying the electrodes that exhibited a significant CCEP (see Methods for details of thresholding). In all but one patient, electrodes exhibiting a significant CCEP demonstrated higher RSFC relative to those which did not exhibit a significant CCEP (*P* < 0.05; Fig.35, a). As is to be expected, the strongest CCEPs and RSFC were observed in electrodes proximal to the stimulation (and 'seed') site. To rule out the possibility that the CCEP/RSFC relationship is based only upon local properties, we repeated the comparison between RSFC and CCEP excluding those within 25mm of the stimulation site. Although RSFC decreased overall, correlations between CCEP and RSFC remained significant (*P* < 0.05; Fig.35, b). Additionally, regression analysis demonstrated that the CCEP/RSFC relationship remained highly significant after the effect of distance was removed from both CCEP responses and RSFC values by regression.

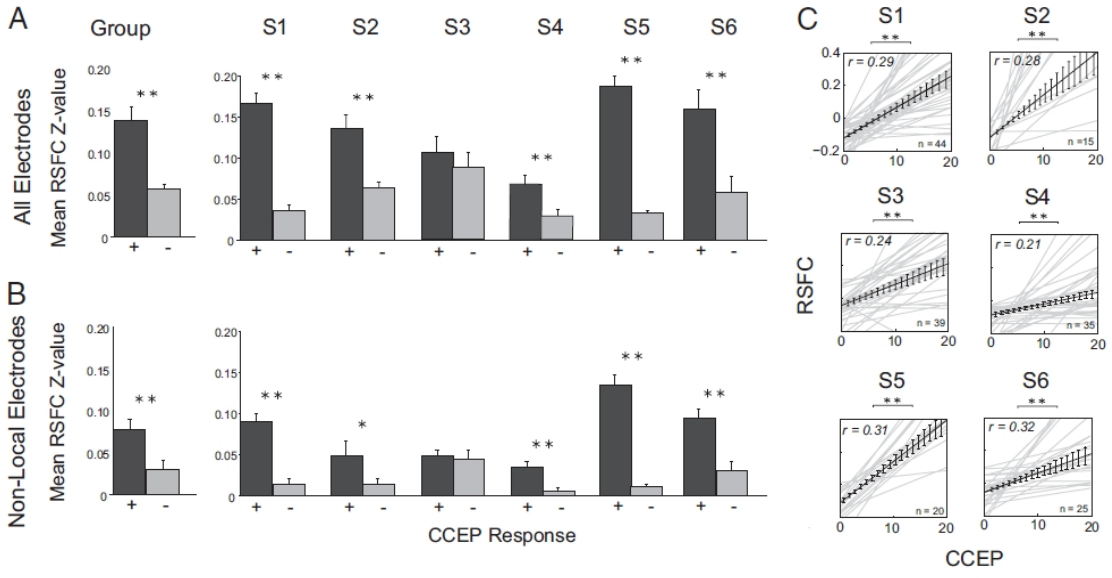

Fig. 35. Relationships between CCEPs and RSFC. (A) Group and single-subject analysis. Across all stimulation sites, electrodes exhibiting significant CCEPs (+, dark gray bars) also exhibited significantly higher RSFC z values than electrodes exhibiting non-significant CCEPs (−, light gray bars), at the group level t(5) = 9.3,

P < 0.001, two-tailed t test), and in all but one of the six individual subjects (S1–S6; *P<0.05; **P<0.01). (B) Exclusion of proximal electrodes. Significantly higher RSFC z values were still observed at electrodes exhibiting significant CCEPs after excluding electrodes within 2.5 cm of the stimulation site (P<0.001, two-tailed t test). (C) Correlation between RSFC and CCEPs. We computed the correlation between CCEP amplitude and RSFC, across all electrodes, for each stimulation/seed site in each subject, regardless of whether a significant CCEP response was observed (gray lines). Two-tailed t tests indicated that the mean relationship across all sites (black line) was significant in each subject (all P<0.001) as well as across all six subjects [t(5) = 21.4, P < 0.001]. By including all electrodes, this correlation is independent of a priori assumptions implied by amplitude thresholding. The mean r-correlation value of all trend lines is reported for each subject (n = number of trend lines = number of stimulation sites). CCEPs are reported as z scores, and RSFC is reported as a Fisher's z value. Patients S1-S6 are the same patients as Pt10-15.

Finally, to assess the correspondence between the spatial distribution of significant CCEPs and RSFC over established functional networks, electrodes overlying expressive and non-expressive language areas as well as hand motor areas were identified using electrical stimulation mapping (ESM, see Methods). For each of these identified electrodes, maps of significant CCEPs and RSFC were calculated and overlaid onto the brain surface (Fig.36). Each figure shows the tight correspondence between spatial distributions of the CCEP and RSFC maps associated with those electrodes. The spatial correspondence is perhaps most impressive for networks associated with expressive (Fig.36, a) and non-expressive (Fig.36, b) language regions, as both methods elicited reciprocal networks of language areas including ventrolateral prefrontal cortex, inferior lateral parietal and temporo-parietal cortex, and superior and middle temporal cortex, in line with previous studies (Kelly et al., 2010, Koyama et al., 2010). Similarly, seeds placed in the hand motor area were associated with significant RSFC across adjacent primary and secondary motor and somato-sensory areas, premotor cortex as well as more distal posterior parietal and lateral prefrontal regions (Fig.36, c), also consistent with previous studies (Biswal et al., 1995, Fox and Raichle, 2007).

DOI:10.14753/SE.2015.1798

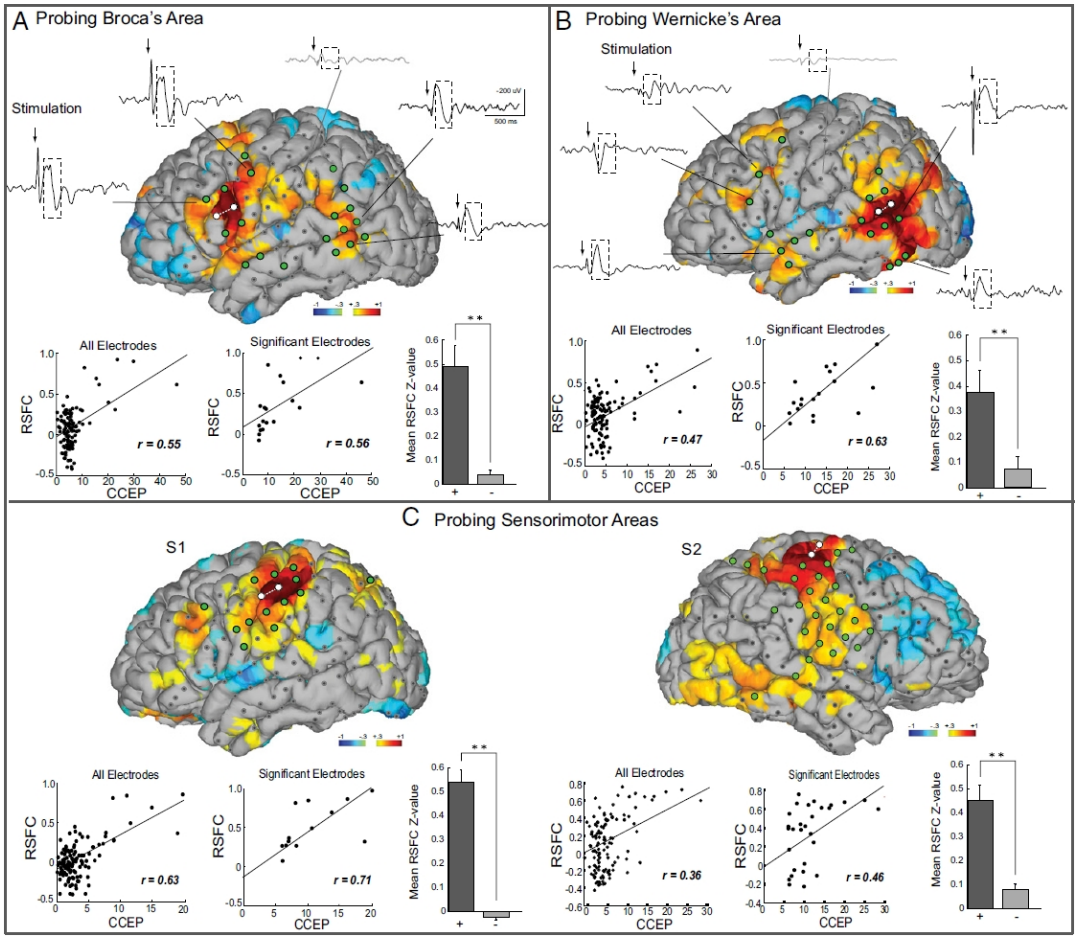

Fig. 36. Probing Broca's area (A) and Wernicke's area (B) in one patient (S1=P10). Patterns of CCEPs and RSFC are overlaid onto subjects' pial surfaces. Selected significant (black lines) and non-significant (gray lines) evoked potentials are shown. The dotted boxes designate the area of interest for determining the significance of the evoked potential (corresponding to the N2 phase). Significant CCEPs (green circles) were observed in close proximity to the stimulation site (e.g., Broca's area) but also in spatially distal areas (e.g., posterior middle and superior temporal cortex). The gray dots indicate electrodes with non-significant CCEPs. Areas exhibiting significant RSFC with the seed ROI underlying the stimulation site are shown in yellow/red (positive RSFC) and blue (negative RSFC). Note the striking overlap of electrodes exhibiting significant CCEPs and regions exhibiting significant RSFC. The scatter plots show the relationship between the RSFC Fisher's z values and CCEP z scores for all recorded electrodes (Left) and for electrodes that exhibited significant CCEPs (Right). The bar graphs show the mean RSFC z values for significant (black) and non-significant CCEP electrodes

[P < 0.001]. (C) Probing sensori-motor areas. The remarkable overlap between patterns of RSFC and CCEPs was also observed using seeds and stimulation sites in sensori-motor areas. Examples from two subjects (Pt10 and Pt11) are shown. CCEPs are reported as z scores, and RSFC is reported as a z-correlation value.

4.6 Anatomico-functional parcellation using graph theoretical measures

4.6.1 Evoked potentials *demonstrate reliable cortical connectivity*

We recorded consistent and statistically significant CCEPs in each of our patients implanted with subdural electrodes. By the following modified criteria (N1 and N2 peaks exceeding 3SD of the baseline), 36% (1012/2505) of N1 and 60% of N2 connections were significant. The time delay from the stimulation artifact for the N1 peak ranged from 10.0 to 49.5ms (median: 21.2ms) and 50.3 to 499.5ms (median: 167.0ms) for the N2 peak. Stimulation at 10mA never resulted in obvious epileptiform discharges for 1088 stimulation sites that were performed outside the epileptogenic zone in 25 patients (see methods).

In order to account for the different CCEP field distributions derived from the same stimulation site using multiple series of stimulation, we computed the intra-subject reliability based on CCEP mapping sessions performed on multiple days in a single patient. CCEP maps recorded on 3 different days within a period of 5 days demonstrated >70% similarity for N1 (70% between day 1 and 4, 71% between day 1 and 5 and 74% between day 4 and 5) and over 75% similarity for N2 (day1-day4: 75%, day1-day5: 76% and day4-day5: 77%).

4.6.2 Evoked potentials demonstrate asymmetry across distributed networks

In general, CCEP connections were often found to be asymmetric (one CCEP connection was stronger than the opposing CCEP connection) based on amplitude criteria. Figure 37 depicts the asymmetry of N1 connections (if in one direction the amplitude exceeded 3SD) with 81% of connections showing a >50% difference and 88% showing a >30% difference in z-scores between directions. A similar profile was

DOI:10.14753/SE.2015.1798

seen with the N2 (not shown), with 73% of connections demonstrating a >50% difference and 82% demonstrating a >30% difference in z-scores between directions.

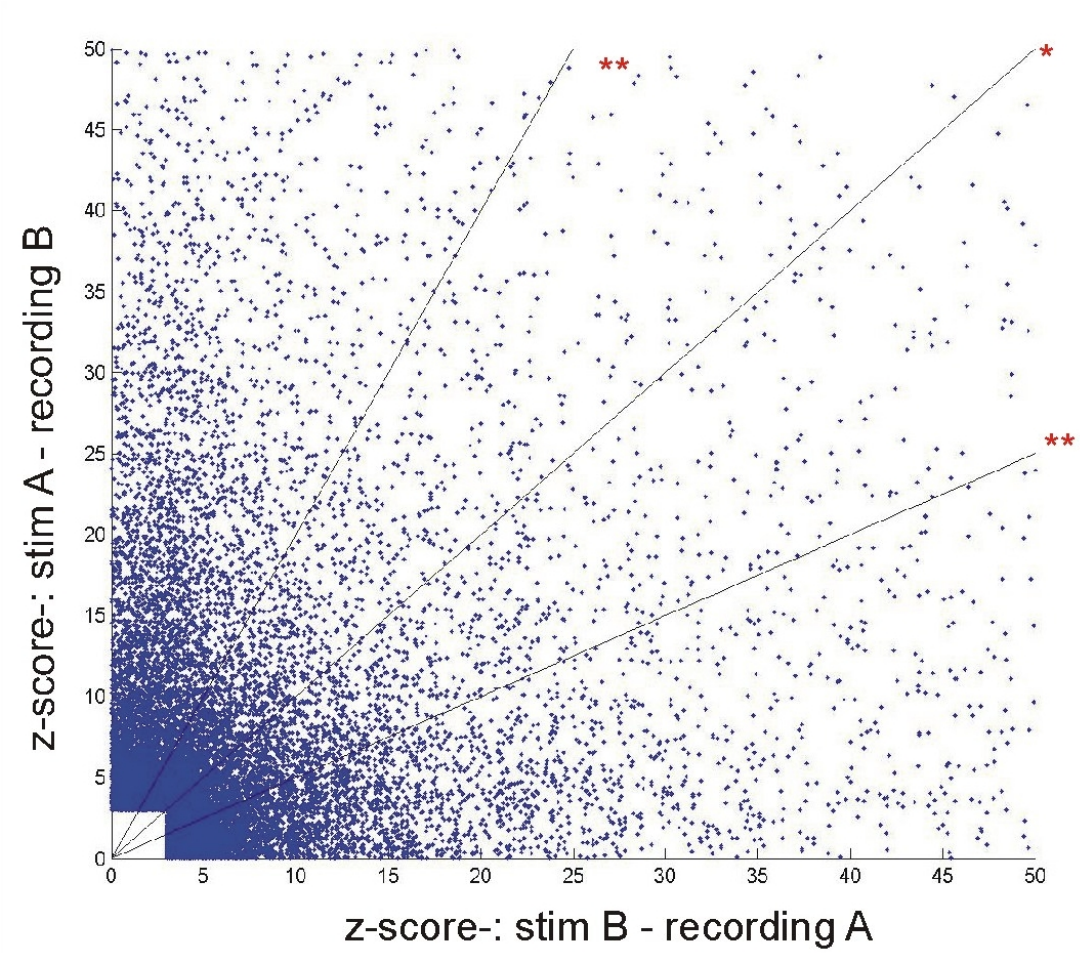

Fig. 37. Defining reciprocity on single electrode level based on N1. Z-scores of all reciprocal connections (at least one direction must fulfill a criteria of 3SD). No linear correlation was found between z-score pairs of reciprocal connections (R2=0.011), which corroborate the directedness of these connections. Diagonal (*) represents connections with equal amplitude, lines above and below (**) represent the threshold for 50% difference in amplitudes.

DOI:10.14753/SE.2015.1798

4.6.3 Effective connectivity decreases with distance

Distances between electrode sites were calculated using the Euclidean distance between the midpoint of the two stimulated electrodes and the center of the recording electrode (Matsumoto et al., 2004). This distance was always the shortest possible route between the two nodes irrespective of the convolutions of the brain. Figure 38 shows that the strength of CCEPs significantly decreased as a function of this distance between stimulating and recording electrodes ($p<0.01$; ANOVA Kruskal-Wallis test). Of all connections that were considered significant, a larger proportion of significant connections were observed locally (<2cm) compared to long-range (>8cm) (67% and 27% for N1, 83% and 51% for N2 respectively). Both in- and out-degree measures were found to be significantly higher for local interactions than long-range connections ($p<0.01$; ANOVA Kruskal-Wallis test). Connectivity appeared to be longer range when considering the N2 component relative to the N1 component, with no observable difference between in- and out-degree connections as a function of distance. We found significantly higher indegree and outdegree for the N2 than the N1 at every distant bin measured (N1 vs. N2 $p<0.02$, Kolmogorov-Smirnov test).

DOI:10.14753/SE.2015.1798

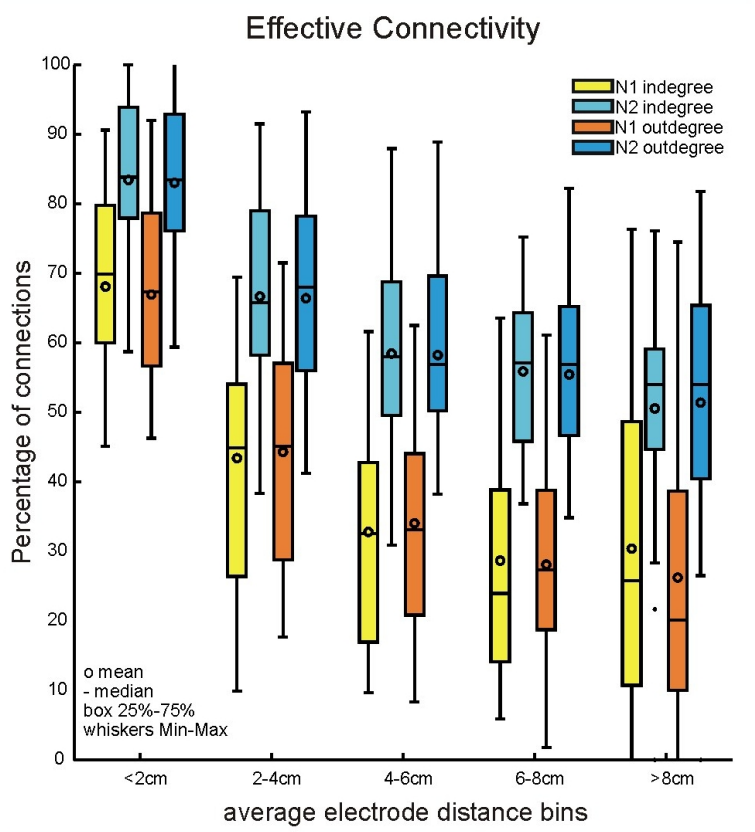

Fig. 38. The bars with lighter colors illustrate the normalized indegree as a function of distance, while the bars with darker colors show the normalized outdegree. CCEP distributions are computed in 2cm bins. Errorbars denote minimum and maximum values. The difference between N1 and N2 is significant in every distance bin ($p<0.05$, Kolmogorov Smirnov) and both for indegree and outdegree. The decrease in connectivity is also significant between the (<2cm) and the (>8cm) bins ($p<0.01$; ANOVA Kruskal-Wallis test) for indegree and outdegree and for N1 and N2 as well.

4.6.4 Connectivity Analysis of the N1 component

As the N1 is considered to reflect the afferent volley of excitation to a given area (Creutzfeldt et al., 1966, Matsumoto et al., 2004, Logothetis et al., 2010), we first analyzed this component in order to assess connectivity. CCEP connectivity was assessed creating a connectivity matrix of z-scores for stimulated and recording BA's for each individual (Fig.39). This yields a relative strength of connections that can be

DOI:10.14753/SE.2015.1798

normalized by z-score for each pair of BA's tested for connectedness. To account for variability in electrode placement, indegree for each BA was normalized by dividing the number of incoming connections by the total number of connections tested. Similarly, outgoing connections from each BA were also normalized by the total number of possible connections within that specific patient.

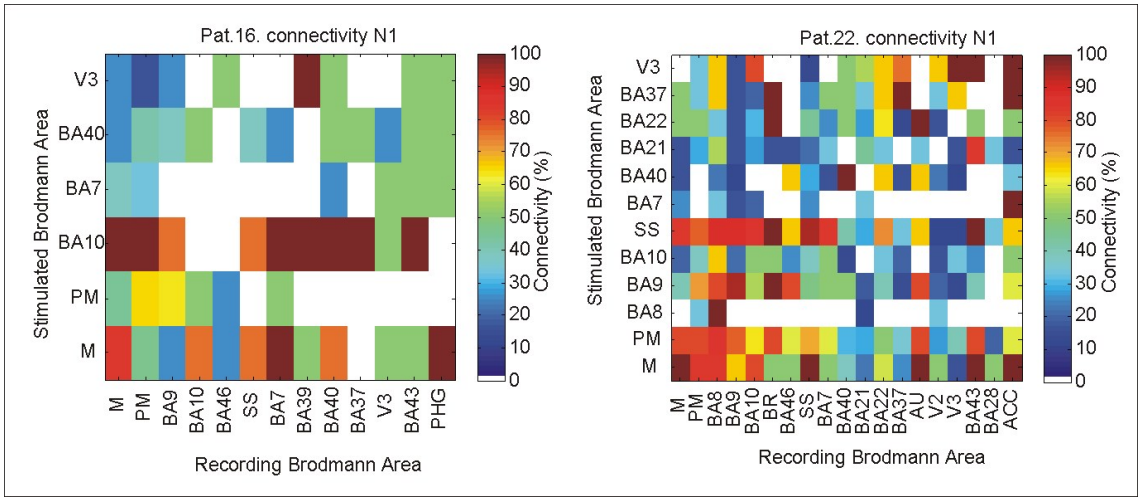

Fig. 39. Connectivity matrices for two representative patients. The matrix shows the connectivity (percentage of connections showing an amplitude of greater than 3SD for the N1 peak versus all possible connections) between regions covered with electrodes.

The CCEP matrix of z-scores for each patient were averaged together to create a group-level CCEP matrix (Fig.40). In general, the largest average z-score values for connectivity were observed between the lateral portion of the frontal, temporal and parietal lobes, with z-scores>12 measured between SS, BA6, BA9, BA40, Heschl's Gyrus and motor cortex. Stimulation of BA 20 revealed strong connections with broad regions of the frontal, temporal lateral and medial, parietal and occipital lobes, while BA 21 and 22 showed the strongest connections with Heschl's gyrus and only moderate connectivity with other cortical areas. Intralobar connections were strong within the occipital lobe. Stimulating V2 and V3 (V1 was not tested) showed strong intralobar connectivity and very well circumscribed strong connections to few regions including Heschl's Gyrus and posterior cingulate areas for V2 and BA22 and 37 and the posterior cingulate areas (for V3) (Fig. 40 for N1 with a threshold of 6SD for better specificity). A directedness of connections is evident between a number of areas. For example,

DOI:10.14753/SE.2015.1798

stimulation of the prefrontal cortex (PFC) results in a larger response in the middle temporal gyrus (BA21) with an average z-score of 10.17 (N1), but the strength of the connection in the opposite direction is weaker, with stimulation in BA21 producing an average z-score of 6.25.

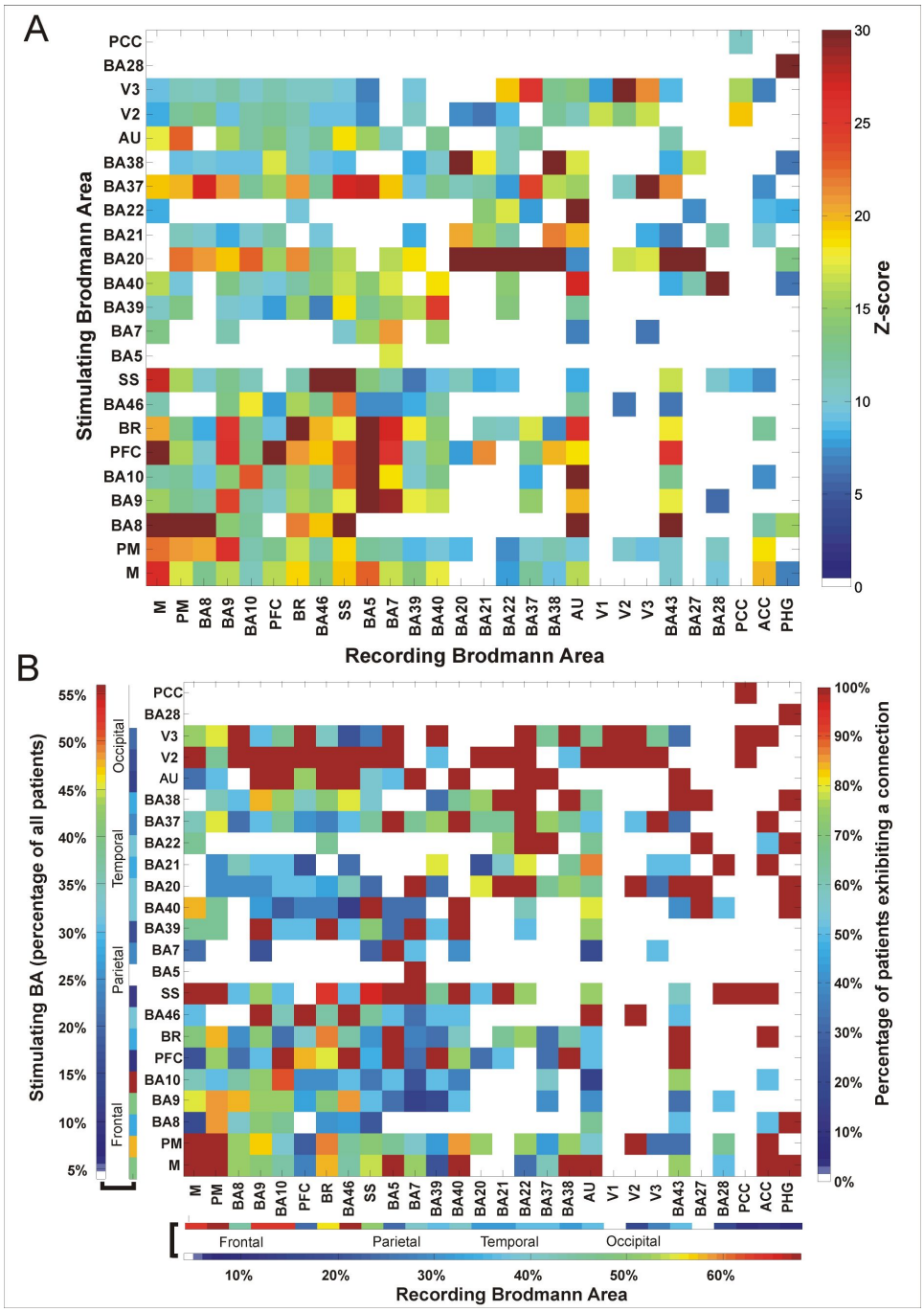

Fig. 40. A: Matrix shows the average z-score between and within regions using the N1 peak as the measure of connection (only z-scores above 6 are shown to highlight stronger connections). B: Evokability of connections between different regions and

BAs. The connectivity matrix represents the percentage of patients that elicited CCEPs >6SD between different BAs using N1.

Consistency of connections across subjects is shown in Figure 40B. Using a 6SD criterion, stimulating BA4 or BA6 resulted in significant CCEPs at almost all recorded BAs, including each other (8/10 subjects). Both BA4 and BA6 demonstrated consistent outgoing connections to BA 9 (11/11 subjects for area 6; 7/8 subjects for motor), BA 10 (9/10 subjects for area 6; 8/9 subjects for motor), BA 46 (9/11 subjects for area 6; 8/10 subjects for motor) and Broca's area (7/9 subjects for area 6; 6/7 subjects for motor). In four subjects with coverage over the posterior cingulate area (a central node of the default mode network; (Fox et al., 2005) all showed responses upon stimulation of the lateral fronto-parietal neocortex.

4.6.5 Connectivity analysis of the N2 component

A separate z-score matrix was created for the N2 peaks to evaluate differences in connectivity during the different time frames. Figure 41 shows the corresponding analyses for the N2 component. N1 connectivity is largely mirrored by analysis of the N2. However we found broader distribution of reciprocal connections with the N2, which could be the result of the yet less understood subcortico-cortical connections as indicated by Figure 41.

Analyzing the N2 component similarly to N1 revealed the central role of the motor, premotor and somato-sensory areas as well, which was very consistent across patients as seen in Figure 41B. Although there are many similarities there are some differences as well. For example stimulating BA20 revealed very strong connections to BA21, 22, 37 and 38 when looking at N1, with the N2 analysis although these connections were present only BA37 showed a very strong connection. When stimulating the somato-sensory (SS) cortex N2 analysis revealed very strong connections to BA7, 39 and 40, which were present when analyzing the N1 but only with lower z-scores, not indicated as a strong connection. A very well studied connection between Broca (BR) and Wernicke (BA22) showed average or lower strength with the N1 analysis, on the other hand it was shown to be very strong with the N2 measurements in both directions.

DOI:10.14753/SE.2015.1798

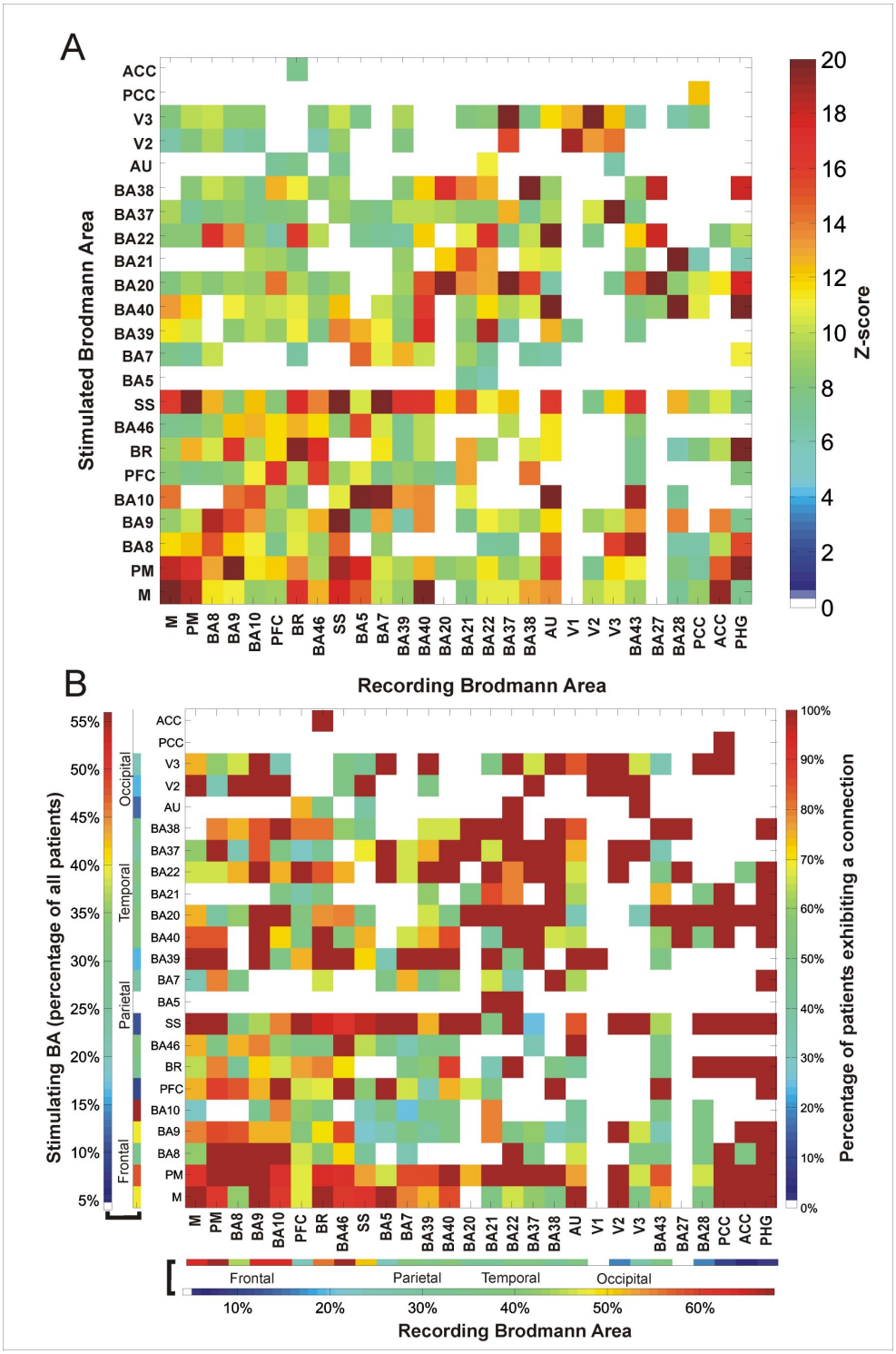

Fig. 41. *A: Matrix shows the average z-score between and within regions using the N2 peak as the measure of connection (only z-scores above 6 are shown to highlight stronger connections). B: Evokability of connections between different regions and BAs.*

The connectivity matrix represents the percentage of patients that elicited CCEPs >6SD between different BAs using N2.

4.6.6 Hubs of connectivity

Next, we localized regions exhibiting the highest degree centrality (cortical hubs) across patients. Somatosensory, motor, premotor area and BA9/10 were identified as cortical hubs (major hubs were defined as those BAs which exhibited total degree measures above the 95th percentile of the maximum) using both the N1 and N2 peak. When hubs were computed using the N2, they were found to be located in Broca's and Wernicke's area as well as portions of the temporal (BA21, BA22) and parietal (BA40) lobes. We do not believe this to be a sampling issue only since there are regions including BA20 and BA38, which were densely sampled in many patients, and were not found to be hubs using this analysis.

After identifying major hub regions (Figure 42; PM, BA9, SS, M, BA10), we examined the network topology within specific functional networks. Areas with eloquent function including motor (BA4, BA6) and language areas (Area: Br and BA22) exhibited more central positions. BA20 and BA9 also occupied central positions in the network.

DOI:10.14753/SE.2015.1798

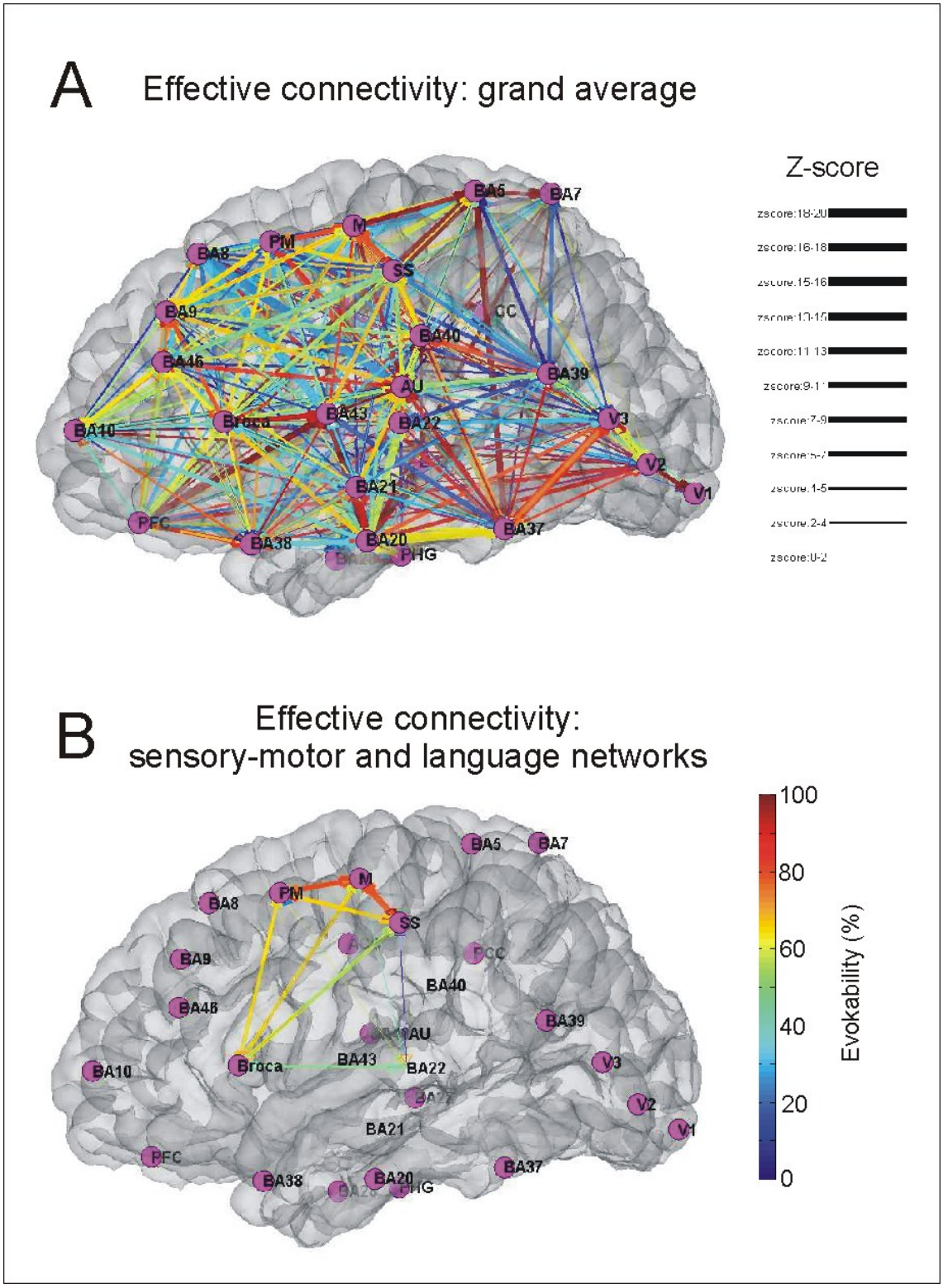

Fig. 42. Expressing directional connections between areas using the group average. A: Graph shows the connections between BAs, based on the connectivity matrix derived from the stimulation data. Grand mean average of all patients is shown for the N1 peak. B: the connections between the somatosensory and motor and the

areas involved in speech and comprehension are highlighted only. The color of the edges represent the evokability (warmer colors represent higher percentage of patients exhibitng the connection), the width of the edge highlights the average z-score between the two areas.

4.6.7 Directedness of Brodmann Area connections

In order to estimate the directedness of connectivity between BAs, a directionality index (DI) was computed as the ratio of the average z-score of the outgoing and incoming connections for each BA for both the N1 and N2 components. Accordingly, a DI greater than 1 represents relatively greater outgoing connections. If the mean strength of all CCEPs for a BA-BA connection did not exceed the significance threshold of z=3 at least in one direction, the directionality index of this connection was not calculated as it is difficult to confidently assess directionality with non-significant CCEPs. 30.4% of BA's exhibited a >50% difference between indegree and outdegree connections and 43.4% of BA's showed a >30% difference using N1. Differences between in- and out-degree for the N2 were 20.8% and 50% of BA's for >50% and >30% of areas, respectively. The distribution of DI's according to BA's is shown in Figure 43 for both the N1 and N2 components. BA 20, 39, V2, showed a large out/in ratio with both analysis (N1 and N2), while the superior temporal gyrus (AU: BA41 and42), some frontal areas (BA5, BA7) and the cingulate cortex demonstrated smaller out/in ratios with both analysis. Interestingly the amplitude differences (z-score) changed dramatically for the motor and premotor cortex between the two methods. Motor areas are showing larger amplitudes for incoming connections with the N1 analysis compared to N2, where outgoing connections evoke larger amplitude CCEPs compared to incoming connections.

DOI:10.14753/SE.2015.1798

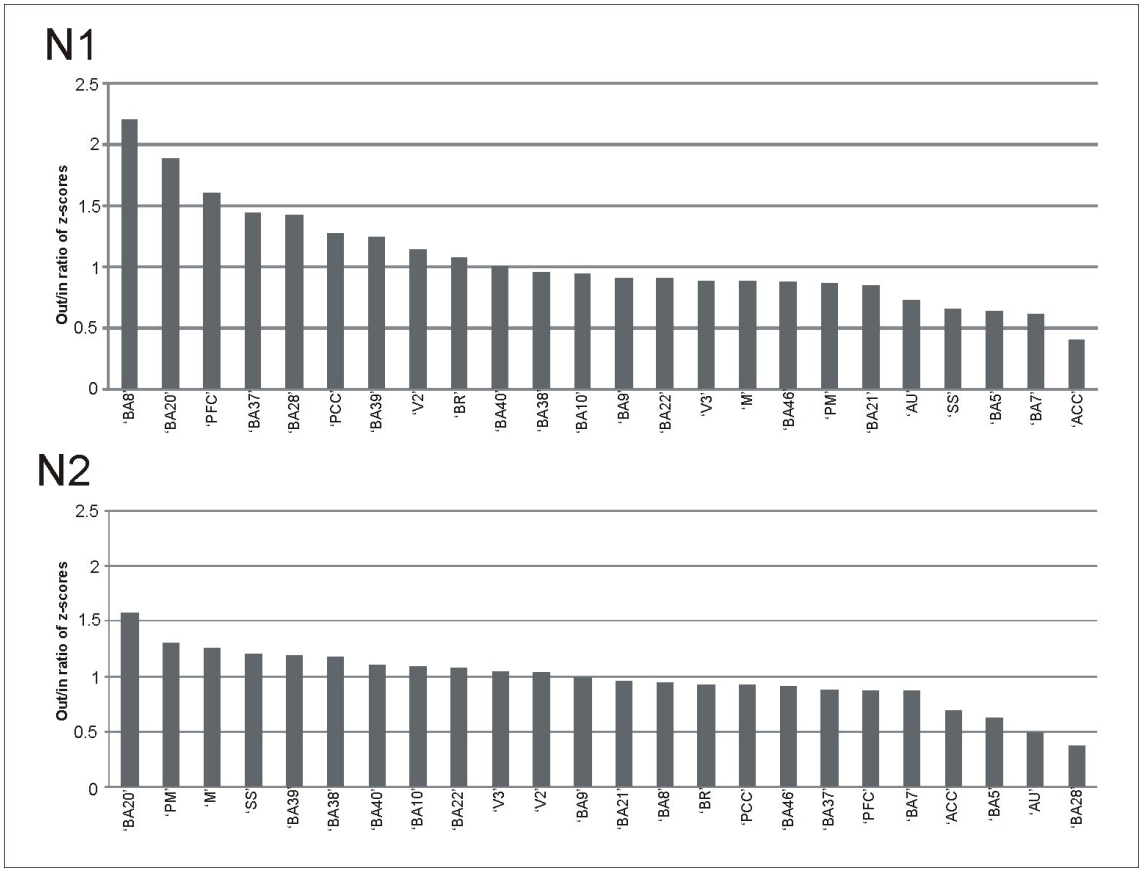

Fig. 43. *Directedness of connections derived from out/in ratio of average z-scores for every region. Upper part show the results for calculating the N1 peak of the CCEP. Lower part represents the results for using the N2 peak of the CCEP. Numbers below 1 represent regions that have higher z-scores for the incoming connections. Numbers above 1 show higher z-scores for the outgoing connections. Only regions with actual values are displayed. Temporal, somato - motor and -sensory regions, but also parietal regions show higher values for outgoing connections and frontal and some temporal regions show higher values for incoming connections.*

DOI:10.14753/SE.2015.1798

5 Discussion

Long time has passed since Dr. Bartholow applied electrical current on one of his patient's brain during an operation in 1874. The effects of direct electrical stimulation of the brain has been widely studied throughout the years. Electrical stimulation mapping is now routinely used in the operating room either on anesthetized or awake patients and also outside of the operating room on epilepsy surgical candidates with implanted electrodes. Electrical stimulation is now not only used as a diagnostic method, but also increasingly applied in selected diseases as a treatment modality. Neurosurgery has developed tremendously over the past decades with ever growing use of the technical advancements during the procedures and treatments. Electrical neuromodulation is now safely used and offered to the patients with epilepsy, movement disorders, psychiatric disease or pain syndromes and the list is growing. During the years epilepsy surgery was always at the fore front of neurosurgical innovations due to the very complex nature of the disease. Surgeons and epileptologists/electrophysiologists were always driven to get closer to the understanding of epilepsy, why some patients after a successful surgery lived seizure free and some worsened. Penfield and Jasper as the founders of modern epilepsy surgery has developed a method to be able to map the cortex before the actual resection would take place. The introduction of intracranial (subdural) electrodes was a milestone in the history of epilepsy surgery. Using the implanted electrodes patients could be observed during their normal daily routine, while having the electrodes over the areas involved in epileptic activity. The electrodes made possible besides the recording of the electrical activity of the brain also the stimulation of the cortex with electrical current. Initially the primary goal of stimulation was to localize the areas of the brain bearing essential functions, such as motor, sensory or language beside others, together also called eloquent areas. With growing stimulation experience the initial use of electrical stimulation has been extended to other aspects of the effect of the current to the brain, such as the stimulation of the epileptogenic area, which may provoke a seizure or electrographic elements which can be the sign of the epileptogenic area. The different epilepsy surgical centers developed their own methods how to perform electrical stimulation mapping in order to reveal eloquent and epileptogenic areas.

In the early 2000's Valentin and his colleagues proposed a new method, which can be used without producing behavioral changes to the patient, but still might be useful for localizing epileptogenic areas (Valentin et al., 2002) by applying brief, single current pulses to the cortex and assessing the responses within 1s after stimulus. SPES became an alternative option and completion to high frequency electrical stimulation in more and more centers due to the growing evidence behind the localization value and cortical mapping value of the evoked responses after the stimulation. The parallel work of Valentin and colleagues and Lüders's group in the usefulness and clinical application of SPES is still not combined as well as the fundamental work of the neuroscientists on the electrophysiological properties of the evoked cortical slow oscillation. This work tries to bridge the different concepts behind the same electrographic phenomenon by applying unique methodologies such as multielectrode recordings from the different layers of the human cortex or comparison of the evoked potential distribution with the results of the analysis of the BOLD fluctuations recorded with fMRI while the patient was at rest.

5.1 General considerations about the effects of SPES on the neocortex recorded with electrocorticography and with a laminar multielectrode recording system in the deeper layers

Our major aim was to study the effects of SPES on the human brain, investigated with subdural and intracortical microelectrodes. We first gave detailed analyzes of the different aspects of the stimulation on the evoked potential. We described the properties of the SPES evoked cortical potential and gave the timeframe of the N1, N2 peak on average in our patient population. We found that the N2 peak appears between 150-200ms on average,. We also looked at the amplitude relationship between the Z-score of the N2 peak and the distance from the stimulation electrodes, which showed some linear anticorrelation, but it was not significant. Applying increasing amount of current does increase the amplitude of the N2 peak, but only up to 9ma. Above 9ma we could not register significant changes. We based our stimulation protocol on this evidence, which we found suites better the needs of comparability among patients and sites compared to the adopted stimulation amplitude used by other centers published in the literature

(Valentin et al., 2002, Matsumoto et al., 2004, Flanagan et al., 2009, Enatsu et al., 2011). We did not observe any evoked seizures or significant behavioral changes with the 35 patients, having over 60 stimulation sessions performed which justifies our protocol.

We first published in the literature the effect of the different vigilance states on the evoked potential. Contrary to the animal literature (Vyazovskiy et al., 2009) and also with the TMS and tDCS studies (Marshall et al., 2004, Marshall et al., 2006, Massimini et al., 2007) a CCEP could also be evoked during awake state and the shape and the latencies did not differ from the one recorded during non-REM sleep.

The potential map of a 48 channel grid electrode did reveal the differences between the N1 and the N2 wave. The N1, which is between 10-40ms is much more circumscribed and therefore represents local activation of the cortex rather than inducing wide spread network changes. On the other hand the potential map of the grid at the maximum of the N2 wave reflects a wide spread hyperpolarization of the cortex even 5-15cm away from the site of the stimulation. In agreement with the propagation patterns revealed during human slow wave sleep, we hypothesize the role of cortico-cortical but also cortico-thalamo-cortical networks in the generation of these potentials. Given the average latency of the N2 peak is between 150-200ms this delay might be the cause of the complex multisynaptic activation needed to generate the N2 wave across the hemisphere and sometimes including the other hemisphere as well, although N1 waves were also recorded contralaterally using subtemporal strips (Umeoka et al., 2009).

Our findings with the time frequency analysis of the subdural electrodes show excellent correlation with the ME recordings from the superficial layers. The wide band power spectrum decrease between 0-200Hz has the same latency as the one recorded in the deeper layers, which is then followed by a rebound power increase. This oscillatory silence is very similar to the one observed during spontaneous sleep (Csercsa et al., 2010).

5.2 Laminar analysis of human Slow wave activity and comparison with the evoked SO

5.2.1 Epilepsy and SWA

Epilepsy is a multi causal disease with diverse etiology. Focal epilepsies have circumscribed seizure initiating regions without severe pathological alterations in other areas. Surgical candidates are selected exclusively from this patient group during the careful pre-operative evaluation, based on several diagnostic findings (CT, MRI, fMRI, PET, SPECT, video-EEG, MEG, functional neurophysiological tests, Wada-test (only at NSLIJ) and seizure semiology). In the present study we included only patients with evidence for focal disease.

The laminar LFPg, CSD, MUA and spectral profile of interictal activity in vivo and in vitro has already been established by our group (Ulbert et al., 2004a, Ulbert et al., 2004b, Fabo et al., 2008, Wittner et al., 2009). We have shown that the initial phase of the interictal discharges are large amplitude brief events characterized by substantial action potential, LFPg, CSD, MUA and spectral surges, often emerging from the granular and infragranular layers of the cortex (Ulbert et al., 2004a). These events are clearly distinctive from the background activity and exquisitely visible in single sweeps. Based on our prior knowledge, we carefully excluded any suspicious pathological events from the analysis presented in the current study, and we also carefully avoided analyzing data derived from electrodes in the proximity of the seizure focus.

Several other considerations suggest that the findings on the neuronal mechanisms underlying SWA, although recorded in epileptic patients, might also apply to healthy subjects. Our SWA morphology corresponded well to those oscillations collected from standard scalp sleep EEG recordings from healthy subjects. Similarities included not only the SWA frequency and rhythmicity (Achermann and Borbely, 1997), but the asymmetric shape, the briefer and sharper deflection in the down-state (Massimini et al., 2004) and higher beta power content in the up-state (Molle et al., 2002). Our results of detection frequency, cycle length and interdetection interval histograms are all comparable with previous findings from healthy subjects (Massimini et al., 2004), despite both the recording and analysis methodologies being different. Minor deviations in the exact numbers are therefore natural and may reflect methodological differences rather than disease related alterations. In addition, neither the firing rate, nor the burst rate exceeded the pathological criteria found for single neurons in SWS (Staba et al., 2002). Finally, the lack of any MRI abnormalities and intact laminarization of the

excised tissue strongly suggests that we recorded from structurally intact regions, free of gross functional alterations.

5.2.2 Comparison of the evoked SO with the spontaneous SO recorded during slow wave sleep

We reported in 2010 our findings on the laminar properties of human slow wave sleep, which shows remarkably similar properties to the evoked N2-P2 waveform (Csercsa et al., 2010). Human slow wave sleep is characterized by a cortical down-state and an up-state. The properties of a downstate is neuronal silence in the middle-upper layers, outward currents from neurons and wide band power decrease on the time-frequency analysis, which are also the properties of disfacilitation (Contreras et al., 1996). According to these criteria we can state that the electrical stimulus evoked cortical potential N2 is a single down-state of a slow oscillation cycle, because the laminar profile we recorded under N2 is the same as it is described here. A cortical up-state is characterized by excessive neuronal firing, inward currents on the CSD and spectral power increase. This all also describes the laminar phenomena observed under the P2 phase of the CCEP, so P2 is also an up-state.

If an evoked N2 is a down-state and the evoked P2 is an up-state, the mini-oscillation we were able to evoke with a single electrical stimulus of the cortex is a single cycle of a slow oscillation. This has never been shown before in humans.

We already know that transcranial electrical and transcranial magnetic stimulation can increase the slow wave activity during non-REM sleep in healthy volunteers, but we do not know what is the exact physiological mechanism underlying this phenomena. According to our finding the common pathway could be the wide spread inhibition of active neuronal elements in almost every layer of the neocortex. This synchronous network event might start the down-state which, using the same mechanisms revealed by Steriade (Steriade et al., 1993c) turns slowly in to an activation process and switches over to an up-state with massive neuronal firing. If the network properties of the local events allow this hyper-synchronous state, than the first cycle is followed by a second and sometimes a third one.

The fact that we were able to evoke the same cortico-cortical potentials also in fully awake state is a new evidence of the general inhibitory mechanisms of the cortex as an

answer to any type of external distracting stimulus (Cash et al., 2009). This common mechanism is so strong that it can even override the actual local processes and put the whole area in to neuronal silence.

The evoked SO shares many features of the spontaneous SO revealed with the laminar and ECoG analysis of the electrophysiological changes. Beside these fundamental similarities the propagation of the evoked potentials over cortical regions might also reflect the same local and global neural networks as the spontaneous SWA. According to the results of the information based analysis of SWA propagation patterns the described local and noncontiguous spread of the SO might be conducted through corticocortical and also cortico thalamocortical pathways. Since the delay of the evoked SO is between 100 and 250ms on average this time window may be necessary to activate complex networks, which can also be modulated by thalamocortical pathways.

5.3 Complex propagation patterns of human slow wave sleep reveals the local and global operations of cortical networks

Here we analyzed the ECoG patterns of sleep slow waves in humans using a nonlinear correlation technique based on mutual information calculations supplemented by linear correlation measures. While high-density scalp EEG provides nearly complete spatial coverage over both hemispheres with a spatial resolution of ≈ 2 cm at the level of the scalp, its localizing capacity is hampered by the spatial smoothing effects of the scalp, skull, pia, and CSF. In contrast, while ECoG recordings provide lower spatial coverage, with a higher spatial resolution of ≈1 cm at the level of the cortical surface, it is not burdened by the spatial smoothing effects of the interleaving tissue (Buzsaki, 2006).

Correlations among SWA cycles recorded from different ECoG channels were highest during the first part of the up states where most of the neuronal spiking interactions take place, confirming that this phase of the oscillation provides an optimal window for neuronal interactions (Luczak et al., 2009). It is also in line with previous findings showing that sleep spindles and hippocampal ripples are phase locked to this segment of the slow-wave cycle, indicating that the flow of information both among cortical regions and between the thalamocortical and hippocampal circuits would be connected to the down-to-up state transition period (Molle et al., 2006, Clemens et al., 2007). SWA, recorded by ECoG, showed complex propagation patterns such as convergence,

divergence, reciprocal propagation, and short circles. Correlations were strongest between neighboring recording sites, although unexpected spatial noncontinuities of slow-wave propagation were also observed. Cortical areas were shown to receive convergent activity from other regions as well as to disseminate SWA. Centers (or hot spots) of SWA propagation with high convergence and divergence rates were identified in all subjects. Hot spots were stable during and, although to a lesser extent, across nights. These complex patterns of SWA propagation might reflect the differential aspects of local and global mechanisms of neural interactions revealed by cortical electrical activity during SWS. Our choice of the nonlinear correlation measure was based on our observation and other reports that, in addition to linear associations, nonlinear dependencies are frequently detected among different brain regions during various brain states (Freiwald et al., 1999, Darvas et al., 2009, Chen et al., 2010).

Functional connections are inferred from linear or nonlinear correlation or coherence measures, such as significant short-latency peaks in cross-correlation functions when established between single neurons (Csicsvari et al., 1998, Bartho et al., 2004, Chen et al., 2010) or significant waveform and phase correlations in cases of neural networks or brain areas (Buzsaki, 2006, Womelsdorf et al., 2007, Bullmore and Sporns, 2009, Uhlhaas et al., 2009). Thus, we speculate that nonlinear correlation of SWA activity might reflect functional connections among brain areas. Associations reported in this study may be mediated by both corticocortical and cortico thalamocortical routes of information transmission (Crunelli and Hughes, 2010). Although it is theoretically possible that the two types of communication operate with different temporal delays, consistent bimodality of propagation time distributions could not be revealed. Also, influences of common information sources cannot completely be ruled out (Hangya et al., 2009), although a recent study suggested that such sources do not necessarily cause detectable correlations (Renart et al., 2010).

Based on the concept of traveling waves, a propagating slow wave rarely if ever reenters previously visited cortical sites. However, anatomical studies of cortical structural connectivity show an especially rich repertoire of reciprocal connections and loops within and across brain areas (Bullmore and Sporns, 2009). In concert with the complex patterns of cortical connectivity, we also found a rich source of reciprocal and short circle propagation patterns, which may suggest that electrical activity underlying

neuronal processing was often bidirectional, or reentered previously visited areas. We propose that cortical centers with high convergence and divergence rates might serve as hot spots for neuronal interaction in sleep. This view is supported by the relative stability of these hot spots and their tendency to have a larger correlation with neighboring cortical areas. Spatial distances between correlated channels were found to be short on average, which further emphasizes the importance of the finely structured, local neuronal circuitry in electrical activity pattern generation. Longer range correlations arose occasionally, presumably as a consequence of the communication between high connectivity centers. These associations could appear as noncontiguous propagation between relatively distant areas. This hypothesis is in agreement with previous results showing that local changes in cortical SWA are largely related to daytime experiences (Huber et al., 2004). We did not observe a systematic change of correlation stability with increasing time after the surgery. However, an effect of gradual recovery after the surgical intervention on the stability of convergence and divergence centers cannot be completely ruled out. Although different placements of the electrode grid on the six patients limited the possibilities of mapping hot spots onto anatomical structures, averaging normalized convergence and divergence rates in different Brodmann's areas showed an elevated activity in the ventrolateral and dorsolateral prefrontal cortex. These observations are in accordance with previous studies showing the strong involvement of human prefrontal areas in memory consolidation and related delta band oscillatory activity during deep stages of sleep (Diekelmann and Born, 2010). Our findings are also in agreement with the prominent participation of the middle and inferior frontal gyri in SWS propagation (Murphy et al., 2009). The long-standing observation that sleep is beneficial to remembering (Jenkins and Dallenbach, 1924) has recently been linked to cortical sleep slow waves (Fowler et al., 1973, Marshall et al., 2006). Although large brain areas can engage in synchronous low-frequency oscillations (Sirota and Buzsaki, 2005, Volgushev et al., 2006), a number of studies showed localized increase of SWA after learning correlated with memory performance after sleep (Huber et al., 2004, Schmidt et al., 2006, Huber et al., 2007, Massimini et al., 2009) and references therein). Thus, a growing body of evidence suggests that memory consolidation during sleep involves localized cortical processes, which are accompanied by regional changes in SWA. In addition to reports of SWA

propagation over wide cortical areas (Massimini et al., 2004, Hill and Tononi, 2005, Murphy et al., 2009) propagation dynamics should be examined at a finer spatial scale to detect phenomena possibly underlying local cortical processing (Luczak et al., 2007, Mohajerani et al., 2010). The use of subdural electrode grids, which lack the major drawbacks of scalp recordings, such as spatial smoothing and attenuation exerted by the intermediate tissues (Buzsaki, 2006, Bangera et al., 2010), allowed us to unravel an unexpected complexity of localized SWA propagation patterns, e.g., short circles and convergence– divergence centers. thus, our results provide the first step in filling the gap between global SWA traveling (Marshall et al., 2004) and local operations of cortical networks (Huber et al., 2004, Mohajerani et al., 2010).

5.4 Electrode localization and surface reconstruction to aid surgical planning and research

At the two epilepsy surgical centers we were able to standardize the preoperative and postoperative brain imaging protocols to be able to visualize the implanted electrodes of each individual on the brain surface. The proposed sequence of multimodal imaging enables, beside precise localization of the electrodes on the brain for surgical planning, the co-registration of functional imaging data to the same three dimensional space. This technical advancement can be the basis of the simultaneous interpretation of the results gained with electrophysiology and any type of structural, functional imaging data. One example was the correlation of the spontaneous BOLD fluctuation recorded at rest in an fMRI with the SPES induced evoked potentials (Keller et al., 2011). The technical and theoretical development of functional neuroimaging is a very promising field for the localization of pathological and functional networks (Lo et al., 2010, van den Heuvel et al., 2010, Wen et al., 2011, Zalesky et al., 2011, Zhang et al., 2011). As of now the clinical relevance of these methods is not yet validated (Ruge et al., 1999, Hill et al., 2000), especially for surgical interventions (Roux et al., 2003), but the growing evidence and clinical experience behind these new methodologies will shortly be incorporated in our daily routine. Such highly sophisticated imaging protocols proposed in this work can be the basis of future developments and the unique possibility to combine direct measurements from the cortex (ECoG) with preoperative structural and functional neuroimaging can be the basis of future clinical applications.

5.5 Resting state fMRI correlates with CCEP

Patients undergoing electrode implantation surgery for epilepsy provide an important population from which noninvasive measures of brain function may be validated and understood in greater detail. The clinical situation of poorly-localized seizures provides a unique invasive window into brain function that would be otherwise difficult to obtain. Several previous studies have demonstrated strong similarities between the structure of temporal correlations among low-frequency BOLD RS-fMRI fluctuations and aspects of the electrocorticography (ECoG) signal recorded from patients with implanted intracranial electrodes. Specifically, similarly correlated slow fluctuations have been observed in neuronal firing rates and in the power of local field potentials in the gamma range (40-100Hz) as well as in lower frequency ranges (<4Hz) (He et al., 2008, Nir et al., 2008). Here, we used CCEP mapping, a less conventional method of probing neuronal activity in vivo, to obtain a direct measure of neuronal connectivity and dynamics. Using this method, we demonstrated that the spatial pattern and magnitude of evoked activity in response to direct cortical stimulation was predicted by the pattern and strength of correlations among low-frequency BOLD signal fluctuations. Although epilepsy is likely to have imparted some abnormal properties to the brains of our participants, it is important to note that we demonstrated significant relationships between RSFC and CCEP in each of six individual participants, all of whom had different forms of focal epilepsy, as well as across the entire group of 6 subjects. Our findings provide strong empirical support for the idea that correlated slow BOLD signal fluctuations provide an intrinsic representation of the brain's repertoire of functional responses (Smith et al., 2009). Future work will benefit from the integration of diffusion imaging-based measurement of the underlying white matter connectivity, which provides the structural foundation upon which the functional architecture is built. The integration of such information will allow us to constrain prediction to those connections shown to be linked by a white-matter tract, and will thus likely demonstrate even better correspondence between the intrinsic architecture and evoked responses.

The excellent correlation between two substantially different methodologies (analyzing BOLD fluctuations at rest vs. applying electrical current on the brain) suggest the same intrinsic architecture in the background, which can be observed many different ways. Probably the networks revealed with the two methodologies would correlate also with

the hubs exhibited with the non-linear analysis of spontaneous SWA propagation pattern. Further investigations are needed to demonstrate this relationship, but the very similar behavior of the SWA to the evoked SO or CCEP suggest the same cortico-cortical or cortico-subcortical mechanisms in the background.

Finally, the present findings suggest that RS-fMRI approaches may provide a non-invasive alternative to more traditional invasive measures to clinically map spatially distributed networks underlying brain function and pathological networks underlying seizure spread.

5.6 Anatomico-functional parcellation of the brain

We present a directional connectivity-based map of the human cortex derived from direct electrophysiological recordings of CCEPs in 25 subjects. This is a multicenter, large scale, multi-lobar evoked effective connectivity study in the awake, human brain using subdural electrodes and adds to the literature using this method to explore brain connectivity (Wilson et al., 1990, Matsumoto et al., 2004, Lacruz et al., 2007, Matsumoto et al., 2007, Catenoix et al., 2011, Matsumoto et al., 2012, David et al., 2013). In doing so, we aim to instruct anatomic and functional connectivity maps and other effective connectivity maps based upon non-interventional methods.

Use of CCEP to map brain connectivity

CCEP's have been used in the clinical setting to improve localization of the epileptogenic focus (Valentin et al., 2002) and to predict outcome after epilepsy surgery (Valentin et al., 2005b). Likewise, the use of CCEP to index physiological brain connectivity has been used by the same groups as a corollary measure. These measures may be obtained with minimally increased clinical resources and even less risk to subjects with a benefit at the individual subject level and beyond.

It is believed that direct electro-cortical stimulation results primarily orthodromic activation of axonal efferents due to 1. direct depolarization of pyramidal neurons and 2. indirect activation of pyramidal neurons by activation of interneurons (Jones and Wise, 1977, Matsumoto et al., 2004). While there is likely to be some antidromic stimulation of presynaptic terminals, their relatively lesser size, density and geometrical organization of compared to pyramidal cells makes orthodromic mechanisms more likely to contribute to the CCEP.

Some studies have focused on identifying individual functional networks, such as motor (Matsumoto et al., 2007), auditory (Brugge et al., 2003) and language (Greenlee et al., 2004, Matsumoto et al., 2004). Heschl's gyrus stimulation results reciprocal polymorphic evoked potentials in the posterolateral superior temporal gyrus (Brugge et al., 2003). We replicate this finding of bidirectional connectivity between BA 41/42 (AU) and area 22 and also demonstrate connectivity with Broca's area and higher order extrastriate cortex (V3). Greenlee et. al. (2004) demonstrated a reciprocal connection between inferior frontal gyrus (Broca's area) and orofacial motor cortex. We also demonstrate this finding with bidirectional connections between Broca's area and motor cortex. In the present report, we add to this understanding of Broca's area by demonstrating reciprocal connectivity also with the premotor area (BA6) and by showing an indegree from BA6 and BA 4 (with N2).

In the pioneering studies using this technique by Matsumoto et al. (2004), a reciprocal connection between the classical Broca's (area 44/45) and Wernicke's (area 22/40) area was shown. This finding argued against a unidirectional interpretation of the Wernicke-Geschwind model, and in support of a bidirectional influence between structures through the arcuate fasciculus or other cortico-subcortico-cortical connections. Our findings confirm Broca's area to be densely and reciprocally connected with areas that subsume the classically-defined Wernicke's area, including the superior temporal gyrus (BA22) and the supramarginal gyrus (BA40). We supplement these findings by demonstrating robust outdegree connections of Broca's area to somato-sensory cortex, BA8, BA21, BA39, BA28, BA41/42, anterior cingulum and parahippocampal gyrus and indegree connections from BA9, PFC, BA38, BA46 and anterior cingulum.

In another large scale study, Lacruz et al. (2007) reported a high incidence of intralobar connections using CCEP mapping. While connectivity outside the frontal and temporal lobes was not assessed, they showed a relatively greater amount of within-lobe connections, especially in the temporal lobe. Frontal lobe stimulation tended to be more likely to produce responses in the contralateral frontal and ipsilateral temporal lobes. This is consistent with our results, though more so in the case of the N2 component than the N1 component. We find an exception to this general scheme in the case of BA20 in the temporal lobe, where we find high connectivity and more outdegree connections.

This may be due to sampling differences between the two studies as well as parcellation differences as Lacruz et al did not specifically look at just the inferior temporal connections.

While the distinction between in- and out-degree was not explored systematically, a number of CCEP studies have shown the basal temporal area to have strong connectivity to a number of other cortical areas (Matsumoto et al., 2004, Umeoka et al., 2009, Koubeissi et al., 2012). Umeoka demonstrated a strong outdegree of the basal temporal language area (BTLA) that extended bilaterally (Umeoka et al., 2009). On the other hand, Matsumoto et al (2004) failed to demonstrate a connection between the superior temporal gyrus (area 22) and the subtemporal areas (area 20). While we did not investigate interhemispheric connectivity, we demonstrate a high outdegree of BA20, which would include the BTLA. Clinical experience has shown stimulation of the BTLA to interfere with language function, often producing speech arrest, but its resection may not cause language deficit (Burnstine et al., 1990, Lüders, 1991, Krauss et al., 1996). Despite the fact ESM may often produce global aphasia by stimulation of the BTLA, gamma band responses related to language often do not include the BTLA, suggesting that clinical ESM may overestimate areas critical to function by producing interference of projections (Crone et al., 2001). The large outdegree of BA20 would be consistent with an area that exerts great influence upon other areas, but is not critical to their function. This observation highlights the importance of understanding directionality of connections for both normal function and disease.

Relationship of CCEP mapping to other measures of connectivity

The latency and amplitude of the N1 demonstrates a positive correspondence with anatomical connectivity defined by diffusion tensor imaging (Conner et al., 2011), while both the N1 and N2 time periods of the CCEP positively correlate with connectivity measures defined by resting state fMRI (Keller et al., 2011). While a number of studies have also shown correspondence between connectivity measures based upon spontaneous electrocorticography and fMRI (He and Liu, 2008, Nir et al., 2008, Keller et al., 2014), different techniques may reveal different network topologies.

Interventional measurements of effective connectivity

DOI:10.14753/SE.2015.1798

The ability to record direct electrophysiological measures following the injection of current provides the most direct technique to measure effective cortico-cortical connectivity in the awake human brain. Furthermore, in this technique we are able to measure the directional influences on inter-regional relationships. We show here that cortico-cortical interactions are not always symmetrically reciprocal, and yet the majority of techniques used to measure large-scale connectivity (DTI, RSFC) assume a non-directional connectivity.

Non-interventional analytic approaches to infer causality have included the use of Granger analysis applied towards fMRI (Goebel et al., 2003, David, 2007) and EEG (Brovelli et al., 2004, Nedungadi et al., 2009). Accordingly, area A Granger causes activity in another area B if the activity in area A better predicts the future activity of area B than area B's past. While refinements including transfer entropy analysis and dynamic causal modeling may improve the application of non-interventional methods (Friston et al., 2003), these methods can only reveal statistical likelihoods of causal interactions. On the other hand, interventional approaches are possible in limited circumstances as in the clinical situation of patients undergoing invasive electrode monitoring for epilepsy or by combining expensive noninvasive methods with lesser spatial accuracy such as TMS and MEG. However, this limited circumstance can provide a standard by which non-interventional implied methods of causality may be examined.

Limitations

A major limitation of this study involves the fact that implanted electrodes sample a limited and variable proportion of the surface of the cerebral cortex. Furthermore, while the lateral aspects of the hemispheres are well-sampled, the medial and inferior aspects are sampled less, and there is no direct recording from the depth of the sulci. By combining databases using the alternative stereo-EEG approach (David et al., 2013), it would be possible to include more sulcal and interhemispheric structures. Non-invasive neuroimaging methods have the advantage of greater sampling and may be used to supplement the current measures by applying noninvasive causality measures that may be instructed by invasive measures.

We chose a Brodmann's scheme supplemented by functional measures to parcellate areas. Other parcellation schemes, for example using Freesurfer, may be used as well and may provide alternative graphical maps. In fact, apparent connectivity would be likely to depend upon the parcellation scheme that is used. Stimulation of cortical areas next to each other within the same BA may result in different CCEP distribution, averaging these results together might reduce the variability and directedness of connections from a single BA. Since our goal was to create a global connectivity map of the brain we focused on large cortical areas and used some degree of summation to be able to combine results from more than one subject. As DTI tractography has been shown to correlate with the N1 component (Conner et al., 2011), this may provide an approach to parcellating areas based on individual anatomy. Data-driven parcellation methods, such as those used in the imaging literature (Craddock et al., 2012) may ultimately be the best approach to account for clustering of connections that may exist only at an individual region. Matsumoto el al. (2007) used such a data driven approach based upon amplitude and N1 latency of CCEP subfields. This represents an alternative means to examine the specific issues such as directionality, effect of distance and graph theory metrics at the individual electrode or set of electrodes level. The future holds promise for applying these analyses into larger databases of subjects with CCEP mapping in order to identify them consistently and test data-driven clustering models. This would be facilitated by a multi-institutional collaboration to create databases of larger numbers of subjects with greater overall sampling of brain areas.

It should also be considered that any measure of directedness is also dependent upon areas sampled. Apparent connectivity will be dependent upon to what degree the sampled regions are connected. For example, if in a certain case, a larger number of areas with low connectivity are measured, the overall connectivity will appear lower. While this is clearly an important consideration regarding interpretation of the present results, we do see similar connections with respect to BA's and their directionality across subjects despite different implantation schemes. A greater sampling with more subjects should reduce this element of bias, again advocating for an effort to increase and combine databases.

Deriving conclusions regarding normal physiological processes from pathological brains is another potential limitation. We aimed to exclude all of the areas which had overt cortical abnormality or it was involved in ictal activity. However, it remains possible that some component of our observations may be biased by the pathophysiology of epilepsy. Since epilepsy is a very heterogeneous disease and the patients included in the study have various etiologies behind the epileptic manifestations, this could also rule out a common factor which would influence our results (David et al., 2013).

Future Directions

The use of CCEP mapping to describe a functional tractography has been advocated in prior reports (Matsumoto et al., 2007, David et al., 2013). While the sampling of each subject's brain by electrodes is somewhat sparse, a more comprehensive map may be possible by combining results of multiple patients and across centers. The grids and strips approach, as in the present study, provides a larger view that is limited to cortical areas located on the brain convexity. Stereoelectroencephalography (SEEG), in which arrays penetrating depth electrodes are placed directly into the brain parenchyma provide sparser sampling, but have the advantage of sampling areas in the cortical sulci. Combination of results derived from SEEG investigations and subdural electrodes, using strict protocols, could reveal the connectivity of regions not typically sampled with only using one of the techniques. For example the insula is very difficult to record from using subdural electrodes, but it is routinely recorded from using SEEG. This combination could reveal the connections from and to the insular cortex to those regions which are typically not covered with SEEG electrodes, such as the parietal or occipital lobes.

While cortical stimulation is performed routinely at many epilepsy centers, SPES for CCEP mapping is not. Evidence for improved clinical outcomes (Valentin et al., 2005b, David et al., 2010) as well as minimal effort and patient risk have resulted in more and more centers performing these protocols for clinical indications. To do so, it will be important to establish protocols by which to perform CCEP mapping (e.g. stimulation parameters, analysis of signals) and means to group findings by using parcellation schemes (e.g. MNI space, Freesurfer) or data-driven methods to cluster data

(Craddock et al., 2012). By doing so, a more comprehensive description of brain connectivity will result by combining databases from multiple centers as has been the case for functional connectivity using resting fMRI (Biswal et al., 2010, Mennes et al., 2013). As we demonstrate here the ease of combining databases from two different centers, adding more data from other centers will surely improve the robustness of findings. We would hope that a similar initiative may be undertaken for connectivity databases based on fMRI and electrocorticography.

The possibility of measuring direct cortical signals after well-localized stimulation of the cortex is a unique opportunity to reveal networks involved in various brain functions. This method can create the basis of future investigations related to specific brain networks and also validate functional neuroimaging data. Future research may be performed to define specific inter-and intralobar as well as the interhemispheric connectivity of the brain. This method may also be used to localize pathological networks, which relate to epilepsy, movement disorders, as well as a host of neuropsychiatric diseases.

DOI:10.14753/SE.2015.1798

6 Conclusions

Single pulse electrical stimulation (SPES) of the human brain is a novel method to map functional and pathological networks. The detailed analysis of the distribution of the evoked potentials on the surface of the brain as well as the laminar properties of the stimulation evoked responses reveal the same cortical generators and intrinsic architecture as it was shown earlier of the spontaneous slow oscillation (SO).

We could establish a stimulation protocol, which can be reliably used for evoking cortico-cortical evoked potentials (CCEP) on the cortex in epilepsy surgical candidates undergoing invasive monitoring to aid localization of epileptogenic tissue.

We performed SPES during sleep, awake and anesthetized states and the recorded CCEPs share the same features between the three different vigilance states.

Thus we are the first group reporting on the possibility to evoke a CCEP, which is essentially the same as one cycle of an evoked slow oscillation in awake state. To prove the concept of an evoked slow oscillation we performed intracortical recordings in some of these patients. The custom built microelectrode recording system enables to record from all six layers of the cortex, which was histologically proven. After reporting on the detailed analysis of the spontaneous slow wave activity we aimed to describe the laminar properties of the evoked cortical responses after SPES. We report firstly on the laminar generators of the CCEPs recorded on the surface of the cortex. We performed the same analysis on the CCEPs as we did with the spontaneous SO, which essentially revealed the same time frequency spectrum (wide band spectral power decrease across the whole cortex, during N2 and wide band power increase during P2), local field potential gradient (negativity in the upper layers during N2 and positivity in the deeper layers, the opposite during P2), multi unit activity (MUA) (significant decrease in MUA in the middle and upper layers during N2 and increase in activity during the early phase of P2) and finally also in the current source density (CSD) profile (current source during N2 in the middle – upper layers, which turns into a current sink in the early phase of the surface P2). According to this the formerly known CCEP is the same as an evoked cortical down-state followed by an up-state.

To describe the propagation patterns of the spontaneous SO we performed a non-linear information based correlation analysis which revealed complex propagation patterns,

contrary to the formerly published linear traveling wave theory. Non-continuities in the SO propagation to distant areas and also electrodes showing high convergence as well as high divergence may be the cortical hubs involved in SO generation and subject to cortico-thalamical inputs.

To reveal the intrinsic architecture behind the propagation pattern of the CCEPs we correlated the results of spontaneous BOLD fluctuations recorded at rest in an MRI. The two substantially different methodologies interestingly correlate significantly meaning that if two areas showed a functional connection with CCEP the exact same two anatomical regions were correlated with resting state functional connectivity (RSFC). We found beside the topological correlation also linear correlation between the amplitudes of the CCEP N2 wave and the fisher's Z score of the same areas with RSFC.

To better visualize the functional connections of different brain regions revealed with CCEP mapping, we developed a method to be able to perform a group analysis between the patients using the cytoarchitectonic map from Brodmann's as a standard space. Using Brodmann's areas (BA) as the reference we created directed graphs of every patient to visualize the interregional connections revealed with CCEP. Beside the individual maps we created a grand mean average of all of the patients included in the analysis, to create a Brodmann's based effective connectivity map of the brain for future reference. We have created the first connectivity based matrices which allows to describe the connectivity between any two (except those which were not covered with electrodes) Brodmann's area. We defined two measures two specify the connection: 1. The average z-score between two BAs show if there is at least one significant connection between the selected two area, 2. the ratio of the z-scores of the in and out going connections for every region regarded as a node of the network. These two measures may describe effective connectivity of the brain on a group level revealing formerly not proven connections directly with direct in vivo electrophysiological measurements.

DOI:10.14753/SE.2015.1798

7 Summary

Cortical electrical stimulation in the field of epilepsy surgery serves four different purposes: 1: As the gold standard tool in neurosurgery enables us to map cortical functions both intraoperatively and extraoperatively using implanted electrodes prior to therapeutic resection, 2: Aids the localization of epileptogenic cortex by evoking afterdischarges or electrographic seizures, 3: electrical stimulation of the brain is more and more often used to treat epilepsy or other neurological disorders and 4: it serves neuroscientific purposes by applying very low single pulses of electrical current, it may reveal the intrinsic architecture of the brain by generating cortico-cortical evoked potentials (CCEP). CCEP consists of an early negative peak called N1 (10-30ms post stimulus) and a delayed negative peak N2 (50-500ms).

We established a reliable stimulation methodology for evoking comparable cortico-cortical evoked potentials within cortical regions and across patients. We compared the effect of the stimulation of the cortex in non-REM sleep, awake and anesthetized states which show no major difference and CCEP is evocable in all three states. By implanting a laminar multielectrode in the cortex we could reveal the intracortical mechanisms behind the surface recorded potentials. We found wide band (0-200Hz) oscillatory power decrease across all 6 layers in parallel with multi-unit activity decrease during N2. Current source density analysis revealed a current source during N2 in the middle-upper layers and a current sink during P2. The comparison with the spontaneous slow oscillation revealed highly correlating results in all aspects of the laminar analysis, which means that the recorded evoked potentials are evoked slow oscillations, which has never been shown before in humans. We described complex propagation patterns of the spontaneous slow waves using a non-linear information based correlation technique contrary to the generally accepted linear propagation mechanism. We developed a method to co-register every electrode to the underlying BA. We created a BA based connectivity matrix of the brain using the evoked potential maps of 25 patients. Z-score of the amplitude of the N2 peak and the ratio of the in-and outgoing connections of every BA are used to describe the connectivity between any two BAs. Comparison of the spontaneous BOLD fluctuations recorded at rest in fMRI with CCEP of the same two area revealed significant correlation between the two measures.

DOI:10.14753/SE.2015.1798

Összefoglaló

Kortikális elektromos ingerlés az epilepszia sebészetben négy különböző célt szolgál: 1: Mint a ‘gold standard’ lehetővé teszi a kortikális funkciók feltérképezését mind intra- mind extraoperatív körülmények között a terápiás rezekció elvégzése előtt. 2: Segít az epileptogén área felfedésében utókisülések vagy elektromos rohamok kiváltásával. 3: Az agy elektromos ingerlését egyre gyakrabban használják terápiás céllal epilepsziában és egyéb neurológiai betegségben. 4: Tudományos célt szolgál amennyiben nagyon kis áramot folyatunk az agykéregbe melynek hatására kortiko-kortikális (CCEP) kiváltott válaszok generálódnak, ami felfedheti az agy belső szerkezetét. A CCEP egy korai negatív potenciálból, N1-s csúcs (10-30ms), továbbá egy késői potenciálból N2 csúcs (50-300ms) áll. Megalkottunk egy ingerlési protokollt amellyel megbízhatóan ki tudunk váltani összevethető CCEP-ket az agyon belül és különböző betegek között. Összehasonlítottuk az ingerlés hatását non-REM alvásban, ébren létben és altatott állapotban, melyek között eltérést nem találtunk. Intrakortikális réteg elektróda implantációja segítségével, fel tudtuk fedni az intrakortikális folyamatokat a felszínen regisztrált kiváltott válasz alatt. Széles spektrumú (0-200Hz) oszcillációs teljesítmény csökkenést regisztráltunk a kéreg mind a hat rétegében, a sok-sejt aktivitás párhuzamos csökkenésével az N2 hullám alatt. Áramforrás sűrűség analízis áram ’forrást’ fedett fel az N2 alatt a középső és felső rétegekben és egy áram ’nyelőt’ a P2 hullám alatt. A spontán lassú oszcillációval (SO) történt összevetés során erősen szignifikáns korrelációt találtunk a réteg elemzés minden területén, ami azt jelenti, hogy a kiváltott potenciál egy SO, amit korábban emberben nem írtak még le. Non-lineáris információ alapú korrelációs technikát alkalmaztunk a spontán SO terjedésének vizsgálatára, mellyel komplex terjedési mintázatokat írtunk le, ami ellenkezik az általánosságban elfogadott lineáris terjedési mechanizmussal. Kidolgoztunk egy protokollt amellyel minden elektródát az alatta fekvő Brodmann áreához (BA) tudunk rendelni és egy standard protokollt az agyfelszín rekonstrukciójához. Ezzel egy BA konnektivitási mátrixot hoztunk létre 25 beteg CCEP profilja alapján. Az N2 csúcs amplitúdójából számított z-szám és a ki/be jövő kapcsolatok aránya lehetővé teszi a konnektivitás leírását bármely két BA között. Szignifikáns korrelációt találtunk a nyugalmi (resting state) fMR során mért spontán BOLD fluktuációk és az ugyanazon területek ingerlésekor mért kiváltott válasz amplitúdója között.

8 References

Achard S, Bullmore E (2007) Efficiency and cost of economical brain functional networks. PLoS computational biology 3:e17.

Achard S, Salvador R, Whitcher B, Suckling J, Bullmore E (2006) A resilient, low-frequency, small-world human brain functional network with highly connected association cortical hubs. The Journal of neuroscience : the official journal of the Society for Neuroscience 26:63-72.

Achermann P, Borbely AA (1997) Low-frequency (< 1 Hz) oscillations in the human sleep electroencephalogram. Neuroscience 81:213-222.

Amzica F, Steriade M (1995) Disconnection of intracortical synaptic linkages disrupts synchronization of a slow oscillation. J Neurosci 15:4658-4677.

Amzica F, Steriade M (1998) Cellular substrates and laminar profile of sleep K-complex. Neuroscience 82:671-686.

Axmacher N, Elger CE, Fell J (2008) Ripples in the medial temporal lobe are relevant for human memory consolidation. Brain 131:1806-1817.

Bangera NB, Schomer DL, Dehghani N, Ulbert I, Cash S, Papavasiliou S, Eisenberg SR, Dale AM, Halgren E (2010) Experimental validation of the influence of white matter anisotropy on the intracranial EEG forward solution. Journal of computational neuroscience 29:371-387.

Bartho P, Hirase H, Monconduit L, Zugaro M, Harris KD, Buzsaki G (2004) Characterization of neocortical principal cells and interneurons by network interactions and extracellular features. J Neurophysiol 92:600-608.

Bassett DS, Bullmore E, Verchinski BA, Mattay VS, Weinberger DR, Meyer-Lindenberg A (2008) Hierarchical organization of human cortical networks in health and schizophrenia. The Journal of neuroscience : the official journal of the Society for Neuroscience 28:9239-9248.

Bassett DS, Nelson BG, Mueller BA, Camchong J, Lim KO (2012) Altered resting state complexity in schizophrenia. Neuroimage 59:2196-2207.

Berger H (1929) Über das Elektroenkephalogramm des Menschen. Archiv für Psychiatrie und Nervenkrankheiten 87:527-570.

Bernhardt BC, Rozen DA, Worsley KJ, Evans AC, Bernasconi N, Bernasconi A (2009) Thalamo-cortical network pathology in idiopathic generalized epilepsy: insights from MRI-based morphometric correlation analysis. Neuroimage 46:373-381.

Biswal B, Yetkin FZ, Haughton VM, Hyde JS (1995) Functional connectivity in the motor cortex of resting human brain using echo-planar MRI. Magnetic resonance in medicine : official journal of the Society of Magnetic Resonance in Medicine / Society of Magnetic Resonance in Medicine 34:537-541.

Biswal BB, Mennes M, Zuo XN, Gohel S, Kelly C, Smith SM, Beckmann CF, Adelstein JS, Buckner RL, Colcombe S, Dogonowski AM, Ernst M, Fair D, Hampson M, Hoptman MJ, Hyde JS, Kiviniemi VJ, Kotter R, Li SJ, Lin CP, Lowe MJ, Mackay C, Madden DJ, Madsen KH, Margulies DS, Mayberg HS, McMahon K, Monk CS, Mostofsky SH, Nagel BJ, Pekar JJ, Peltier SJ, Petersen SE, Riedl V, Rombouts SA, Rypma B, Schlaggar BL, Schmidt S, Seidler RD, Siegle GJ, Sorg C, Teng GJ, Veijola J, Villringer A, Walter M, Wang L, Weng XC, Whitfield-Gabrieli S, Williamson P, Windischberger C, Zang YF, Zhang HY, Castellanos FX, Milham MP (2010) Toward discovery science of human brain function. Proceedings of the National Academy of Sciences of the United States of America 107:4734-4739.

Born J, Rasch B, Gais S (2006) Sleep to remember. Neuroscientist 12:410-424.

Bragin A, Wilson CL, Staba RJ, Reddick M, Fried I, Engel J, Jr. (2002) Interictal high-frequency oscillations (80-500 Hz) in the human epileptic brain: entorhinal cortex. Ann Neurol 52:407-415.

Brodmann K (1909) Vergleichende Lokalisationslehre der Großhirnrinde in ihren Prinzipien dargestellt auf Grund des Zellenbaues. Leipzig, Germany: Verlag von Johann Ambrosius Barth.

Brovelli A, Ding M, Ledberg A, Chen Y, Nakamura R, Bressler SL (2004) Beta oscillations in a large-scale sensorimotor cortical network: directional influences revealed by Granger causality. Proceedings of the National Academy of Sciences of the United States of America 101:9849-9854.

Brugge JF, Volkov IO, Garell PC, Reale RA, Howard MA, 3rd (2003) Functional connections between auditory cortex on Heschl's gyrus and on the lateral superior temporal gyrus in humans. J Neurophysiol 90:3750-3763.

Bullmore E, Sporns O (2009) Complex brain networks: graph theoretical analysis of structural and functional systems. Nature reviews Neuroscience 10:186-198.

Bullmore ET, Bassett DS (2011) Brain graphs: graphical models of the human brain connectome. Annual review of clinical psychology 7:113-140.

Burnstine TH, Lesser RP, Hart J, Jr., Uematsu S, Zinreich SJ, Krauss GL, Fisher RS, Vining EP, Gordon B (1990) Characterization of the basal temporal language area in patients with left temporal lobe epilepsy. Neurology 40:966-970.

Buzsaki G (2006) Rhythms of the Brain. New York, New York: Oxford University Press, Inc.

Buzsaki G, Draguhn A (2004) Neuronal oscillations in cortical networks. Science 304:1926-1929.

Cash SS, Halgren E, Dehghani N, Rossetti AO, Thesen T, Wang C, Devinsky O, Kuzniecky R, Doyle W, Madsen JR, Bromfield E, Eross L, Halasz P, Karmos G, Csercsa R, Wittner L, Ulbert I (2009) The human K-complex represents an isolated cortical down-state. Science 324:1084-1087.

Catenoix H, Magnin M, Guenot M, Isnard J, Mauguiere F, Ryvlin P (2005) Hippocampal-orbitofrontal connectivity in human: an electrical stimulation study. Clinical neurophysiology : official journal of the International Federation of Clinical Neurophysiology 116:1779-1784.

Catenoix H, Magnin M, Mauguiere F, Ryvlin P (2011) Evoked potential study of hippocampal efferent projections in the human brain. Clinical neurophysiology : official journal of the International Federation of Clinical Neurophysiology 122:2488-2497.

Chauvette S, Volgushev M, Timofeev I (2010) Origin of Active States in Local Neocortical Networks during Slow Sleep Oscillation. Cereb Cortex.

Chen CC, Kilner JM, Friston KJ, Kiebel SJ, Jolly RK, Ward NS (2010) Nonlinear coupling in the human motor system. The Journal of neuroscience : the official journal of the Society for Neuroscience 30:8393-8399.

Clemens Z, Molle M, Eross L, Barsi P, Halasz P, Born J (2007) Temporal coupling of parahippocampal ripples, sleep spindles and slow oscillations in humans. Brain : a journal of neurology 130:2868-2878.

Conner CR, Ellmore TM, Disano MA, Pieters TA, Potter AW, Tandon N (2011) Anatomic and electro-physiologic connectivity of the language system: A combined DTI-CCEP study. Computers in biology and medicine.

Contreras D, Timofeev I, Steriade M (1996) Mechanisms of long-lasting hyperpolarizations underlying slow sleep oscillations in cat corticothalamic networks. The Journal of physiology 494 (Pt 1):251-264.

Cossart R, Aronov D, Yuste R (2003) Attractor dynamics of network UP states in the neocortex. Nature 423:283-288.

Cox RW (1996) AFNI: software for analysis and visualization of functional magnetic resonance neuroimages. Comput Biomed Res 29:162-173.

Craddock RC, James GA, Holtzheimer PE, 3rd, Hu XP, Mayberg HS (2012) A whole brain fMRI atlas generated via spatially constrained spectral clustering. Human brain mapping 33:1914-1928.

Crepon B, Navarro V, Hasboun D, Clemenceau S, Martinerie J, Baulac M, Adam C, Le Van Quyen M (2010) Mapping interictal oscillations greater than 200 Hz recorded with intracranial macroelectrodes in human epilepsy. Brain 133:33-45.

Creutzfeldt OD, Watanabe S, Lux HD (1966) Relations between EEG phenomena and potentials of single cortical cells. I. Evoked responses after thalamic and erpicortical stimulation. Electroencephalography and clinical neurophysiology 20:1-18.

Crone NE, Hao L, Hart J, Jr., Boatman D, Lesser RP, Irizarry R, Gordon B (2001) Electrocorticographic gamma activity during word production in spoken and sign language. Neurology 57:2045-2053.

Crunelli V, Hughes SW (2010) The slow (<1 Hz) rhythm of non-REM sleep: a dialogue between three cardinal oscillators. Nature neuroscience 13:9-17.

Csercsa R, Dombovari B, Fabo D, Wittner L, Eross L, Entz L, Solyom A, Rasonyi G, Szucs A, Kelemen A, Jakus R, Juhos V, Grand L, Magony A, Halasz P, Freund TF, Magloczky Z, Cash SS, Papp L, Karmos G, Halgren E, Ulbert I (2010) Laminar analysis of slow wave activity in humans. Brain : a journal of neurology 133:2814-2829.

Csicsvari J, Hirase H, Czurko A, Buzsaki G (1998) Reliability and state dependence of pyramidal cell-interneuron synapses in the hippocampus: an ensemble approach in the behaving rat. Neuron 21:179-189.

Dalal SS, Edwards E, Kirsch HE, Barbaro NM, Knight RT, Nagarajan SS (2008) Localization of neurosurgically implanted electrodes via photograph-MRI-radiograph coregistration. Journal of neuroscience methods 174:106-115.

Dale AM, Fischl B, Sereno MI (1999) Cortical surface-based analysis. I. Segmentation and surface reconstruction. Neuroimage 9:179-194.

Damasio H, Damasio AR (1980) The anatomical basis of conduction aphasia. Brain : a journal of neurology 103:337-350.

Damoiseaux JS, Greicius MD (2009) Greater than the sum of its parts: a review of studies combining structural connectivity and resting-state functional connectivity. Brain structure & function 213:525-533.

Darvas F, Ojemann JG, Sorensen LB (2009) Bi-phase locking - a tool for probing non-linear interaction in the human brain. Neuroimage 46:123-132.

David O (2007) Dynamic causal models and autopoietic systems. Biological research 40:487-502.

David O, Bastin J, Chabardes S, Minotti L, Kahane P (2010) Studying network mechanisms using intracranial stimulation in epileptic patients. Frontiers in systems neuroscience 4:148.

David O, Job AS, De Palma L, Hoffmann D, Minotti L, Kahane P (2013) Probabilistic functional tractography of the human cortex. Neuroimage 80:307-317.

Delorme A, Makeig S (2004) EEGLAB: an open source toolbox for analysis of single-trial EEG dynamics including independent component analysis. J Neurosci Methods 134:9-21.

Diekelmann S, Born J (2010) The memory function of sleep. Nature reviews Neuroscience 11:114-126.

Duncan JS, Papademetris X, Yang J, Jackowski M, Zeng X, Staib LH (2004) Geometric strategies for neuroanatomic analysis from MRI. Neuroimage 23 Suppl 1:S34-45.

Dykstra A, Halgren E, Thesen T, C. C, A. T, Kuzniecky R, Eskandar E, Cash SS (2010) Correlates of Auditory Streaming Measured with Direct Cortical Recordings in Behaving Humans. In: Human Brain Mapping Barcelona, Spain.

Dykstra AR, Chan AM, Quinn BT, Zepeda R, Keller CJ, Cormier J, Madsen JR, Eskandar EN, Cash SS (2011) Individualized localization and cortical surface-based registration of intracranial electrodes. Neuroimage.

Ebersole JS, Pedley TA (2003) Current practice of clinical electroencephalography. Philadelphia: Lippincott Williams & Wilkins.

Enatsu R, Matsumoto R, Piao Z, O'Connor T, Horning K, Burgess RC, Bulacio J, Bingaman W, Nair DR (2013) Cortical negative motor network in comparison with sensorimotor network: a cortico-cortical evoked potential study. Cortex; a journal devoted to the study of the nervous system and behavior 49:2080-2096.

Enatsu R, Piao Z, O'Connor T, Horning K, Mosher J, Burgess R, Bingaman W, Nair D (2011) Cortical excitability varies upon ictal onset patterns in neocortical epilepsy: A cortico-cortical evoked potential study. Clinical neurophysiology : official journal of the International Federation of Clinical Neurophysiology.

Entz L, Fabo D, Eross L, Halasz P, Wittner L, Karmos G, Ulbert I (2009) Single pulse cortical electrical stimulation induced slow oscillation in different vigilance states in epileptic patients. In: 28th International Epilepsy Congress, vol. 50, pp 93-93 Budapest, Hungary.

Entz L, Toth E, Keller CJ, Bickel S, Groppe DM, Fabo D, Kozak LR, Eross L, Ulbert I, Mehta AD (2014) Evoked effective connectivity of the human neocortex. Human brain mapping.

Eross L, Bago AG, Entz L, Fabo D, Halasz P, Balogh A, Fedorcsak I (2009) Neuronavigation and fluoroscopy-assisted subdural strip electrode positioning: a simple method to increase intraoperative accuracy of strip localization in epilepsy surgery. Journal of neurosurgery 110:327-331.

Euston DR, Tatsuno M, McNaughton BL (2007) Fast-forward playback of recent memory sequences in prefrontal cortex during sleep. Science (New York, NY 318:1147-1150.

Fabo D (2008) Properties of spontaneous and evoked discharges in the human subiculum. In: Semmelweis University, vol. PhD Budapest: Semmelweis University.

Fabo D, Magloczky Z, Wittner L, Pek A, Eross L, Czirjak S, Vajda J, Solyom A, Rasonyi G, Szucs A, Kelemen A, Juhos V, Grand L, Dombovari B, Halasz P, Freund TF, Halgren E, Karmos G, Ulbert I (2008) Properties of in vivo interictal spike generation in the human subiculum. Brain 131:485-499.

Felleman DJ, Van Essen DC (1991) Distributed hierarchical processing in the primate cerebral cortex. Cereb Cortex 1:1-47.

Flanagan D, Valentin A, Garcia Seoane JJ, Alarcon G, Boyd SG (2009) Single-pulse electrical stimulation helps to identify epileptogenic cortex in children. Epilepsia 50:1793-1803.

Foerster O, Penfield W (1930) Der Narbenzug am und im Gehirn bei trumatischer Epilepsie in seiner Bedeutung für das Zustandekommen der Anfaelle und für die therapeutische Bekaempfung derselben. Zeitschrift der Geselschaft für Neurologie und Psychiatrie 125:475-572.

Fowler MJ, Sullivan MJ, Ekstrand BR (1973) Sleep and memory. Science 179:302-304.

Fox MD, Raichle ME (2007) Spontaneous fluctuations in brain activity observed with functional magnetic resonance imaging. Nat Rev Neurosci 8:700-711.

Fox MD, Snyder AZ, Vincent JL, Corbetta M, Van Essen DC, Raichle ME (2005) The human brain is intrinsically organized into dynamic, anticorrelated functional networks. Proceedings of the National Academy of Sciences of the United States of America 102:9673-9678.

Fox MD, Snyder AZ, Vincent JL, Raichle ME (2007) Intrinsic fluctuations within cortical systems account for intertrial variability in human behavior. Neuron 56:171-184.

Freeman JA, Nicholson C (1975) Experimental optimization of current source-density technique for anuran cerebellum. J Neurophysiol 38:369-382.

Fregni F, Thome-Souza S, Nitsche MA, Freedman SD, Valente KD, Pascual-Leone A (2006) A controlled clinical trial of cathodal DC polarization in patients with refractory epilepsy. Epilepsia 47:335-342.

Freiwald WA, Valdes P, Bosch J, Biscay R, Jimenez JC, Rodriguez LM, Rodriguez V, Kreiter AK, Singer W (1999) Testing non-linearity and directedness of interactions between neural groups in the macaque inferotemporal cortex. Journal of neuroscience methods 94:105-119.

Friston KJ, Harrison L, Penny W (2003) Dynamic causal modelling. Neuroimage 19:1273-1302.

Goebel R, Roebroeck A, Kim DS, Formisano E (2003) Investigating directed cortical interactions in time-resolved fMRI data using vector autoregressive modeling and Granger causality mapping. Magnetic resonance imaging 21:1251-1261.

Goldring S, Harding GW, Gregorie EM (1994) Distinctive electrophysiological characteristics of functionally discrete brain areas: a tenable approach to functional localization. Journal of neurosurgery 80:701-709.

Gordon B, Lesser RP, Rance NE, Hart J, Jr., Webber R, Uematsu S, Fisher RS (1990) Parameters for direct cortical electrical stimulation in the human: histopathologic confirmation. Electroencephalography and clinical neurophysiology 75:371-377.

Greenlee JD, Oya H, Kawasaki H, Volkov IO, Kaufman OP, Kovach C, Howard MA, Brugge JF (2004) A functional connection between inferior frontal gyrus and orofacial motor cortex in human. J Neurophysiol 92:1153-1164.

Greicius M (2008) Resting-state functional connectivity in neuropsychiatric disorders. Curr Opin Neurol 21:424-430.

Grzeszczuk R, Tan KK, Levin DN, Pelizzari CA, Hu X, Chen GT, Beck RN, Chen CT, Cooper M, Milton J, et al. (1992) Retrospective fusion of radiographic and MR data for localization of subdural electrodes. Journal of computer assisted tomography 16:764-773.

Guye M, Bettus G, Bartolomei F, Cozzone PJ (2010) Graph theoretical analysis of structural and functional connectivity MRI in normal and pathological brain networks. MAGMA 23:409-421.

Hagmann P, Cammoun L, Gigandet X, Meuli R, Honey CJ, Wedeen VJ, Sporns O (2008) Mapping the structural core of human cerebral cortex. PLoS biology 6:e159.

Haider B, Duque A, Hasenstaub AR, McCormick DA (2006) Neocortical network activity in vivo is generated through a dynamic balance of excitation and inhibition. J Neurosci 26:4535-4545.

Halgren E, Wang C, Schomer DL, Knake S, Marinkovic K, Wu J, Ulbert I (2006) Processing stages underlying word recognition in the anteroventral temporal lobe. NeuroImage 30:1401-1413.

Hamberger MJ (2007) Cortical language mapping in epilepsy: a critical review. Neuropsychology review 17:477-489.

Hampson M, Driesen NR, Skudlarski P, Gore JC, Constable RT (2006) Brain connectivity related to working memory performance. J Neurosci 26:13338-13343.

Hangya B, Borhegyi Z, Szilagyi N, Freund TF, Varga V (2009) GABAergic neurons of the medial septum lead the hippocampal network during theta activity. The Journal of neuroscience : the official journal of the Society for Neuroscience 29:8094-8102.

Hangya B, Tihanyi BT, Entz L, Fabo D, Eross L, Wittner L, Jakus R, Varga V, Freund TF, Ulbert I (2011) Complex propagation patterns characterize human cortical activity during slow-wave sleep. The Journal of neuroscience : the official journal of the Society for Neuroscience 31:8770-8779.

He B, Liu Z (2008) Multimodal functional neuroimaging: integrating functional MRI and EEG/MEG. IEEE reviews in biomedical engineering 1:23-40.

He BJ, Shulman GL, Snyder AZ, Corbetta M (2007a) The role of impaired neuronal communication in neurological disorders. Curr Opin Neurol 20:655-660.

He BJ, Snyder AZ, Zempel JM, Smyth MD, Raichle ME (2008) Electrophysiological correlates of the brain's intrinsic large-scale functional architecture. Proc Natl Acad Sci U S A 105:16039-16044.

He Y, Chen ZJ, Evans AC (2007b) Small-world anatomical networks in the human brain revealed by cortical thickness from MRI. Cereb Cortex 17:2407-2419.

He Y, Evans A (2010) Graph theoretical modeling of brain connectivity. Current opinion in neurology 23:341-350.

Hermes D, Miller KJ, Noordmans HJ, Vansteensel MJ, Ramsey NF (2010) Automated electrocorticographic electrode localization on individually rendered brain surfaces. Journal of neuroscience methods 185:293-298.

Hill DL, Smith AD, Simmons A, Maurer CR, Jr., Cox TC, Elwes R, Brammer M, Hawkes DJ, Polkey CE (2000) Sources of error in comparing functional magnetic resonance imaging and invasive electrophysiological recordings. Journal of neurosurgery 93:214-223.

Hill S, Tononi G (2005) Modeling sleep and wakefulness in the thalamocortical system. J Neurophysiol 93:1671-1698.

Horsley V (1909) The Linacre Lecture ON THE FUNCTION OF THE SO-CALLED MOTOR AREA OF THE BRAIN: Delivered to the Master and Fellows of St. John's College, Cambridge, May 6th, 1909. British medical journal 2:121-132.

Huang X, Xu W, Liang J, Takagaki K, Gao X, Wu JY (2010) Spiral wave dynamics in neocortex. Neuron 68:978-990.

Huber R, Esser SK, Ferrarelli F, Massimini M, Peterson MJ, Tononi G (2007) TMS-induced cortical potentiation during wakefulness locally increases slow wave activity during sleep. PloS one 2:e276.

Huber R, Ghilardi MF, Massimini M, Tononi G (2004) Local sleep and learning. Nature 430:78-81.

Hunter JD, Hanan DM, Singer BF, Shaikh S, Brubaker KA, Hecox KE, Towle VL (2005) Locating chronically implanted subdural electrodes using surface reconstruction. Clinical neurophysiology : official journal of the International Federation of Clinical Neurophysiology 116:1984-1987.

Iber C, Ancoli-Israel S, Chesson A, Quan SF (2007) The AASM Manual for the Scoring of Sleep and Associated Events: Rules, Terminology and Technical Specifications. Westchester: American Academy of Sleep Medicine.

Isomura Y, Sirota A, Ozen S, Montgomery S, Mizuseki K, Henze DA, Buzsaki G (2006) Integration and segregation of activity in entorhinal-hippocampal subregions by neocortical slow oscillations. Neuron 52:871-882.

Iturria-Medina Y, Sotero RC, Canales-Rodriguez EJ, Aleman-Gomez Y, Melie-Garcia L (2008) Studying the human brain anatomical network via diffusion-weighted MRI and Graph Theory. Neuroimage 40:1064-1076.

Jacobs J, Levan P, Chatillon CE, Olivier A, Dubeau F, Gotman J (2009) High frequency oscillations in intracranial EEGs mark epileptogenicity rather than lesion type. Brain 132:1022-1037.

Jenkins JC, Dallenbach KM (1924) Obliviscence during sleep and waking. Am J Psychol 605-612.

Jirsch JD, Urrestarazu E, LeVan P, Olivier A, Dubeau F, Gotman J (2006) High-frequency oscillations during human focal seizures. Brain 129:1593-1608.

Jones EG, Wise SP (1977) Size, laminar and columnar distribution of efferent cells in the sensory-motor cortex of monkeys. The Journal of comparative neurology 175:391-438.

Kaiser M, Hilgetag CC (2006) Nonoptimal component placement, but short processing paths, due to long-distance projections in neural systems. PLoS computational biology 2:e95.

Kajikawa Y, Hackett TA (2005) Entropy analysis of neuronal spike train synchrony. Journal of neuroscience methods 149:90-93.

Keller CJ, Bickel S, Entz L, Ulbert I, Milham MP, Kelly C, Mehta AD (2011) Intrinsic functional architecture predicts electrically evoked responses in the human brain. Proceedings of the National Academy of Sciences of the United States of America 108:10308-10313.

Keller CJ, Bickel S, Honey CJ, Groppe DM, Entz L, Craddock RC, Lado FA, Kelly C, Milham M, Mehta AD (2013) Neurophysiological investigation of spontaneous correlated and anticorrelated fluctuations of the BOLD signal. The Journal of neuroscience : the official journal of the Society for Neuroscience 33:6333-6342.

Keller CJ, Cash SS, Narayanan S, Wang C, Kuzniecky R, Carlson C, Devinsky O, Thesen T, Doyle W, Sassaroli A, Boas DA, Ulbert I, Halgren E (2009) Intracranial microprobe for evaluating neuro-hemodynamic coupling in unanesthetized human neocortex. Journal of neuroscience methods 179:208-218.

Keller CJ, Honey CJ, Entz L, Bickel S, Groppe DM, Toth E, Ulbert I, Lado FA, Mehta AD (2014) Corticocortical evoked potentials reveal projectors and integrators in human brain networks. The Journal of neuroscience : the official journal of the Society for Neuroscience 34:9152-9163.

Kelly C, Uddin LQ, Shehzad Z, Margulies DS, Castellanos FX, Milham MP, Petrides M (2010) Broca's region: linking human brain functional connectivity data and non-human primate tracing anatomy studies. The European journal of neuroscience 32:383-398.

Kinoshita M, Ikeda A, Matsuhashi M, Matsumoto R, Hitomi T, Begum T, Usui K, Takayama M, Mikuni N, Miyamoto S, Hashimoto N, Shibasaki H (2005) Electric cortical stimulation suppresses epileptic and background activities in neocortical epilepsy and mesial temporal lobe epilepsy. Clin Neurophysiol 116:1291-1299.

Knake S, Wang CM, Ulbert I, Schomer DL, Halgren E (2007) Specific increase of human entorhinal population synaptic and neuronal activity during retrieval. NeuroImage 37:618-622.

Koubeissi MZ, Lesser RP, Sinai A, Gaillard WD, Franaszczuk PJ, Crone NE (2012) Connectivity between perisylvian and bilateral basal temporal cortices. Cereb Cortex 22:918-925.

Kovalev D, Spreer J, Honegger J, Zentner J, Schulze-Bonhage A, Huppertz HJ (2005) Rapid and fully automated visualization of subdural electrodes in the presurgical evaluation of epilepsy patients. AJNR American journal of neuroradiology 26:1078-1083.

Koyama MS, Kelly C, Shehzad Z, Penesetti D, Castellanos FX, Milham MP (2010) Reading networks at rest. Cereb Cortex 20:2549-2559.

Kramer MA, Eden UT, Lepage KQ, Kolaczyk ED, Bianchi MT, Cash SS (2011) Emergence of persistent networks in long-term intracranial EEG recordings. The Journal of neuroscience : the official journal of the Society for Neuroscience 31:15757-15767.

Krause F (1911) Chirurgie des Gehirns und Rückenmarks nach eigenen Erfahrungen. Berlin, Wien: Urban, Schwarzenberg.

Krause F (1931-1932) Die spezielle Chirurgie der Gehirnkrankheiten 2. Bd. Die epileptischen Erkrankungen Stuttgart: Enke

Krauss GL, Fisher R, Plate C, Hart J, Uematsu S, Gordon B, Lesser RP (1996) Cognitive effects of resecting basal temporal language areas. Epilepsia 37:476-483.

Kurth S, Ringli M, Geiger A, LeBourgeois M, Jenni OG, Huber R (2010) Mapping of cortical activity in the first two decades of life: a high-density sleep electroencephalogram study. The Journal of neuroscience : the official journal of the Society for Neuroscience 30:13211-13219.

Lacruz ME, Garcia Seoane JJ, Valentin A, Selway R, Alarcon G (2007) Frontal and temporal functional connections of the living human brain. The European journal of neuroscience 26:1357-1370.

Lakatos P, Karmos G, Mehta AD, Ulbert I, Schroeder CE (2008) Entrainment of neuronal oscillations as a mechanism of attentional selection. Science (New York, NY 320:110-113.

Lakatos P, Shah AS, Knuth KH, Ulbert I, Karmos G, Schroeder CE (2005) An oscillatory hierarchy controlling neuronal excitability and stimulus processing in the auditory cortex. Journal of neurophysiology 94:1904-1911.

Lo CY, Wang PN, Chou KH, Wang J, He Y, Lin CP (2010) Diffusion tensor tractography reveals abnormal topological organization in structural cortical networks in Alzheimer's disease. The Journal of neuroscience : the official journal of the Society for Neuroscience 30:16876-16885.

Logothetis NK, Augath M, Murayama Y, Rauch A, Sultan F, Goense J, Oeltermann A, Merkle H (2010) The effects of electrical microstimulation on cortical signal propagation. Nature neuroscience 13:1283-1291.

Loomis AL, Harvey EN, Hobart GA (1937) Cerebral states during sleep, as studied by human brain potentials. Journal of Experimental Psychology 21:127-144.

Luczak A, Bartho P, Marguet SL, Buzsaki G, Harris KD (2007) Sequential structure of neocortical spontaneous activity in vivo. Proceedings of the National Academy of Sciences of the United States of America 104:347-352.

Lüders HO (1991) Epilepsy Surgery. New York: Raven Press Ltd.

Magnin M, Rey M, Bastuji H, Guillemant P, Mauguiere F, Garcia-Larrea L (2010) Thalamic deactivation at sleep onset precedes that of the cerebral cortex in humans. Proceedings of the National Academy of Sciences of the United States of America 107:3829-3833.

Mahvash M, Konig R, Wellmer J, Urbach H, Meyer B, Schaller K (2007) Coregistration of digital photography of the human cortex and cranial magnetic

resonance imaging for visualization of subdural electrodes in epilepsy surgery. Neurosurgery 61:340-344; discussion 344-345.

Marshall L, Helgadottir H, Molle M, Born J (2006) Boosting slow oscillations during sleep potentiates memory. Nature 444:610-613.

Marshall L, Molle M, Hallschmid M, Born J (2004) Transcranial direct current stimulation during sleep improves declarative memory. The Journal of neuroscience : the official journal of the Society for Neuroscience 24(44):9985-92.:T - ppublish.

Massimini M, Ferrarelli F, Esser SK, Riedner BA, Huber R, Murphy M, Peterson MJ, Tononi G (2007) Triggering sleep slow waves by transcranial magnetic stimulation. Proceedings of the National Academy of Sciences of the United States of America 104:8496-8501.

Massimini M, Ferrarelli F, Huber R, Esser SK, Singh H, Tononi G (2005) Breakdown of cortical effective connectivity during sleep. Science (New York, NY 309:2228-2232.

Massimini M, Huber R, Ferrarelli F, Hill S, Tononi G (2004) The sleep slow oscillation as a traveling wave. J Neurosci 24:6862-6870.

Massimini M, Tononi G, Huber R (2009) Slow waves, synaptic plasticity and information processing: insights from transcranial magnetic stimulation and high-density EEG experiments. The European journal of neuroscience 29:1761-1770.

Matsumoto R, Nair DR, Ikeda A, Fumuro T, Lapresto E, Mikuni N, Bingaman W, Miyamoto S, Fukuyama H, Takahashi R, Najm I, Shibasaki H, Luders HO (2012) Parieto-frontal network in humans studied by cortico-cortical evoked potential. Human brain mapping 33:2856-2872.

Matsumoto R, Nair DR, LaPresto E, Bingaman W, Shibasaki H, Luders HO (2007) Functional connectivity in human cortical motor system: a cortico-cortical evoked potential study. Brain : a journal of neurology 130:181-197.

Matsumoto R, Nair DR, LaPresto E, Najm I, Bingaman W, Shibasaki H, Luders HO (2004) Functional connectivity in the human language system: a cortico-cortical evoked potential study. Brain : a journal of neurology 127:2316-2330.

McIntosh AR, Gonzalez-Lima F (1994) Structural equation modeling and its application to network analysis in functional brain imaging. Human brain mapping 2:2-22.

Mehta AD, Klein G (2010) Clinical utility of functional magnetic resonance imaging for brain mapping in epilepsy surgery. Epilepsy research 89:126-132.

Mena-Segovia J, Sims HM, Magill PJ, Bolam JP (2008) Cholinergic brainstem neurons modulate cortical gamma activity during slow oscillations. The Journal of physiology 586:2947-2960.

Mennes M, Biswal BB, Castellanos FX, Milham MP (2013) Making data sharing work: the FCP/INDI experience. Neuroimage 82:683-691.

Miller KJ, Makeig S, Hebb AO, Rao RP, denNijs M, Ojemann JG (2007) Cortical electrode localization from X-rays and simple mapping for electrocorticographic research: The "Location on Cortex" (LOC) package for MATLAB. Journal of neuroscience methods 162:303-308.

Mohajerani MH, McVea DA, Fingas M, Murphy TH (2010) Mirrored bilateral slow-wave cortical activity within local circuits revealed by fast bihemispheric voltage-sensitive dye imaging in anesthetized and awake mice. The Journal of neuroscience : the official journal of the Society for Neuroscience 30:3745-3751.

Molle M, Marshall L, Gais S, Born J (2002) Grouping of spindle activity during slow oscillations in human non-rapid eye movement sleep. J Neurosci 22:10941-10947.

Molle M, Yeshenko O, Marshall L, Sara SJ, Born J (2006) Hippocampal sharp wave-ripples linked to slow oscillations in rat slow-wave sleep. Journal of neurophysiology 96:62-70.

Morgan JP (1982) The first reported case of electrical stimulation of the human brain. Journal of the history of medicine and allied sciences 37:51-64.

Murphy M, Riedner BA, Huber R, Massimini M, Ferrarelli F, Tononi G (2009) Source modeling sleep slow waves. Proceedings of the National Academy of Sciences of the United States of America 106:1608-1613.

Na SH, Jin SH, Kim SY, Ham BJ (2002) EEG in schizophrenic patients: mutual information analysis. Clinical neurophysiology : official journal of the International Federation of Clinical Neurophysiology 113:1954-1960.

Nedungadi AG, Rangarajan G, Jain N, Ding M (2009) Analyzing multiple spike trains with nonparametric Granger causality. Journal of computational neuroscience 27:55-64.

Nelles M, Koenig R, Kandyba J, Schaller C, Urbach H (2004) Fusion of MRI and CT with subdural grid electrodes. Zentralblatt fur Neurochirurgie 65:174-179.

Nicholson C, Freeman JA (1975) Theory of current source-density analysis and determination of conductivity tensor for anuran cerebellum. J Neurophysiol 38:356-368.

Nir Y, Mukamel R, Dinstein I, Privman E, Harel M, Fisch L, Gelbard-Sagiv H, Kipervasser S, Andelman F, Neufeld MY, Kramer U, Arieli A, Fried I, Malach R (2008) Interhemispheric correlations of slow spontaneous neuronal fluctuations revealed in human sensory cortex. Nature neuroscience 11:1100-1108.

Noordmans HJ, van Rijen PC, van Veelen CW, Viergever MA, Hoekema R (2001) Localization of implanted EEG electrodes in a virtual-reality environment. Computer aided surgery : official journal of the International Society for Computer Aided Surgery 6:241-258.

Ostojic S, Brunel N, Hakim V (2009) How connectivity, background activity, and synaptic properties shape the cross-correlation between spike trains. The Journal of neuroscience : the official journal of the Society for Neuroscience 29:10234-10253.

Panzeri S, Senatore R, Montemurro MA, Petersen RS (2007) Correcting for the sampling bias problem in spike train information measures. J Neurophysiol 98:1064-1072.

Paz R, Gelbard-Sagiv H, Mukamel R, Harel M, Malach R, Fried I (2010) A neural substrate in the human hippocampus for linking successive events. Proceedings of the National Academy of Sciences of the United States of America 107:6046-6051.

Peckham PH, Krames ES, Rezai AR (2009) Neuromodulation: A comprehensive handbook.: Academic Press.

Petrides M, Pandya DN (2009) Distinct parietal and temporal pathways to the homologues of Broca's area in the monkey. PLoS biology 7:e1000170.

Pinsk MA, Kastner S (2007) Neuroscience: unconscious networking. Nature 447:46-47.

Purpura DP, Pool JL, Ransohoff J, Frumin MJ, Housepian EM (1957) Observations on evoked dendritic potentials of human cortex. Electroencephalography and clinical neurophysiology 9:453-459.

Renart A, de la Rocha J, Bartho P, Hollender L, Parga N, Reyes A, Harris KD (2010) The asynchronous state in cortical circuits. Science 327:587-590.

Rosenberg DS, Mauguiere F, Catenoix H, Faillenot I, Magnin M (2009) Reciprocal thalamocortical connectivity of the medial pulvinar: a depth stimulation and evoked potential study in human brain. Cereb Cortex 19:1462-1473.

Roux FE, Boulanouar K, Lotterie JA, Mejdoubi M, LeSage JP, Berry I (2003) Language functional magnetic resonance imaging in preoperative assessment of language areas: correlation with direct cortical stimulation. Neurosurgery 52:1335-1345; discussion 1345-1337.

Rubinov M, Sporns O (2010) Complex network measures of brain connectivity: uses and interpretations. Neuroimage 52:1059-1069.

Ruge MI, Victor J, Hosain S, Correa DD, Relkin NR, Tabar V, Brennan C, Gutin PH, Hirsch J (1999) Concordance between functional magnetic resonance imaging and intraoperative language mapping. Stereotactic and functional neurosurgery 72:95-102.

Sadaghiani S, Scheeringa R, Lehongre K, Morillon B, Giraud AL, Kleinschmidt A (2010) Intrinsic connectivity networks, alpha oscillations, and tonic alertness: a simultaneous electroencephalography/functional magnetic resonance imaging study. J Neurosci 30:10243-10250.

Sakata S, Harris KD (2009) Laminar structure of spontaneous and sensory-evoked population activity in auditory cortex. Neuron 64:404-418.

Salvador R, Suckling J, Coleman MR, Pickard JD, Menon D, Bullmore E (2005) Neurophysiological architecture of functional magnetic resonance images of human brain. Cereb Cortex 15:1332-1342.

Sanchez-Vives MV, McCormick DA (2000) Cellular and network mechanisms of rhythmic recurrent activity in neocortex. Nature neuroscience 3:1027-1034.

Schevon CA, Trevelyan AJ, Schroeder CE, Goodman RR, McKhann G, Jr., Emerson RG (2009) Spatial characterization of interictal high frequency oscillations in epileptic neocortex. Brain 132:3047-3059.

Schmidt C, Peigneux P, Muto V, Schenkel M, Knoblauch V, Munch M, de Quervain DJ, Wirz-Justice A, Cajochen C (2006) Encoding difficulty promotes postlearning changes in sleep spindle activity during napping. The Journal of neuroscience : the official journal of the Society for Neuroscience 26:8976-8982.

Scholvinck ML, Maier A, Ye FQ, Duyn JH, Leopold DA (2010) Neural basis of global resting-state fMRI activity. Proc Natl Acad Sci U S A 107:10238-10243.

Schroeder CE, Lakatos P (2009) Low-frequency neuronal oscillations as instruments of sensory selection. Trends Neurosci 32:9-18.

Shannon CE (1948) A MATHEMATICAL THEORY OF COMMUNICATION. Bell System Technical Journal 27:379-423.

Shmuel A, Leopold DA (2008) Neuronal correlates of spontaneous fluctuations in fMRI signals in monkey visual cortex: Implications for functional connectivity at rest. Hum Brain Mapp 29:751-761.

Shu Y, Hasenstaub A, McCormick DA (2003) Turning on and off recurrent balanced cortical activity. Nature 423:288-293.

Siapas AG, Wilson MA (1998) Coordinated interactions between hippocampal ripples and cortical spindles during slow-wave sleep. Neuron 21:1123-1128.

Sirota A, Buzsaki G (2005) Interaction between neocortical and hippocampal networks via slow oscillations. Thalamus & related systems 3:245-259.

Smith JF, Pillai A, Chen K, Horwitz B (2011) Effective Connectivity Modeling for fMRI: Six Issues and Possible Solutions Using Linear Dynamic Systems. Frontiers in systems neuroscience 5:104.

Smith SM, Fox PT, Miller KL, Glahn DC, Fox PM, Mackay CE, Filippini N, Watkins KE, Toro R, Laird AR, Beckmann CF (2009) Correspondence of the brain's functional architecture during activation and rest. Proc Natl Acad Sci U S A 106:13040-13045.

Smith SM, Jenkinson M, Woolrich MW, Beckmann CF, Behrens TE, Johansen-Berg H, Bannister PR, De Luca M, Drobnjak I, Flitney DE, Niazy RK, Saunders J,

Vickers J, Zhang Y, De Stefano N, Brady JM, Matthews PM (2004) Advances in functional and structural MR image analysis and implementation as FSL. Neuroimage 23 Suppl 1:S208-219.

Staba RJ, Wilson CL, Fried I, Engel J, Jr. (2002) Single neuron burst firing in the human hippocampus during sleep. Hippocampus 12:724-734.

Stam CJ, van Straaten EC (2012) The organization of physiological brain networks. Clinical neurophysiology : official journal of the International Federation of Clinical Neurophysiology 123:1067-1087.

Steinvorth S, Wang C, Ulbert I, Schomer D, Halgren E (2009) Human entorhinal gamma and theta oscillations selective for remote autobiographical memory. Hippocampus.

Steriade M (2003) The corticothalamic system in sleep. Front Biosci 8:d878-899.

Steriade M (2006) Grouping of brain rhythms in corticothalamic systems. Neuroscience 137:1087-1106.

Steriade M, Amzica F (1996) Intracortical and corticothalamic coherency of fast spontaneous oscillations. Proc Natl Acad Sci U S A 93:2533-2538.

Steriade M, Contreras D, Curro Dossi R, Nunez A (1993a) The slow (< 1 Hz) oscillation in reticular thalamic and thalamocortical neurons: scenario of sleep rhythm generation in interacting thalamic and neocortical networks. J Neurosci 13:3284-3299.

Steriade M, Nunez A, Amzica F (1993b) Intracellular analysis of relations between the slow (< 1 Hz) neocortical oscillation and other sleep rhythms of the electroencephalogram. J Neurosci 13:3266-3283.

Steriade M, Nunez A, Amzica F (1993c) A novel slow (< 1 Hz) oscillation of neocortical neurons in vivo: depolarizing and hyperpolarizing components. J Neurosci 13:3252-3265.

Steriade M, Timofeev I (2003) Neuronal plasticity in thalamocortical networks during sleep and waking oscillations. Neuron 37:563-576.

Steriade M, Timofeev I, Grenier F (2001) Natural waking and sleep states: a view from inside neocortical neurons. Journal of neurophysiology 85:1969-1985.

Tao JX, Hawes-Ebersole S, Baldwin M, Shah S, Erickson RK, Ebersole JS (2009) The accuracy and reliability of 3D CT/MRI co-registration in planning epilepsy

surgery. Clinical neurophysiology : official journal of the International Federation of Clinical Neurophysiology 120:748-753.

Timofeev I, Grenier F, Steriade M (2001) Disfacilitation and active inhibition in the neocortex during the natural sleep-wake cycle: an intracellular study. Proceedings of the National Academy of Sciences of the United States of America 98:1924-1929.

Tononi G, Sporns O, Edelman GM (1994) A measure for brain complexity: relating functional segregation and integration in the nervous system. Proceedings of the National Academy of Sciences of the United States of America 91:5033-5037.

Uhlhaas PJ, Pipa G, Lima B, Melloni L, Neuenschwander S, Nikolic D, Singer W (2009) Neural synchrony in cortical networks: history, concept and current status. Frontiers in integrative neuroscience 3:17.

Ulbert I, Halgren E, Heit G, Karmos G (2001a) Multiple microelectrode-recording system for human intracortical applications. Journal of neuroscience methods 106:69-79.

Ulbert I, Heit G, Madsen J, Karmos G, Halgren E (2004a) Laminar analysis of human neocortical interictal spike generation and propagation: current source density and multiunit analysis in vivo. Epilepsia 45 Suppl 4:48-56.

Ulbert I, Karmos G, Heit G, Halgren E (2001b) Early discrimination of coherent versus incoherent motion by multiunit and synaptic activity in human putative MT+. Human brain mapping 13:226-238.

Ulbert I, Magloczky Z, Eross L, Czirjak S, Vajda J, Bognar L, Toth S, Szabo Z, Halasz P, Fabo D, Halgren E, Freund TF, Karmos G (2004b) In vivo laminar electrophysiology co-registered with histology in the hippocampus of patients with temporal lobe epilepsy. Exp Neurol 187:310-318.

Umeoka S, Terada K, Baba K, Usui K, Matsuda K, Tottori T, Usui N, Nakamura F, Inoue Y, Fujiwara T, Mihara T (2009) Neural connection between bilateral basal temporal regions: cortico-cortical evoked potential analysis in patients with temporal lobe epilepsy. Neurosurgery 64:847-855; discussion 855.

Urrestarazu E, Chander R, Dubeau F, Gotman J (2007) Interictal high-frequency oscillations (100-500 Hz) in the intracerebral EEG of epileptic patients. Brain 130:2354-2366.

Valentin A, Alarcon G, Garcia-Seoane JJ, Lacruz ME, Nayak SD, Honavar M, Selway RP, Binnie CD, Polkey CE (2005a) Single-pulse electrical stimulation identifies epileptogenic frontal cortex in the human brain. Neurology 65:426-435.

Valentin A, Alarcon G, Honavar M, Garcia Seoane JJ, Selway RP, Polkey CE, Binnie CD (2005b) Single pulse electrical stimulation for identification of structural abnormalities and prediction of seizure outcome after epilepsy surgery: a prospective study. Lancet neurology 4:718-726.

Valentin A, Anderson M, Alarcon G, Seoane JJ, Selway R, Binnie CD, Polkey CE (2002) Responses to single pulse electrical stimulation identify epileptogenesis in the human brain in vivo. Brain 125:1709-1718.

van den Heuvel MP, Mandl RC, Stam CJ, Kahn RS, Hulshoff Pol HE (2010) Aberrant frontal and temporal complex network structure in schizophrenia: a graph theoretical analysis. The Journal of neuroscience : the official journal of the Society for Neuroscience 30:15915-15926.

Volgushev M, Chauvette S, Mukovski M, Timofeev I (2006) Precise long-range synchronization of activity and silence in neocortical neurons during slow-wave oscillations [corrected]. The Journal of neuroscience : the official journal of the Society for Neuroscience 26:5665-5672.

Vyazovskiy VV, Cirelli C, Pfister-Genskow M, Faraguna U, Tononi G (2008) Molecular and electrophysiological evidence for net synaptic potentiation in wake and depression in sleep. Nat Neurosci 11:200-208.

Vyazovskiy VV, Faraguna U, Cirelli C, Tononi G (2009) Triggering slow waves during NREM sleep in the rat by intracortical electrical stimulation: effects of sleep/wake history and background activity. Journal of neurophysiology 101:1921-1931.

Wang C, Ulbert I, Schomer DL, Marinkovic K, Halgren E (2005) Responses of human anterior cingulate cortex microdomains to error detection, conflict monitoring, stimulus-response mapping, familiarity, and orienting. J Neurosci 25:604-613.

Wang JH, Zuo XN, Gohel S, Milham MP, Biswal BB, He Y (2011) Graph theoretical analysis of functional brain networks: test-retest evaluation on short- and long-term resting-state functional MRI data. PloS one 6:e21976.

Wellmer J, von Oertzen J, Schaller C, Urbach H, Konig R, Widman G, Van Roost D, Elger CE (2002) Digital photography and 3D MRI-based multimodal imaging for individualized planning of resective neocortical epilepsy surgery. Epilepsia 43:1543-1550.

Wen W, Zhu W, He Y, Kochan NA, Reppermund S, Slavin MJ, Brodaty H, Crawford J, Xia A, Sachdev P (2011) Discrete neuroanatomical networks are associated with specific cognitive abilities in old age. The Journal of neuroscience : the official journal of the Society for Neuroscience 31:1204-1212.

Wilson CL, Isokawa M, Babb TL, Crandall PH (1990) Functional connections in the human temporal lobe. I. Analysis of limbic system pathways using neuronal responses evoked by electrical stimulation. Experimental brain research Experimentelle Hirnforschung Experimentation cerebrale 82:279-292.

Winkler PA, Vollmar C, Krishnan KG, Pfluger T, Bruckmann H, Noachtar S (2000) Usefulness of 3-D reconstructed images of the human cerebral cortex for localization of subdural electrodes in epilepsy surgery. Epilepsy research 41:169-178.

Wittner L, Huberfeld G, Clemenceau S, Eross L, Dezamis E, Entz L, Ulbert I, Baulac M, Freund TF, Magloczky Z, Miles R (2009) The epileptic human hippocampal cornu ammonis 2 region generates spontaneous interictal-like activity in vitro. Brain : a journal of neurology 132:3032-3046.

Wolansky T, Clement EA, Peters SR, Palczak MA, Dickson CT (2006) Hippocampal slow oscillation: a novel EEG state and its coordination with ongoing neocortical activity. The Journal of neuroscience : the official journal of the Society for Neuroscience 26:6213-6229.

Womelsdorf T, Schoffelen JM, Oostenveld R, Singer W, Desimone R, Engel AK, Fries P (2007) Modulation of neuronal interactions through neuronal synchronization. Science 316:1609-1612.

Worrell GA, Gardner AB, Stead SM, Hu S, Goerss S, Cascino GJ, Meyer FB, Marsh R, Litt B (2008) High-frequency oscillations in human temporal lobe: simultaneous microwire and clinical macroelectrode recordings. Brain 131:928-937.

Worrell GA, Parish L, Cranstoun SD, Jonas R, Baltuch G, Litt B (2004) High-frequency oscillations and seizure generation in neocortical epilepsy. Brain 127:1496-1506.

Zalesky A, Fornito A, Seal ML, Cocchi L, Westin CF, Bullmore ET, Egan GF, Pantelis C (2011) Disrupted axonal fiber connectivity in schizophrenia. Biological psychiatry 69:80-89.

Zhang Z, Liao W, Chen H, Mantini D, Ding JR, Xu Q, Wang Z, Yuan C, Chen G, Jiao Q, Lu G (2011) Altered functional-structural coupling of large-scale brain networks in idiopathic generalized epilepsy. Brain : a journal of neurology 134:2912-2928.

DOI:10.14753/SE.2015.1798

9 List of Author's publications

9.1 Publications related to the present thesis:

1 Entz L; Toth E; Keller CJ; Bickel S; Groppe DM; Fabo D; Kozak LR; Eross L; Ulbert I;Mehta AD. Evoked effective connectivity of the human neocortex. *HUMAN BRAIN MAPPING* 2014 Dec;35(12):5736-53

2 Keller CJ, Honey CJ, Entz L, Bickel S, Groppe DM, Toth E, Ulbert, Lado FA, Mehta AD. Corticocortical evoked potentials reveal projectors and integrators in human brain networks. *JOURNAL OF NEUROSCIENCE 34:(27) pp. 9152-9163. (2014)*

3 Keller CJ, Bickel S, Honey CJ, Groppe DM, Entz L, Craddock RC, Lado FA, Kelly C, Milham M, Mehta AD. Neurophysiological investigation of spontaneous correlated and anticorrelated fluctuations of the BOLD signal. *JOURNAL OF NEUROSCIENCE* 33:(15) *pp. 6333-6342.* (2013)

4 Keller CJ, Bickel S, Entz L, Ulbert I, Milham MP, Kelly C, Mehta AD. Intrinsic functional architecture predicts electrically evoked responses in the human brain. *PROCEEDINGS OF THE NATIONAL ACADEMY OF SCIENCES OF THE UNITED STATES OF AMERICA.* 108:(25) pp. 10308-10313. (2011)

5 Hangya B, Tihanyi BT, Entz L, Fabo D, Eross L, Wittner L, Jakus R, Varga V, Freund TF, Ulbert I. Complex Propagation Patterns Characterize Human Cortical Activity during Slow-Wave Sleep. *JOURNAL OF NEUROSCIENCE* 31:(24) pp. 8770-8779. (2011)

6 Csercsa R, Dombovari B, Fabo D, Wittner L, Eross L, Entz L, Solyom A, Rasonyi G, Szucs A, Kelemen A, Jakus R, Juhos V, Grand L, Magony A, Halasz P, Freund TF, Magloczky Z, Cash SS, Papp L, Karmos G, Halgren E, Ulbert I. Laminar analysis of slow wave activity in humans. *BRAIN* 133:(Pt 9) pp. 2814-2829. (2010)

7 Erőss L, Bagó AG, Entz L, Fabó D, Halász P, Balogh A, Fedorcsák I. Neuronavigation and fluoroscopy-assisted subdural strip electrode positioning: a simple method to increase intraoperative accuracy of strip localization in epilepsy surgery. *JOURNAL OF NEUROSURGERY* 110:(2) pp. 327-331. (2009)

9.2 Publications not related to the present thesis:

1 Tamás G, Takáts A, Radics P, Rózsa I, Csibri É, Rudas G, Golopencza P, Entz L, Fabó D, Erőss L. A mély agyi stimuláció hatékonysága Parkinson-kóros betegeink kezelésében. *IDEGGYÓGYÁSZATI SZEMLE/CLINICAL NEUROSCIENCE* 66:(3-4) pp. 115-120. (2013)

2 Erőss L, Fekete G, Entz L, Fabó D, Borbély C, Kozák LR, Andrejkovics M, Czirják S, Fedorcsák I, Novák L, Bognár L. Az intraoperatív elektromos agyi stimuláció szerepe a nyelvi és beszédfunkciók megőrzése céljából éber betegeken végzett idegsebészeti beavatkozások során. *IDEGGYÓGYÁSZATI SZEMLE* 65:(9-10) pp. 333-341. (2012)

3 Muller K, Fabo D, Entz L, Kelemen A, Halasz P, Rasonyi G, Eross L. Outcome of vagus nerve stimulation for epilepsy in Budapest. *EPILEPSIA* 51 Suppl 3: pp. 98-101. (2010)

4 Wittner L, Huberfeld G, Clémenceau S, Eross L, Dezamis E, Entz L, Ulbert I, Baulac M, Freund TF, Maglóczky Z, Miles R. The epileptic human hippocampal cornu ammonis 2 region generates spontaneous interictal-like activity in vitro *BRAIN* 132:(11) pp. 3032-3046. (2009)

5 Nagy A, Sax B, Entz L Jr, Barat E, Toma I, Becker D, Merkely B, Kekesi V. Comparison of elimination and cardiovascular effects of adenine nucleosides administered intrapericardially or intravenously in anesthetized dog. *JOURNAL OF CARDIOVASCULAR PHARMACOLOGY* 54:(4) pp. 341-347. (2009)

6 Erőss L, Entz L, Fabó D, Jakus R, Szűcs A, Rásonyi GY, Kelemen A, Barcs G, Juhos V, Balogh A, Barsi P, Clemens ZS, Halász P. Interhemispheric propagation of seizures in mesial temporal lobe epilepsy. *IDEGGYÓGYÁSZATI SZEMLE* 62:(9-10) pp. 319-325. (2009)

7 Toma I, Sax B, Nagy A, Entz L Jr, Rusvai M, Juhasz-Nagy A, Kekesi V. Intrapericardial angiotensin II stimulates endothelin-1 and atrial natriuretic peptide formation of the in situ dog heart. *EXPERIMENTAL BIOLOGY AND MEDICINE* 231:(6) pp. 847-851. (2006)

DOI:10.14753/SE.2015.1798

10 Acknowledgements

First of all I would like to thank my mentors Dr. István Ulbert and Prof. Péter Halász for their continuous support and guidance during these years. I especially would like to express my gratitude to István Ulbert who stood behind me on a daily basis and gave me scientific, material and personal support throughout the years.

Dr. Loránd Erőss, my clinical mentor, who beside giving me the opportunity to perform my research on the patients he implanted, whereof I am mostly thankful, he also introduced me to the field of neurosurgery and especially into the subspecialty of functional neurosurgery and gave me endless opportunities to learn the field.

I would like to thank for the Fulbright Foundation to making me possible to spend one year in New York under the mentorship of Dr. Ashesh Mehta. Dr. Mehta allowed me to perform research on his patients and gave me support in every sense for what I always will be thankful. He showed me how to perform high quality research parallel with the daily work at a neurosurgical ward. Dr. Dániel Fabó worked with me on a daily basis and introduced me to many aspects of epileptology and epilepsy research whereof I will be always thankful.

Dr. Stephan Bickel introduced me to functional neuroimaging research and helped me throughout the years with continues support and great questions.

I would like to thank Dr. Lucia Wittner, Corey J. Keller and Dr. Balázs Hangya to the work we did together which resulted in high impact publications.

Emília Tóth was enormously helpful in performing much of the data analysis and writing the Matlab scripts.

I would like to thank Prof. István Nyáry and Prof. Zoltán Nagy directors of the Institute for making me possible to perform the research we have planned. Here, I also would like to thank the colleagues at the National Institute of Clinical Neuroscience for every help I received from them.

I started my research career at the Research Laboratory of the Cardiovascular Surgery Dept. of Semmelweis University under the guidance of Prof. Alexander Juhász-Nagy and Dr. Violetta Kékesi who turned my interest towards physiology and taught me how to perform, analyze and understand experiments and basic physiology. Dr. Andrea Nagy

as my first mentor helped me to gain basic skills in research and presenting at conferences.

I would like to thank my parents for the continues support I received during my education and especially my father Prof. László Entz, whose attitude towards patients and knowledge of medicine and surgery has driven me always to become a doctor.

I would like to thank my wife, Dr. Zsófia Entz-Tóth who stood behind me and supported me continuously in every sense so I could focus on my research.

Finally I would like to thank the cooperation of all patients and their families, who volunteered to participate in the research.